



**Identification and characterisation of
suppressor mutants complementing a photorespiratory
defect in the *Arabidopsis* mutant *er-ant1***

vom Fachbereich Biologie der Universität Kaiserslautern zur Verleihung des
akademischen Grades „Doktor der Naturwissenschaften“ genehmigte

Dissertation

D 386

vorgelegt von

Jacqueline Sabrina Altensell

Kaiserslautern, im Juni 2019

Tag der wissenschaftlichen Aussprache: 26. Juli 2019

Berichterstatter:

1. Prof. Dr. H. Ekkehard Neuhaus
2. Prof. Dr. Poul Erik Jensen

Table of contents

Abstract.....	1
Dansk abstrakt.....	2
Deutsche Zusammenfassung.....	3
1 Introduction	5
1.1 Energy translocation in the plant cell.....	5
1.2 Use of forward genetics allows unbiased research	8
1.3 Forward genetics and Next-generation sequencing – a powerful combination	10
1.4 Objectives.....	10
2 Methods.....	11
2.1 Plant material and growth conditions.....	11
2.1.1 Cultivation on soil.....	11
2.1.2 Cultivation in hydroponic culture.....	11
2.1.3 Cultivation in sterile agar culture	11
2.2 Microbiological and molecular biology methods.....	12
2.2.1 Bacteria strains and plasmids.....	12
2.2.2 Cultivation of bacteria	13
2.2.3 Oligonucleotides.....	14
2.2.4 Recombinant DNA technologies	15
2.2.5 Agarose gel electrophoresis	16
2.2.6 Plasmid isolation from <i>E. coli</i> cells	16
2.2.7 Gateway cloning	17
2.2.8 Isolation of RNA.....	19
2.2.9 Quantitative real-time PCR (qRT-PCR)	19
2.2.10 Transformation of <i>A. thaliana</i> ("floral dip" method)	19

2.2.11	Histochemical analyses by GUS staining	20
2.2.12	Isolation and transient transformation of <i>A. thaliana</i> protoplasts.....	20
2.2.13	GFP fluorescence analyses	20
2.2.14	Quantification of amino acids	21
2.2.15	Chlorophyll determination	21
2.2.16	Transcriptome analysis.....	22
2.2.17	TEM analysis	22
2.2.18	Chlorophyll fluorescence measurements	22
2.2.19	Investigation of photosynthetic complexes	24
2.2.20	EMS mutagenesis and suppressor screen	25
2.2.21	Bioinformatic tools used for identification of conserved domains.....	29
2.2.22	Biochemical characterisation of the HAD-type phosphatase	30
3	Results	31
3.1	Metabolic analysis of <i>er-ant1</i>	31
3.1.1	Amino acid content of <i>er-ant1</i> mutants.....	31
3.1.2	Comparison of the amino acid profile of <i>er-ant1</i> with that of photorespiration mutants	35
3.2	Transcriptomic analyses	36
3.2.1	Influence of perturbations on <i>ER-ANT1</i> expression.....	36
3.2.2	Transcriptomic analysis of <i>er-ant1</i> mutants.....	40
3.2.3	The interplay between CO ₂ assimilation and nitrate metabolism in <i>er-ant1</i>	44
3.2.4	Jasmonate synthesis is affected in <i>er-ant1</i>	47
3.2.5	Analysis of serine-metabolism in <i>er-ant1</i> leaves	49
3.2.6	Analysis of the S-adenosylmethionine metabolism in <i>er-ant1</i> leaves	51
3.2.7	The <i>er-ant1</i> plants show alterations in the cellular redox state	54
3.2.8	Expression signature of genes encoding mitochondrial proteins in <i>er-ant1</i>	56

3.2.9	Fermentation in <i>er-ant1</i>	58
3.2.10	Hypoxia-associated reprogramming in <i>er-ant1</i>	60
3.3	Effect of vitamin B ₆ on <i>er-ant1</i>	62
3.4	Identification of <i>er-ant1</i> suppressor mutants	64
3.5	Characterisation of <i>er-ant1</i> suppressor mutants	66
3.5.1	Morphology of M ₃ <i>er-ant1</i> suppressor plants	66
3.5.2	Chlorophyll content of suppressor plants	67
3.5.3	Glycine quantification in the suppressor plants	68
3.5.4	Photosystem II performance of suppressor mutants	69
3.5.5	Assembly of photosynthetic complexes	72
3.5.6	Ultrastructure of <i>er-ant1</i> suppressor mutant chloroplasts	74
3.6	Identification and verification of suppressor candidate genes	77
3.6.1	Identification of suppressor candidates using Next-Generation Sequencing	77
3.6.2	Bulked segregant Next-Generation Sequencing analysis	78
3.6.3	Identification of single nucleotide polymorphisms	79
3.6.4	Identification of candidate suppressor mutations	80
3.6.5	Confirmation of candidate SNPs via Sanger sequencing	84
3.7	Confirmation of the AT2G33255 suppressor mutation	84
3.7.1	Isolation of <i>had</i> T-DNA insertion mutants	85
3.7.2	Morphology of <i>had-2</i> and <i>had-3</i> plants	86
3.7.3	Crossing of <i>er-ant1</i> with <i>had-2</i>	86
3.7.4	Amino acid content in <i>had</i> knockout mutants and <i>had-2 x er-ant1</i>	88
3.8	Characterisation of HAD	88
3.8.1	Expression analysis <i>in silico</i>	89
3.8.2	Promotor activity of <i>HAD in vivo</i>	90
3.8.3	Subcellular localisation of HAD	91

3.8.4	Haloacid dehalogenase-like hydrolase superfamily.....	93
3.8.5	Conserved domains of HAD.....	94
3.8.6	HAD comparison to characterised PLP phosphatases	96
3.8.7	Heterologous expression and purification of the recombinant HAD	98
3.8.8	Substrate specificity of HAD	99
4	Discussion	103
4.1.1	From PLP to photorespiration	103
4.1.2	From photorespiration to redox homeostasis	106
4.1.3	Hypoxia	107
4.1.4	Amino acid metabolism.....	110
4.1.5	ER-ANT1 and cancer	112
4.1.6	How can absence of ER-ANT1 affect PLP metabolism	114
4.2	Outlook.....	118
5	Literature cited	120
6	Appendix.....	143

Abstract

More than ten years ago, ER-ANT1 was shown to act as an ATP/ADP antiporter and to exist in the endoplasmic reticulum (ER) of higher plants. Because structurally different transporters generally mediate energy provision to the ER, the physiological function of ER-ANT1 was not directly evident.

Interestingly, mutant plants lacking ER-ANT1 exhibit a photorespiratory phenotype. Although many research efforts were undertaken, the possible connection between the transporter and photorespiration also remained elusive. Here, a forward genetic approach was used to decipher the role of ER-ANT1 in the plant context and its association to photorespiration.

This strategy identified that additional absence of a putative HAD-type phosphatase partially restored the photorespiratory phenotype. Localisation studies revealed that the corresponding protein is targeted to the chloroplast. Moreover, biochemical analyses demonstrate that the HAD-type phosphatase is specific for pyridoxal phosphate. These observations, together with transcriptional and metabolic data of corresponding single (ER-ANT1) and double (ER-ANT1, phosphatase) loss-of-function mutant plants revealed an unexpected connection of ER-ANT1 to vitamin B₆ metabolism.

Finally, a scenario is proposed, which explains how ER-ANT1 may influence B₆ vitamer phosphorylation, by this affects photorespiration and causes several other physiological alterations observed in the corresponding loss-of-function mutant plants.

Dansk abstrakt

For over ti år siden blev det påvist at ER-ANT1 fungerer som en ATP/ADP antiporter der findes i planters ER membraner. Dog var det på det tidspunkt uklart hvad physiologisk funktion ER-ANT1 havde, eftersom ER systemets energibehov opfyldes af mange strukturelt forskellige transportproteiner. Overraskende nok udviste planter uden ER-ANT1 tegn på forstyrret fotorespiration. Trods gentagne forsøg er det ikke lykket at redegøre for forbindelsen mellem ER-ANT1s transporter funktion og fotorespirationen. I dette værk beskrives et forsøg på at udrede netop denne forbindelse mellem ER-ANT1s rolle in planten og dennes betydning for fotorespirationen. Ved hjælp af en fremad genetisk fremgang er det lykket at identificere en yderligere faktor, HAD-type fosfatase, hvis fravær delvist redder den fotorespirationsrelaterede fenotype. En undersøgelse af lokaliseringen af denne fosfatase viser at den findes i kloroplasterne, og udfra biokemiske undersøgelser fremgår det at denne HAD-type fosfatase udviser præference for pyridoxal fosfat. Sammen med transkriptions og stofskifte data fra ER-ANT1 enkelt- og ER-ANT1/fosfatase dobbeltmutanter peger disse observationer på en hidtil ukendt rolle i vitamin B₆ stofskiftet. Afsluttende i dette værk præsenteres en model der sammendrager de eksperimentielle observationer og beskriver hvordan ER-ANT1 har indfyldelse på forforylering af vitamin B₆ gennem dets påvirkning af fotorespiration, og hvordan dette forklarer mange af de fysiologiske ændringer der forekommer i planter der mangler ER-ANT1 proteinet.

Deutsche Zusammenfassung

Vor mehr als zehn Jahren konnte gezeigt werden, dass ER-ANT1 in der Membran des endoplasmatischen Retikulums höherer Pflanzen lokalisiert ist und dort als ATP/ADP-Antiporter fungiert. Da die generelle Energieversorgung des endoplasmatischen Retikulums offensichtlich durch andere Transporter vermittelt wird, ist die genaue physiologische Bedeutung des ER-ANT1 nicht auf den ersten Blick ersichtlich.

Arabidopsis-Mutanten, denen der funktionelle ER-ANT1 fehlt, weisen interessanterweise einen Photorespirationsphänotyp auf. Viele Anstrengungen wurden unternommen, um die Rolle des ER-ANT1 im pflanzlichen Kontext aufzuklären. Jedoch blieb völlig unklar, wie ein fehlender ATP/ADP-Transporter im endoplasmatischen Retikulum eine Störung in der Photorespiration auslösen kann. Um neue Einblicke zu erlangen und sich unvoreingenommen der möglichen Rolle des ER-ANT1 im pflanzlichen Stoffwechsel und dessen Verbindung zur Photorespiration zu nähern, wurde im Rahmen dieser Arbeit ein vorwärtsgenetischer Ansatz angewendet.

Es konnten hierdurch Suppressor-Mutanten identifiziert und betroffene Gene mittels Next-Generation Sequencing bestimmt werden. Die Untersuchung der ersten Kandidaten führte zur Erkenntnis, dass der Wachstumsdefekt der *er-ant1* Mutante durch die zusätzliche Abwesenheit einer putativen HAD-Typ Phosphatase teilweise aufgehoben wird.

Da die Funktion dieser Phosphatase nicht beschrieben ist, wurde eine initiale Charakterisierung durchgeführt. GFP-basierte Targetingstudien ergaben, dass sie in Chloroplasten lokalisiert ist. Des Weiteren wurde die HAD-Typ Phosphatase heterolog in *E. coli* exprimiert, anschließend gereinigt und in Enzymtests eingesetzt. Es stellte sich heraus, dass die HAD-Typ Phosphatase Pyridoxalphosphat mit hoher Spezifität hydrolysiert. Zusammen mit Transkriptom- und Metabolomdaten der jeweiligen Einzel- (Fehlen von ER-ANT1) und Doppel-Mutanten (Fehlen von ER-ANT1 und HAD-Typ Phosphatase), deutete diese Beobachtung auf eine unerwartete Verbindung des ER-ANT1 mit dem Vitamin-B₆-Metabolismus hin. Überdies wurden die Transkriptom- und Metabolomdaten der *er-ant1* Mutante mit entsprechenden Daten klassischer Photorespirationsmutanten verglichen. Auf diese Weise konnte bestimmt werden, welche Veränderungen auf den Photorespirationsdefekt zurückzuführen sind und welche exklusiv *er-ant1* betreffen.

Auf Basis der neuen Erkenntnisse, wurde ein Szenario vorgeschlagen, welches erklärt, wie das Fehlen von ER-ANT1 die Phosphorylierung der B₆-Vitamere beeinflussen könnte, dadurch Einfluss auf die Photorespiration nimmt und verschiedene andere physiologische Veränderungen in der Mutante bedingt.

1 Introduction

1.1 Energy translocation in the plant cell

Nucleotides are building blocks of the genetic information, act as cofactors in enzyme reactions, are required for the activation of precursors during the production of polymers or may function as second messengers in signal cascades. Among the different nucleotides, ATP plays a key role because it represents the major energy currency of the cell. Eukaryotes regenerate most of their ATP via oxidative phosphorylation in mitochondria. Plants are also capable of regenerating vast amounts of ATP during photosynthesis in their chloroplasts.

Moreover, glycolysis and fermentation processes may contribute to the production of chemical energy. However, these pathways are comparatively inefficient and costly in terms of carbohydrate consumption. Although the majority of cellular energy is produced in mitochondria and chloroplasts, its use is not restricted to these two locations. ATP-dependent reactions occur almost everywhere in the cell, and thus, highly efficient transport systems are required to provide ATP to the places where needed.

In terms of energy metabolism, chloroplasts are quite autarkic since they can fuel endogenous processes with photosynthetic ATP. Heterotrophic plastids, however, rely on ATP uptake and the same holds true for chloroplasts in the night or during phases of limited photosynthetic activity (Tjaden *et al.*, 1998; Reinhold *et al.*, 2007). Members of the major facilitator superfamily, the nucleoside triphosphate transporters (NTTs), catalyse the required energy translocation across the inner envelope membrane (Winkler and Neuhaus, 1999). Interestingly, NTT-mediated ATP uptake occurs in exchange with ADP and phosphate, and thus energy provision to the plastid is accompanied by the simultaneous removal of the two products of energy consumption (Trentmann *et al.*, 2008).

Although recent studies suggest that NTTs may deliver energy to the cytosol (Voon *et al.*, 2018), mitochondria play clearly the main function in this process. ADP/ATP carriers (AACs) represent the most abundant transporters in the inner mitochondrial membrane, catalyse a highly efficient ATP export and by this supply the cytosol and indirectly other organelles with mitochondrial energy (Millar and Heazlewood, 2003). The concomitant ADP import provides the substrate for oxidative phosphorylation to the matrix. AACs physiologically interact with

phosphate carriers, which import the second substrate for ATP regeneration into the mitochondrion (Kunji *et al.*, 2016).

AACs and phosphate importers belong to the mitochondrial carrier family (MCF), which comprises 58 members in *Arabidopsis* (Palmieri *et al.*, 2011). MCF proteins are structurally and phylogenetically related but highly heterogeneous in terms of their substrate specificity. They exhibit a molecular mass of about 30–35 kDa, consist of six transmembrane domains and contain specific conserved domains (Kuan and Saier, 1993; Nury *et al.*, 2006). They transport structurally highly diverse substrates, such as nucleotides or phosphate but also di- and tricarboxylates, different cofactors, amino acids, sulfate or even protons. Most MCF proteins are located in the inner mitochondrial membrane; however, some members reside in other organelles like peroxisomes, chloroplasts or the endoplasmic reticulum (Haferkamp and Schmitz-Esser, 2012). The proteins that mediate energy provision to peroxisomes (Linka *et al.*, 2008) and possibly also to glyoxysomes are MCF transporters with moderate relation to the AACs (Fukao *et al.*, 2001). However, different from the AACs, they import ATP and export ADP and thus mediate the opposed translocation of the substrates.

Endoplasmic Reticulum Adenylate Transporter 1 (ER-ANT1), the transporter of this study, also belongs to the MCF. The detailed characterisation of various MCF proteins revealed that members with related substrate spectra often cluster together in phylogenetic analyses (Haferkamp and Schmitz-Esser, 2012; Palmieri *et al.*, 2011). Interestingly, ER-ANT1 forms a monophyletic subcluster with the AACs (Leroch *et al.*, 2008; Haferkamp and Schmitz-Esser, 2012) which implies that ER-ANT1 acts as an ATP/ADP antiporter. Biochemical analyses demonstrated that ER-ANT1 is, in fact, specific for ATP and ADP and operates in a counter exchange mode (Leroch *et al.*, 2008). However, it shows a lower affinity for ATP and ADP than the AACs. Moreover, different from the AACs, ER-ANT1 lacks the N-terminal transit peptide for mitochondrial import and is targeted to the endoplasmic reticulum (ER) membrane (Leroch *et al.*, 2008).

The ER harbours various highly energy consuming processes in the lumen but lacks the capacity for ATP production (Hirschberg *et al.*, 1998; Depaoli *et al.*, 2019). Therefore, high amounts of ATP have to be imported from the cytosol (Hirschberg *et al.*, 1998; Depaoli *et al.*, 2019). Although the existence of an ATP-transport capacity at the ER membrane was

demonstrated as early as 1992 (Clairmont *et al.*, 1992), the identity of the corresponding transport proteins remained unknown for a long time. In this context, ER-ANT1 was the first promising candidate, since it acts as an ATP/ADP antiporter in the ER of *Arabidopsis* (Leroch *et al.*, 2008).

The role for ER-ANT1 in energy supply to the ER is supported by the fact that ER-ANT1 is highly expressed in organs and tissues that show intense activities of luminal chaperones and thus of ATP consuming processes (Leroch *et al.*, 2008). Moreover, it has been shown that mRNA levels of ATP-dependent enzymes, such as the ER chaperones BiP1 to BiP3 and the calcium-dependent protein kinase 2, are strongly reduced in mutant plants lacking ER-ANT1 (*er-ant1*). In addition, *er-ant1* plants exhibit decreased seed lipid- and seed storage-protein levels, which further point to an involvement of ER-ANT1 in cellular processes classically related to the ER function (Leroch *et al.*, 2008).

However, ER-ANT1 apparently does not represent the long-sought major ATP supplier in the ER. This is because energy provision to the ER is a basal process and required in all eukaryotes, but ER-ANT1 homologs are restricted to higher plants (Haferkamp and Schmitz-Esser, 2012; Hoffmann *et al.*, 2013). Furthermore, *er-ant1* knockout plants suffer severely under ambient air but remain rather unaffected under conditions of high CO₂ availability (Hoffmann *et al.*, 2013). This observation suggests that basal ATP supply to the ER is guaranteed and thus mediated by a different uptake system (Leroch *et al.*, 2008).

Very recent studies identified the major ATP/ADP transporter of the ER in mammalian cells, AXER (Klein *et al.*, 2018). The corresponding sequence is conserved among all eukaryotes. Moreover, the initial characterisation of the two AXER homologs from plants revealed that they act as ATP/ADP antiporters in the membrane of the ER (unpublished, Plant Physiology, TUK) and that they are essential for plant survival (Reyes *et al.*, 2010).

However, these discoveries do not minimise the relevance of ER-ANT1 in higher plants. In fact, plants lacking ER-ANT1 (*er-ant1*) show stunted growth and reduced chlorophyll contents under ambient CO₂ conditions. It became clear that *er-ant1* is defective in photorespiration as this mutant shows massive accumulation of the photorespiratory key-intermediate glycine, is impaired in CO₂ fixation and has a higher CO₂ compensation point than the wild type

(Hoffmann *et al.*, 2013). Moreover, the *er-ant1* dwarf phenotype can be reversed by suppressing photorespiration (Hoffmann *et al.*, 2013).

The current data in sum suggest that ER-ANT1 may be involved in energy delivery to the ER and apparently fulfils a specific role in plants that is essential for photorespiration.

1.2 Use of forward genetics allows unbiased research

Arabidopsis thaliana exhibits many features that make it an excellent plant model organism. For example, its small size limits the requirements for huge growth facilities. But particularly its short generation cycle, the small genome with comparatively few repetitive sequences and its efficient reproduction through self-pollination made *Arabidopsis* an early favourite for studying mutations in plants (Koornneef and Meinke, 2010; Page and Grossniklaus, 2002).

Another reason for its success is that *Arabidopsis* is suitable for reverse as well as for forward genetic screens. Whereas reverse genetics strategies rely upon sequence information and try to gain insight into the underlying function of a gene by studying resulting phenotypes, forward genetics aim to discover changes in sequences that underlie a specific mutant phenotype (Peters *et al.*, 2003). In general, forward genetics were proven to be a powerful tool for the identification of components involved in a specific biological process without the need for prior assumptions (Qu and Qin, 2014; Page and Grossniklaus, 2002).

One chemical mutagen widely used in forward genetics is ethyl methanesulfonate (EMS) (Qu and Qin, 2014). EMS leads to random point mutations in the genome by alkylating guanine (G) residues, forming O⁶-ethylguanine. Usually, G pairs with cytosine (C), however, O⁶-ethylguanine can pair with thymine (T) exclusively. Followed by subsequent DNA repair, original G/C pairs are replaced by A (adenine)/T pairs (Kim *et al.*, 2006).

Within forward genetics, EMS can be used to perform so-called secondary screens (Page and Grossniklaus, 2002). For this, mutant plants, which are affected in a particular metabolic or developmental pathway, are again mutagenised with EMS, followed by the screening for second-site mutations which either enhance (worsen) or suppress (alleviate) the phenotype caused by the primary mutation (Page and Grossniklaus, 2002).

In theory, four types of suppression can result from second site mutations (Li and Zhang, 2016). The first is the epistatic suppression, in which mutations affecting an upstream step of a signalling pathway are suppressed by downstream antagonistic mutations (Li and Zhang, 2016). An example for this is BDA1 (bian da 1; Chinese for “becoming big 1”) which is a signalling component acting downstream of SNC2 (Suppressor of NPR1, Constitutive2) in the regulation of plant immunity in *Arabidopsis* (Yang *et al.*, 2012). BDA1 was identified in a suppressor screen, in which the loss-of-function mutation in *BDA1* suppressed the dwarf phenotype and the constitutive defence responses in *snc2-1D npr1-1* mutant plants (Yang *et al.*, 2012).

The second type of suppression is achieved by the removal of proteins that otherwise would result in toxic effects (Li and Zhang, 2016). This was, for example, observed in the *Arabidopsis* gain-of-function mutant *snc1* (suppressor of *npr1-1* constitutive 1), which exhibits a constitutive defence response (Xu *et al.*, 2012). Here, the identified suppressor mutation in *MOS12* (Modifier Of SNC1,12) eventually resulted in altered splicing patterns of *SNC1*, which alleviated the toxic effects caused by the increased accumulation of SNC1 in the *snc1* mutant (Xu *et al.*, 2012; Li and Zhang, 2016).

In rare occasions, a mutation in an interaction partner of the mutant protein can suppress the mutant phenotype (Li and Zhang, 2016). For example, the fusion of the Cdc2 kinase in yeast with the cyclin Cdc13 was predicted and validated after the identification of the Cdc13 gene in a Cdc2 mutant suppressor screen (Booher and Beach, 1987; Booher *et al.*, 1989).

The fourth suppression results from the activation of alternative pathways (Li and Zhang, 2016), as observed for a growth-defective yeast which lacks specific members of the nuclear pore complex. The fitness of the yeast mutant was restored by a mutation in a nuclear envelope protein, which supposed to reduce nuclear membrane fluidity (van Leeuwen *et al.*, 2017).

In general, forward genetic suppressor screens might provide new insights into the pathway affected by a mutation (Page and Grossniklaus, 2002). Although various biological studies used the mutagenesis-based approach in *Arabidopsis*, this method still has its difficulties as, for example, the identification of the second-site mutations by map-based cloning is very laborious and time-consuming (Uchida *et al.*, 2014).

1.3 Forward genetics and Next-generation sequencing – a powerful combination

Next-generation sequencing (NGS) technologies evolved during the past 15 years and led to substantial improvements in the quality and yield of the resulting data. Furthermore, the price for whole-genome sequencing became more and more affordable: In 2006, sequencing of a whole human genome cost approximately 14 million US Dollar, whereas eight years later, the price dropped below 1000 US Dollar (van Dijk *et al.*, 2014). This opened up new possibilities for the application of NGS in everyday scientific life. By coupling NGS to forward genetic screens, time-consuming processes, such as the common outcrossing of the suppressor mutant in another accession line as well as laborious steps, like PCR-based mapping with molecular markers, were no longer required (Uchida *et al.*, 2014; Qu and Qin, 2014).

1.4 Objectives

Although ER-ANT1 was biochemically characterised more than ten years ago and *er-ant1* mutants were analysed quite detailed, the role of this transport protein in the cellular context is still elusive, and its connection to photorespiration is entirely unknown. The aim of this study is to gain deeper insights into the plant-specific function of ER-ANT1 and to explain how its absence is linked to photorespiration. For this, a forward genetic screen should be conducted. This method aimed to identify candidates suppressing the growth defect of *er-ant1* by using a combination of a bulked segregant analysis and NGS. Subsequently, the correctness of the identified candidate(s) should be verified by reverse genetic approaches. The newly identified candidate(s) might help to place ER-ANT1 into the physiological context and to clarify how far ER-ANT1 is involved in energy supply to the ER. In order to dissect characteristics unique for *er-ant1* mutants from those commonly associated with photorespiration, metabolic and transcriptomic data from ER-ANT1 should be compared with those from other characterised photorespiration mutants. This approach might be suited to identify the connection between ATP/ADP translocation at the ER and photorespiration.

2 Methods

2.1 Plant material and growth conditions

Studies were performed with *Arabidopsis thaliana* wild type plants (ecotype Columbia-0) and T-DNA insertion mutants in Col-0 background. The used T-DNA insertion mutants are listed in Table 2-1.

Table 2-1: List of used T-DNA insertion mutants.

TAIR Locus	Name	NASC ID
AT5G17400	<i>er-ant1</i>	N543626
AT2G33255	<i>had-1</i>	N664249
AT2G33255	<i>had-2</i>	N682264
AT2G33255	<i>had-3</i>	N863636

2.1.1 Cultivation on soil

Before germination, seeds were incubated for 2 d in the dark at 4°C on standardised ED73 soil (Weigel and Glazebrook, 2002). If not stated otherwise, plants were grown diurnally for 10 h at 22°C and 120 $\mu\text{mol photons m}^{-2} \text{s}^{-1}$ light intensity followed by 14 h at 18°C without light. Plants were either grown at ambient CO₂ levels (~ 400 ppm) or high CO₂ levels (2000 ppm) in Fitotron plant climate chambers (Weiss Technik, Reiskirchen, Germany).

2.1.2 Cultivation in hydroponic culture

Cultivation of *Arabidopsis* in hydroponic culture was performed according to Conn *et al.*, 2013.

2.1.3 Cultivation in sterile agar culture

Before cultivation in sterile culture, plants were surface sterilised. After preincubation for 5 min in 70 % EtOH, seeds were sterilised with 5 % sodium hypochlorite for 10 min and subsequently washed three times with sterilised water. Seeds were stratified for 2 d dark at 4°C in water before the transfer to sterile ½ MS agar plates.

1 litre ½ MS-media:

- **2.2 g** MS salts incl. vitamins
- **10 g** sucrose
- **0.5 g** MES
- **8 g** Agar
- **pH** 5.7
- **(Optional** different concentrations of pyridoxine HCl)

2.2 Microbiological and molecular biology methods

2.2.1 Bacteria strains and plasmids

Within this study, *Escherichia coli* (*E. coli*) and *Agrobacterium tumefaciens* (*A. tumefaciens*) were used. Properties of the used bacteria strains are listed in Table 2-2.

Table 2-2: Bacteria strains.

Strain	Resistance	Source
<i>E. coli</i> XL1 Blue	Tet ^R	Bullock, 1987
<i>E. coli</i> DH5α	-	Taylor <i>et al.</i> , 1993
<i>E. coli</i> Rosetta 2 (DE3)	Clm ^r	Merck, Darmstadt
<i>A. tumefaciens</i>	Rif ^R , Gen ^R	Koncz and Schell, 1986

Plasmids used in this study are listed in Table 2-3.

Table 2-3: Plasmids

Plasmid	Relevant properties	Source
pBSK	Amp ^r , cloning vector	Stratagene, Heidelberg
pDONR™/Zeo	Zeo ^r , <i>ccdB</i> , Gateway entry vector	Life technologies, Darmstadt
pBGWFS7	Bar ^r , GUS:GFP, Gateway destination vector	Karimi <i>et al.</i> , 2002
pET16b	Amp ^r , expression vector	Novagen, Heidelberg

2.2.2 Cultivation of bacteria

E. coli cells were cultivated at 37°C at aerobic conditions in either sterile LB-media (*E. coli* DH5α) or sterile YT media (*E. coli* XL1 Blue, *E. coli* Rosetta 2 (DE3)).

YT-Media:

- 0.8 % (w/v) Peptone
- 0.5 % (w/v) Yeast extract
- 0.25 % (w/v) NaCl
- pH 7.0
- (1.5 % (w/v) Agar for plates)

LB-Media:

- 1 % (w/v) Peptone
- 0.5 % (w/v) Yeast extract
- 0.5 % (w/v) NaCl
- pH 7.0
- (1.5 % (w/v) Agar for plates)

Antibiotics for *E. coli* selection were added after autoclaving. Used concentrations of antibiotics are listed in Table 2-4.

Table 2-4: Concentrations of antibiotics for *E. coli* selection.

Antibiotic	End concentration [$\mu\text{g/ml}$]
Ampicillin	200
Tetracycline	10
Chloramphenicol	12.5
Zeocin	50
Spectinomycin	50

A. tumefaciens cells were cultivated at 30°C. Antibiotics for *A. tumefaciens* selection were added after autoclaving. Used concentrations of antibiotics are listed in Table 2-5.

Table 2-5: Concentrations of antibiotics for *A. tumefaciens* selection

Antibiotic	End concentration [$\mu\text{g/ml}$]
Rifampicin	100
Gentamycin	25
Spectinomycin	100

Recombinant bacteria cells were stored from overnight cultures in 15 % (v/v) glycerol at 80°C.

2.2.3 Oligonucleotides

Oligonucleotides for amplification of DNA-fragments with PCR and for expression studies via qRT-PCR are listed in Table 2-6.

Table 2-6: Oligonucleotides.

Primer	Sequence 5'→3'
T3	AATTAACCCTCACTAAAGGG
T7	TAATACGACTCACTATAGGG
M13-fwd	GTAAAACGACGGCCAG
M13-rev	CAGGAAACAGCTATGAC
attB1	CAAGTTTGTACAAAAAAGCAG
attB2	CCACTTTGTACAAGAAAGC
Seq-AT2G33255-fwd	TAGAGCCCCACATCACGATT
Seq-AT2G33255-rev	TATGCAACAGCGGGTCTGG
LBb1.3	ATTTTGCCGATTTTCGGAAC
SAIL-LB3	TAGCATCTGAATTTTCATAACCAATCTCGATACAC
HAD-KO-1-LP	TCCCATTTCATCATCTTATCGC
HAD-KO-1-RP	ATCAGACGAAAACCCAAATCC
HAD-KO-2-LP	TCAAAGCAGAGAGCCCTAGTG
HAD-KO-2-RP	GCTATGGAGAAAGGGTTGACC
HAD-KO-3-LP	TTGCATACACCAGATTTTGCTC
HAD-KO-3-RP	ATCAGACGAAAACCCAAATCC
qRT-HAD-fwd	GCTTCAAATCATGCCTGGTACTGC
qRT-HAD-rev	CGTTGATGGAAGATGTCGATTGCC
qRT-SAND-fwd	AACTCTATGCAGCATTTGATCCACT
qRT-SAND-rev	TGATTGCATATCTTTATCGCCATC

2.2.4 Recombinant DNA technologies

2.2.4.1 Transformation of *E. coli* cells

Transformation of plasmid DNA into competent *E. coli* cells was performed using the heat shock method (Froger and Hall, 2007).

2.2.4.2 Transformation of *A. tumefaciens* cells

The transformation of competent *A. tumefaciens* cells was performed according to the protocol of the "freeze-thaw" method (Höfgen and Willmitzer, 1988).

2.2.5 Agarose gel electrophoresis

Agarose gel electrophoresis was carried out according to Sambrook and Russell, 2001 and was performed in a horizontal gel apparatus at constant voltage (80-120 V). Depending on the size of the molecules to be separated, 0.8-2 % agarose gels were prepared. For this purpose, the agarose was boiled in 1-fold TAE buffer, cooled with stirring to about 50° C and mixed with ethidium bromide (final concentration 0.5 g / ml), which intercalated into the DNA. The ethidium bromide fluoresces orange under UV light excitation ($\lambda = 260$ nm). The solution was then poured into a gel chamber with a pocket former. DNA samples to be separated were prepared with 10x TAE loading buffer medium for gel-run. As a measure of the fragment sizes, a corresponding DNA marker (GeneRuler™ Mix Ladder, Thermo Fisher, Waltham USA) was separated parallel to the samples.

50x TAE loading buffer (1 litre):

- **242 g** Tris free base
- **57.1 ml** Glacial acetic acid
- **18.61 g** Disodium EDTA

Fill up to 1 litre with H₂O

2.2.6 Plasmid isolation from *E. coli* cells

To isolate plasmid DNA for sequencing and gateway cloning, the “Nucleospin Plasmid® Kit” (Macherey + Nagel, Düren) was used. This was done according to the manufacturer’s instructions.

Plasmid isolation for other purposes was carried out according to the principle of alkaline lysis. This is based on the fact that plasmid DNA, genomic DNA, RNA and proteins have different precipitation properties (Sambrook and Russell, 2001). For the plasmid isolation, 4 ml of overnight culture were harvested (centrifugation for 1 min at 15000 g). The supernatant was subsequently discarded and resuspended with 150 μ l P1 buffer (Qiagen, Hilden) containing 1 mg x ml⁻¹ DNase-free RNase. Subsequently, 150 μ l of SDS-containing P2 buffer (Qiagen, Hilden) were added, whereby the alkaline lysis of the cells took place. The NaOH contained in the P2 buffer denatures the proteins liberated during lysis and chromosomal DNA. Thereafter, 150 μ l

of P3 buffer (Qiagen, Hilden), which stops the reaction, and 2 drops of chloroform were added to purify the plasmid DNA. After careful inverting, the lysate was centrifuged for 5 min at 15000 g. The supernatant (about 400µl) was transferred to a new centrifuge tube. By the addition of 800 µl isopropanol, the DNA was precipitated. The mixture was then centrifuged for 10 min at 15000 g and 4°C and the supernatant discarded. The resulting pellet was washed by the addition of 1 ml 80 % ethanol and again centrifuged for 10 min at 15000 g and 4°C. The supernatant was discarded, and the pellet dried until it became transparent. Finally, the dry pellet was dissolved in 40 µl H₂O.

2.2.6.1 Manipulation of DNA with restriction enzymes

DNA restriction has been used for both, to clone vector DNA and to analyse constructs from vector DNA. For the restriction approach, the buffer media and incubation temperatures given by the manufacturers (NEB) were used. The cut DNA was then fractionated by agarose gel electrophoresis and the fragment sought was excised from the gel using a scalpel. Elution of the DNA was done using the Gel Extraction Kit "NucleoSpin Extract II" (Macherey & Nagel, Düren). T4 DNA ligase was used to target ligation as an assembly of specific DNA fragments. This enzyme has the property to catalyse the covalent attachment of complementary DNA ends. Thus, after the restriction of a vector and a specific fragment with the same restriction enzymes, the ligase can covalently link the vector with the specific DNA fragment via phosphodiester bonds. The ligations were carried out with the enzyme T4 DNA ligase (Thermo Scientific, Waltham) according to the manufacturer.

2.2.7 Gateway cloning

Starting from *A. thaliana* cDNA, attB recombination sites were added to the respective sequence via PCR and the use of primers. The primers carried attB sites overlaps at the 5' ends. These recombination sites are recognised by recombinases. The PCR product was transformed into a donor vector by the so-called BP reaction. The recombination sites attB of the PCR product and attP from the donor vector react specifically with each other. As a result, the attL sequences are generated in the resulting input clone. The donor vector exhibits a Clm resistance and contains the gene ccdB. Its gene product inhibits the gyrase and thus die. The ccdB gene is replaced by the PCR product during the BP reaction and is no longer present in

the resulting input clone. The contained antibiotic sequences (Spec, Clm in the donor vector, Zeocin in the entry clone) allows two independent selections. The LR reaction creates so-called destination clones. They are formed by the recombination of the entry clone with the target vector, the attL sites of the entry clone react with the attR sites of the target vector and attB sites are generated again. Double selection is again enabled by a *ccdB* gene in the target vector between the attR sites as well as the use of antibiotic resistance to spectinomycin in the destination vector.

To generate an entry clone, a BP reaction was performed between an attB flanked DNA fragment and a donor vector containing attP sites. The BP reaction mixture without proteinase K was incubated at 25°C for one hour. Subsequently, the proteinase K was added to stop the reaction by incubation for 10 min at 37° C. Competent *E. coli* (DH5α) were transformed and selected on LB plates with a suitable antibiotic.

BP reaction mixture:

- **100-150 ng DNA** PCR product
- **1 µl** pDONR_{zeo}
- **2 µl** BP clonase
- **1 µl** Proteinase K
- **Fill up to 10 µl** TE-Buffer (pH 8.0)

To generate a destination clone, an LR reaction was performed between an entry clone with attL sites and a target vector with attR sites. The LR reaction batch without proteinase K was incubated at 25°C for one hour. Subsequently, the proteinase K was added, and the batch was incubated for 10 min at 37°C. Competent *E. coli* (DH5α) were transformed and selected on LB-plates with a suitable antibiotic.

LR reaction mixture:

- **100-150 ng DNA** Entry clone
- **1 µl** Destination clone
- **2 µl** LR clonase
- **1 µl** Proteinase K
- **Fill up to 10 µl** TE-Buffer (pH 8.0)

2.2.8 Isolation of RNA

For qRT-PCR analyses, total *A. thaliana* RNA was isolated. For this purpose, leaves were harvested and ground in liquid nitrogen. Total RNA was isolated from 50 mg of the triturated material using the "NucleoSpin RNA Plant Kit" according to the manufacturer's instructions (Macherey & Nagel, Düren). The RNA concentration was determined by photometric measurement at a nanodrop machine (Peqlab, Erlangen).

2.2.9 Quantitative real-time PCR (qRT-PCR)

With reverse transcriptase (Verso-Kit, Thermo Fisher Scientific, Karlsruhe), the contained mRNA from total RNA was rewritten into cDNA. The amplification for determining the expression of individual genes was carried out using "PerfeCTa® SYBR® Green" according to the manufacturer's instructions (Quantabio, Gaithersburg, USA). The amplification and fluorescence detection were performed with the qRT-PCR machine MyiQ iCycler (Bio-Rad, Munich). The relative quantification was done, using the $2^{-\Delta\Delta Ct}$ method (Livak and Schmittgen, 2001).

2.2.10 Transformation of *A. thaliana* ("floral dip" method)

The production of transgenic *A. thaliana* plants was carried out by means of *A. tumefaciens*-mediated transformation (Clough and Bent, 1998). For this purpose, 250 ml of the *Agrobacterium* overnight culture were centrifuged at 5000 g for 15 min. The cell pellet was then resuspended in 500 ml sucrose solution (5 %) with 0.01 % Silwet L77 (BASF, Ludwigshafen). To transform the *Arabidopsis thaliana* wild-type plants, the entire

inflorescences were immersed in the *Agrobacterium* suspension and then incubated in the dark for one day at room temperature. Finally, the transformed plants were grown under long-day conditions until seed ripening and harvesting.

2.2.11 Histochemical analyses by GUS staining

The gene of β -glucuronidase (GUS) from *E. coli* was used as a gene fusion marker for the analysis of gene expression in transformed *A. thaliana*. The promoter region of AT2G33255 was fused to the GUS reporter gene and transformed into *A. thaliana* via floral dip so that gene expression can be documented by histochemical staining *in planta*. For detection, the synthetic substrate X-Gluc (5-bromo-4-chloro-3-indolyl-beta-D-glucuronic acid) is used, which forms after oxidative condensation and cleavage a blue colour precipitate at the exact synthesis site of the GUS reporter (and thus the promoter to be examined). The staining was carried out in accordance with Sessions *et al.*, 1999: The plants were incubated for 20 min in pre-cooled acetone on ice. After removal of the acetone, the plants were washed twice with staining buffer on ice. Thereafter, the plants were mixed with the staining solution and vacuum-sealed for 30 min. This was followed by incubation of the plants in staining solution overnight at 37°C. The next day, the plants were destained with increasing concentrations of ethanol (20 %, 35 %, 50 %, 70 %; 30 min each concentration) and then examined for blue staining. The stained plant tissue was stored in the dark in 70 % ethanol.

2.2.12 Isolation and transient transformation of *A. thaliana* protoplasts

Protoplasts from *A. thaliana* were isolated and transiently transformed according to Yoo *et al.*, 2007.

2.2.13 GFP fluorescence analyses

Observation of the transformed *Arabidopsis* protoplasts was performed using a confocal laser microscope.

Details on microscopic analysis for subcellular localisation of GFP fusion proteins:

- **Microscope** Leica TCS SP52
- **Software** Leica Application Suite
Advanced Fluorescence
Version 2.5.2.6939
- **Objective** HCX PL APO lambda blue 63.0x1.20 WATER UV
- **Excitation wavelength laser** 488nm (Argon laser)
- **Filter bandwidth emission** GFP: 495nm-540nm
Autofluorescence chloroplasts: 651nm-704nm

2.2.14 Quantification of amino acids

For the determination of metabolites, *A. thaliana* leaves were harvested and transferred directly into liquid nitrogen. Subsequently, the leaves were ground in liquid nitrogen, and the powder was stored at -80°C. 500 µl water were added to 100 mg of triturated material, and the mixture was shaken for 15 min at 99°C (600 rpm). The contained starch and cell debris were sedimented by centrifugation at 20000 g. For the measurement, 20 µl of the sample supernatant were mixed with 60 µl borate buffer (0.2 M boric acid, pH 8.8) and then derivatised with 20 µl AQC (fluorescent reagent 6-aminoquinolyl-N-hydroxysuccinimidylcarbamate; Watrex, Prague) The quantification of the amino acids was carried out with an HPLC system consisting of P680 HPLC Dionex pump, ASI 100 Dionex autosampler, RF 2000 fluorescence detector, UCI 50 Dionex interface and an UVD 170 U Dionex UV detector. Nucleodur cc 250/4 100-5 c18ec served as HPLC column. Aliquots of 25 µl were applied to the column by the pump. The flow was constant at 1 ml/min. The samples were heated to 37°C on an autosampler. The chromatograms were evaluated using the software Chromeleon 6.7 (Thermo Fisher, Waltham, USA) .

2.2.15 Chlorophyll determination

Plant material for chlorophyll determination was ground in liquid nitrogen. For the chlorophyll (Chl) quantification, the extinctions of leaf extracts at the red absorption maxima of Chl_a

(~663 nm) and Chl_b (~646 nm) were measured. The samples were prepared, and chlorophyll content was determined according to Porra, 2002.

2.2.16 Transcriptome analysis

Leaf material of five plants per genotype was harvested and ground in liquid nitrogen. The preparation of samples for whole transcriptome expression analysis with “GeneChip® Whole Transcript (WT) Expression Arrays” was performed with the “GeneChip® WT PLUS Reagent Kit” (Affymetrix, USA) according to the manufacturer's instructions. The samples of each genotype were pooled prior to the analysis. Therefore, the data per genotype represent the mean of five individual samples.

2.2.17 TEM analysis

For TEM analysis, leaf material of *A. thaliana* grown permanently at high CO₂ conditions and adapted to ambient air was collected. Sample preparation was performed, according to Armbruster *et al.*, 2013. In brief, leaves were cut into small squares (~ 1 x 1 mm²) and fixed with 2.5 % glutaraldehyde in 0.1 M sodium cacodylate buffer (pH 7) for 2 h. Subsequently, samples were washed two times with cacodylate buffer and postfixed with 1 % osmium tetroxide for 2 h. After that, samples were washed with water, dehydrated in acetone, and embedded in Spurr's low-viscosity resin. 60 nm thin sections were prepared using a diamond knife (microtome) and mounted on copper grids coated with Pioloform (polyvinyl butyral). The sections were poststained with lead citrate. Electron microscopy was performed by Anurag Sharma (CPSC, University of Copenhagen, Denmark) as described previously by (Armbruster *et al.*, 2013).

2.2.18 Chlorophyll fluorescence measurements

The PAM 101/103 system was used to determine F_v/F_m , $Y(II)$ and NPQ as described before (Varotto *et al.*, 2000). Experiments were performed with plants permanently grown at high CO₂ conditions for five weeks and with plants at high CO₂ conditions for four weeks and subsequently adapted to ambient air for one week. For measurements, four to seven plants per genotype were dark adapted for 15 min. Then leaves were exposed to actinic light (0, 73,

219, 534 and 1290 $\mu\text{mol photons m}^{-2} \text{ s}^{-1}$) for 5 min to determine the photosynthetic parameters.

Dark-adapted plants were used to measure the maximum quantum yield of PSII (F_v/F_m). When plants are dark-adapted, all their PSII centres are open. After dark-adaptation, actinic light of intensity too low to induce PSII electron transport but high enough to elicit a minimum chlorophyll fluorescence was applied (Murchie and Lawson, 2013). This measured minimum chlorophyll fluorescence is termed F_0 . Subsequently, a saturating light pulse was applied to induce the closure of all reaction centres, producing a maximal possible value for fluorescence (F_m). F_v describes the difference between F_0 and F_m . The maximum quantum yield is expressed by the following formula:

$$\frac{F_m - F_0}{F_m} = \frac{F_v}{F_m}$$

To investigate PSII performance also in light-adapted states Y(II) and NPQ intensities were monitored after adaption to increasing actinic light. First, F_0 and F_m in plants which have been dark adapted for 15 minutes were determined. Then the leaves were illuminated stepwise for 5 min at increasing actinic light intensities. At the end of each incremental step, a saturation light pulse was applied to determine the photosynthetic parameters.

The effective PSII quantum yield Y(II) was calculated according to Genty et al. (1989) by the formula:

$$Y(II) = \frac{F_m' - F'}{F_m'}$$

F' describes the steady-state fluorescence of the leaf in continuous actinic light and F_m' the maximum fluorescence in the light-adapted state. In principle, Y(II) may vary between the values 0 and 1. The value 0.5 would mean that 50 % of the absorbed quanta are converted into chemically fixed energy by charge separation in PSII, whereas the other 50 % is dissipated into fluorescence and heat (Baker *et al.*, 1989).

The NPQ is a measure of non-photochemical fluorescence quenching. This process acts as a 'safety' mechanism as it dissipates excess excitation energy by heat and thereby prevents the

likelihood of singlet oxygen formation. In this study, the NPQ value was calculated using the equation of Bilger and Björkmann (1990):

$$NPQ = \frac{F_m' - F_m}{F_m'}$$

On the one hand, a high NPQ indicates an excessive photon flux density. On the other hand, a high NPQ shows that the plant retained physiological mechanisms to protect itself.

2.2.19 Investigation of photosynthetic complexes

2.2.19.1 Thylakoid isolation

Thylakoids were isolated from leaves of plants permanently grown at high CO₂ conditions for five weeks and from leaves of plants grown at high CO₂ conditions for four weeks and subsequently adapted to ambient air for one week. Thylakoid membranes were prepared as described earlier (Bassi *et al.*, 1985). Thylakoid amounts were normalised on the basis of chlorophyll concentration (Porra, 2002).

2.2.19.2 2D-BN-PAGE

All experimental steps were carried out at 4°C. For native PAGE analysis, thylakoid samples equivalent to 10 µg chlorophyll were solubilised in 25BTH20G Buffer (25 mM BisTris/HCl, pH 7.0, 20 % (w/v) glycerol and 0.25mg/ml Pefabloc (Sigma Aldrich, USA) containing 2 % (w/v) digitonin or dodecyl-β-D-maltoside (β-DM) for 5 min in the dark. β-DM has strong delipidating properties which enable the release of all protein complexes from the entire thylakoid membrane network (Aro *et al.*, 2005; Järvi *et al.*, 2011). However, it commonly destroys weak hydrophobic interactions in protein complexes (Wittig *et al.*, 2006). Therefore, also digitonin was used, maintaining weak interactions between protein complexes. Because of its large structure, this detergent only solubilises proteins from non-appressed regions. Therefore, proteins from the grana core fractions stay insolubilised when digitonin is the detergent of choice (Wittig *et al.*, 2006; Suorsa *et al.*, 2015).

Traces of unsolubilised material were removed by 20 min centrifugation at 18000 g and 1 h on a rotary wheel. The solubilised pigment-protein complexes were fractionated by nondenaturing BN-PAGE as described previously (Schägger and Jagow, 1991).

SDS-PAGE in the second dimension was performed as previously described (Armbruster *et al.*, 2010). For protein visualisation, gels were stained with silver (Blum *et al.*, 1987).

2.2.20 EMS mutagenesis and suppressor screen

For the suppressor screen, *er-ant1* seeds were mutagenised with ethyl methanesulfonate (EMS). EMS acts by alkylating guanine (G) residues, forming O⁶-ethylguanine. Usually, G pairs with cytosine (C). However, O⁶-ethylguanine can pair with thymine (T) exclusively. Followed by subsequent DNA repair, original G/C pairs are replaced by A (adenine)/T pair (Kim *et al.*, 2006). The mutagenesis was performed by Dr. Tatjana Kleine (LMU, Munich, Germany) as previously described (Kim *et al.*, 2006). The next screening steps were performed by Dr. Sebastian Hassler (University of Kaiserslautern, Germany). The resulting M₁ generation was composed of plants with random point mutations. *A. thaliana*, as a diploid plant, underlies the principles of heredity/dominance. Because dominant mutant phenotypes are much less common than recessive phenotypes in *Arabidopsis*, the M₁ generation was not screened for possible suppressor mutants (Meinke, 2013). Instead, pools of 500 M₁ plants were cultivated at high CO₂ (2000 ppm) conditions to ensure proper plant growth and seed development. Afterwards, the seeds of these pools were harvested individually. The most apparent phenotype of *er-ant1* plants is their reduced growth when cultivated at ambient air conditions. Therefore, plants of the M₂ Generation were cultivated at ambient CO₂ conditions. The identified suppressor mutants were isolated to avoid crossing events and for seed production. Before using the plants for the following experiments, the *er-ant1* specific T-DNA insertion was verified with a PCR based T-DNA insertion screen. By this verification, it was ensured that the chosen plants maintained their homozygosity for the recessive *er-ant1* mutant allele.

2.2.20.1 Bulk segregant analysis and next-generation sequencing

To identify mutations causative for the suppression bulk segregant analysis (BSA) was combined with whole genome Next-Generation Sequencing (NGS) similar as previously described by Song *et al.*, 2017.

2.2.20.2 Creation of the mapping populations

To create a mapping population, individual M₃ plants from various suppressor mutant lines were backcrossed with the original *er-ant1* mutant. Since always both parents, *er-ant1* and the respective suppressor mutant, were homozygous for the *er-ant1* T-DNA insertion, also all individuals of the backcross F₁ were homozygous for this modification. To get information about the dominance of the suppressor trait, which was important for following genetic filtering procedures, the F₁ generation was cultivated at ambient air. The BC₁F₁ plants self-pollinated and resulted in the segregating F₂ generation (mapping population) which is still homozygous *er-ant1* knockout. Due to segregation, also traits for the suppressor mutant became homozygous resulting in plants whose *er-ant1* dwarf phenotype was partly complemented.

2.2.20.3 gDNA preparation for NGS

For each investigated suppressor line, gDNA was extracted from 50 larger plants of the F₂-generation (positive pool) and from 50 plants showing the *er-ant1* phenotype (negative pool). In addition, one pooled sample was prepared, consisting of gDNA extracted from 50 plants of the original *er-ant1* T-DNA insertion line (*er-ant1* pool). The gDNA was extracted as previously described (Pallotta *et al.*, 2000). The pooled gDNA samples of 13 mapping populations and pooled gDNA of 50 original *er-ant1* mutant plants were used for Next-Generation Sequencing.

2.2.20.4 Whole genome resequencing

The whole genome resequencing was provided by Novogene (Beijing, China). Briefly, the genomic DNA was randomly sheared into fragments of about 350 bp and subjected to library construction using the “Illumina® TruSeq Library Construction Kit” (Illumina, San Diego, USA) according to the manufacturer's instructions. After library quality control, pair-end sequencing

was performed on the “Illumina® HiSeq” platform (Illumina, San Diego, USA), with the read length of 150 bp at each end.

2.2.20.5 NGS bioinformatic pipeline

The bioinformatics data analysis of the raw NGS data was provided by Novogene (Beijing, China). Briefly, the original sequencing data acquired by the high-throughput sequencing platform were recorded in image files. To perform the data analysis, the image files were firstly transformed to sequence reads by base calling with CASAVA software (version 1.8, Illumina, San Diego, USA). The sequences and corresponding sequencing quality information, represented by Phred scores, were stored in FASTQ files. To detect base positions with an unusually low sequencing quality, the sequencing quality distribution was examined over the full length of all sequences. The Phred score (Q) describes the probability of a base call being incorrect by the formula:

$$Q = -10 \log_{10}P$$

P represents the sequencing error rate. To decrease the complexity of downstream analyses, sequencing data contaminated with adapter and low-quality reads were removed. The effective sequencing data were aligned with the reference sequence TAIR10 (ftp://ftp.Arabidopsis.org/home/tair/Genes/TAIR10_genome_release/) through BWA software (Li and Durbin, 2009). The duplicates were removed with SAMtools (Li *et al.*, 2009). To evaluate the similarity between each sample and the reference genome, mapping statistics such as mapping rate, average sequencing depth and coverage, were evaluated. Single nucleotide polymorphisms (SNPs) were detected with SAMtools. To reduce the error rate in SNP detection, results were filtered, so that only SNPs were taken into account with more than four supporting reads and a mapping quality Q higher than 20. The software ANNOVAR was used to annotate the detected SNPs (Wang *et al.*, 2010).

2.2.20.6 Identification of candidate suppressor SNPs

For the visualisation of SNP localisation on chromosomes and for receiving more information about the effects each SNP has on the genetic information, the software CandiSNP was used (Etherington *et al.*, 2014).

To use this software, the allele frequency of all SNPs had to be calculated, first. The allele frequency (AF; also known as gene frequency) describes the proportion of the total gene copies that are of a particular allele in a defined population (Brenner *et al.*, 2002). The AF of each SNP was estimated with the following equation

$$AF = \frac{alt_{depth}}{(alt_{depth} + ref_{depth})}$$

Here, alt_{depth} (variant allele depth) is the number of reads containing the variant base (SNP) and ref_{depth} (reference allele depth) the number of reads containing the reference base.

Several filtering steps were performed to identify putative suppressor mutation causing SNPs (candidate SNPs). The dominance of the suppression causing SNP is described in section 2.2.20.2. It was observed that all suppression causing SNPs resulted in recessive phenotypes. Thus, all homozygous SNPs in any plant of the negative pool could be removed. Therefore, all SNPs with $AF \geq 0.5$ were dismissed from the *er-ant1* pool and the negative pool. The remaining SNPs with $AF < 0.5$ in the *er-ant1* pool and the respective negative pool were used for filtering the positive pool with the goal to exclude SNPs which were already present in the original *er-ant1* mutant and to exclude non-causative SNPs, which were randomly generated during the EMS-mutagenesis. Because EMS mutagenesis primarily results in G/C to A/T transitions, in the next filtering step, all SNPs generated by different base exchanges were removed (Maple and Møller, 2007).

SNPs can be either localised to a coding or non-coding region. Although introns and other non-coding regions can be causative for a suppressor phenotype, too (for example Thole *et al.*, 2008), this study focussed first on SNPs localised to coding exon regions to reduce the number of candidate SNPs. Within the coding region, SNPs can have various effects. An SNP can be non-synonymous, which results in an amino acid exchange or can lead to the gain of a preliminary start-codon or stop-codon. It is also possible that the SNP is synonymous, which means that it will have no effect because the variant codon codes for the same amino acid as the reference codon. To obtain only those that have an obvious impact on the resulting protein version, all synonymous mutations were removed.

Accumulations of SNPs with high AFs on chromosomes indicate that a corresponding sequence region is essential for the phenotype used for selection. It was assumed that only

plants homozygous for the suppressor mutation were used as a positive pool. Therefore SNPs with lower AFs than the maximum AF reached in each analysis were sorted out thoroughly. Often, several candidate SNPs with the maximal possible AF = 1 were observed in a single line. The focus was mainly on these SNPs, but SNPs with slightly lower AFs were also considered, taking possible sequencing errors into account. Candidate SNPs of lines with maximal AFs < 1 were also chosen. Lower AFs can have different origins, beside the not excludable possibility that also false-positive plants were included in the positive pool. For example, the used NGS platform itself has an error rate of 0.1 % and depends strongly on the quality of the used samples (Pfeiffer *et al.*, 2018; Fox *et al.*, 2014).

Since NGS is not free from errors (Fox *et al.*, 2014), chosen candidate SNPs were confirmed via “Sanger”-sequencing (Seq-IT, Kaiserslautern, Germany) prior to further analyses. For this, gDNA was extracted from at least 10 individual plants of the respective M₃ suppressor line. Furthermore, specific primers were designed for sequencing the genomic regions containing candidate SNPs. In parallel, also gDNA of wild type and *er-ant1* plants was sequenced to confirm, that the respective SNPs were absent in the non-suppressor mutant plants.

2.2.21 Bioinformatic tools used for identification of conserved domains

2.2.21.1 NCBI CD-Search

One promising candidate suppressor mutation was identified in AT2G33255. This gene encodes a putative HAD-type phosphatase.

NCBI CD-Search (Conserved Domain-Search) was used to identify conserved domains in the corresponding amino acid sequence. CD-search is a web-based tool for the detection of conserved domains in protein sequences (<https://www.ncbi.nlm.nih.gov/Structure/cdd/wrpsb.cgi>). It uses RPS-BLAST to compare query protein sequences against conserved domain models. If CD-Search finds a specific hit, there is high confidence in the association between the protein query sequence and a conserved domain (Marchler-Bauer *et al.*, 2017; Marchler-Bauer and Bryant, 2004).

For the identification of conserved domains, CD-Search was used with the 245 amino acid long AT2G33255 protein sequence. It was searched against the CDD v3.17 database, including NCBI-curated domains and data imported from Pfam, SMART, COG, PRK, and TIGRFAM

(https://www.ncbi.nlm.nih.gov/Structure/cdd/cdd_help.shtml#RPSBSearchDb). To avoid false positive results, the expectation value threshold was set to 0.01 (https://www.ncbi.nlm.nih.gov/Structure/cdd/cdd_help.shtml#WRPSBExpect). Furthermore, the by default enabled “composition based statistics adjustment” was used, which abolishes the need to mask out compositionally biased regions in query sequences (https://www.ncbi.nlm.nih.gov/Structure/cdd/cdd_help.shtml#WRPSBCompositionBasedScoring).

2.2.22 Biochemical characterisation of the HAD-type phosphatase

For the heterologous expression of the HAD-type phosphatase in *E. coli* and subsequent protein purification, the corresponding sequence was fused with a C-terminal 10x histidine-tag (His-Tag). This was achieved by its directed insertion into the vector pET16b. In pET16b expression of the protein of interest is under the control of the *lacI*-promoter and thus inducible by IPTG. The expression construct was used to transform competent *E. coli* Rosetta cells. Protein expression, purification via IMAC and immunostaining were performed as previously described (Trentmann *et al.*, 2007). However, in contrast to Trentmann *et al.*, the soluble fraction was used for protein enrichment.

The biochemical characterisation of the purified HAD-type phosphatase was assayed as previously described (Sussman and Avron, 1981). The used reaction mixture contained 20 mM Tris-HCl pH 7.0, 5 mM MgCl₂, 1mM NaMoO₄ and up to 10 mM of the tested substrates in a total volume of 1 ml. Approximately 25 µg/ml of purified protein was used in the enzymatic reactions. Reactions were stopped by adding perchloric acid to the reaction mixture. Subsequently, 200 µl of the mixture was used for phosphate determination. The released inorganic phosphate was determined as previously described (Ames, 1966).

3 Results

3.1 Metabolic analysis of *er-ant1*

3.1.1 Amino acid content of *er-ant1* mutants

Under photorespiratory conditions, mutant plants lacking ER-ANT1 massively accumulate glycine, probably due to a decreased activity of the glycine decarboxylase complex (GDC) (Hoffmann *et al.*, 2013). However, the residual 40 % GDC activity in *er-ant1* is apparently sufficient to degrade glycine during the night (Hoffmann *et al.*, 2013)

Interestingly, besides glycine, also other amino acid levels are changed in *er-ant1* mutant leaves (Hoffmann *et al.*, 2013). To further investigate the effect of missing ER-ANT1 on the amino acid metabolism, the levels of various amino acids in *er-ant1* were quantified and compared with those of corresponding wild-type plants. It was of particular interest to identify pathways affected in *er-ant1* as well as changes not resulting from disturbed photorespiration. For this, it was necessary to get a detailed overview of changes in amino acid concentrations, first. Accordingly, the different amino acids were determined in leaves not only during the day but also at the end of the night phase, when photorespiration was inactive for several hours. Furthermore, amino acids in the heterotrophic root tissue, which is basically not capable of photorespiration, were quantified.

First of all, the increased day glycine content in leaves of *er-ant1* mutants was verified: The glycine level was approximately 67-fold higher than that of the wild type (Figure 3-1 A). During the night, the glycine contents in wild-type and *er-ant1* leaves decreased, but that of *er-ant1* ($\sim 2.5 \mu\text{mol/g FW}$) was still significantly higher than that of the wild type ($\sim 0.01 \mu\text{mol/g FW}$). Also, *er-ant1* roots contained more glycine than the wild-type roots.

During the light phase, the serine content of the *er-ant1* shoot tissue was similar to that of the wild type ($\sim 2 \mu\text{mol/g fresh weight (FW)}$) (Figure 3-1 B). In contrast to this, serine was substantially increased during the night, whereas the corresponding wild-type level dropped. Interestingly, wild-type plants exhibited less serine in roots than in shoots, whereas *er-ant1* mutants accumulated more serine in roots than in shoots.

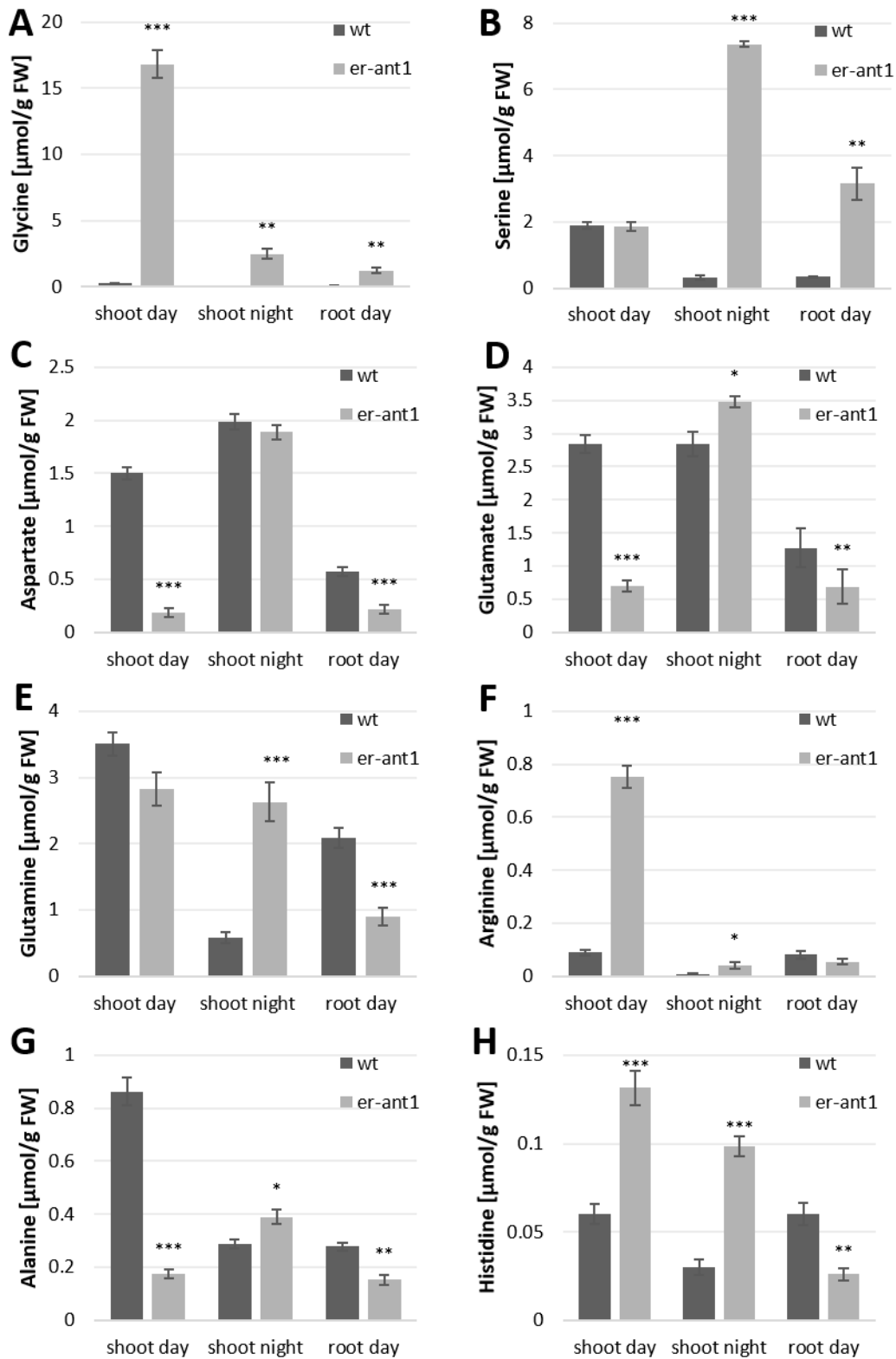


Figure 3-1: HPLC determined amino acid content in leaves and roots of *er-ant1* and wild-type plants. Plants were grown at 2000 ppm CO₂ in a light/dark cycle of 16/8 h for four weeks and subsequently shifted to ambient air. Samples were harvested after 5 d of adaptation, 5 h after onset of light. Shown are mean values of \geq four individual replicates, \pm SE. Asterisks indicate the significance level between wild-type and mutant plants according to Student's t-test (* $P < 0.05$, ** $P < 0.01$, *** $P < 0.001$) wt: wild type. FW: fresh weight.

Like previously reported, *er-ant1* mutant leaves exhibit decreased levels of aspartate during the light phase (Hoffmann *et al.*, 2013). This result was verified (Figure 3-1 C); however, at the end of the night phase, aspartate levels of *er-ant1* and wild-type leaves were quite similar. The aspartate concentration in *er-ant1* roots was significantly lower ($\sim 0.21 \mu\text{mol/g FW}$) than in the corresponding wild-type roots ($\sim 0.57 \mu\text{mol/g FW}$), but here the difference was not as pronounced as in the illuminated shoots.

Glutamate has a central position in the amino acid metabolism of plants. It is directly involved in the assimilation and dissimilation of ammonia, and it is used in aminotransferase reactions forming different amino acids (Forde and Lea, 2007). Leaves of *er-ant1* exhibited decreased glutamate levels ($\sim 0.7 \mu\text{mol/g FW}$) compared to wild-type leaves ($\sim 2.8 \mu\text{mol/g FW}$), as previously reported (Figure 3-1 D; Hoffmann *et al.*, 2013). Wild-type leaves showed identical daytime and nocturnal glutamate contents. The glutamate content in *er-ant1* mutants was, however, much higher at the end of the night phase than during the day. With $\sim 3.5 \mu\text{mol/g FW}$ in *er-ant1* leaves at the end of the night phase, the glutamate level was even significantly higher than that of the corresponding wild-type plants ($\sim 2.84 \mu\text{mol/g FW}$). By contrast, the glutamate level of wild-type roots was with $\sim 1.3 \mu\text{mol/g FW}$ approximately twice as high as that of the *er-ant1* roots.

The glutamine synthetase/glutamate synthase cycle represents the main entry of inorganic nitrogen into the plants' pool of nitrogen compounds. Within this cycle, the glutamine synthetase assimilates ammonia, which is for example released during photorespiration, into glutamine. This glutamine may serve as a precursor for glutamate and other nitrogen compounds required for plant growth (Kirby *et al.*, 2006). After illumination, no significant difference between the glutamine contents of wild-type ($\sim 3.5 \mu\text{mol/g FW}$) and *er-ant1* ($\sim 2.8 \mu\text{mol/g FW}$) leaves (Figure 3-1 E) was detected. However, the glutamine content in wild-type leaves harvested at the end of the dark phase dropped to $\sim 0.6 \mu\text{mol/g FW}$, whereas that of *er-ant1* remained high ($\sim 2.6 \mu\text{mol/g FW}$). Moreover, *er-ant1* roots contained significantly less glutamine ($\sim 0.9 \mu\text{mol/g FW}$) compared to wild-type roots ($\sim 2.1 \mu\text{mol/g FW}$).

Among the 21 proteinogenic amino acids, arginine has the highest nitrogen to carbon ratio. In plants, arginine serves as major storage and transport form for organic nitrogen. Besides its use for protein synthesis, arginine is also a precursor for polyamines as well as for nitric oxide

(Winter *et al.*, 2015). In illuminated leaves, arginine levels of *er-ant1* were highly elevated ($\sim 0.8 \mu\text{mol/g FW}$) compared to the wild type ($\sim 0.09 \mu\text{mol/g FW}$) (Figure 3-1 F). In the night, the arginine concentration decreased in wild-type and *er-ant1* leaves. However, the arginine content of *er-ant1* was with $\sim 0.04 \mu\text{mol/g FW}$ still significantly higher than that of wild-type leaves ($\sim 0.008 \mu\text{mol/g FW}$). Compared to that, no significant differences between the arginine levels of wild-type and *er-ant1* roots was observed.

Alanine is formed by the reversible transfer of one amino group from glutamate to pyruvate which is catalysed by alanine:oxoglutarate aminotransferase. The alanine metabolism in plants is not entirely clarified. However, it has had been observed that alanine accumulates during hypoxic conditions in roots, probably to prevent loss of nitrogen and carbon from anaerobic fermentation (Sousa and Sodek, 2003; Miyashita *et al.*, 2007). During the day, *er-ant1* leaves showed a significantly decreased alanine content compared to wild-type leaves ($\sim 0.2 \mu\text{mol/g FW}$ versus $\sim 0.9 \mu\text{mol/g FW}$) (Figure 3-1 G). During the night, the alanine levels of *er-ant1* leaves increased ($\sim 0.4 \mu\text{mol/g FW}$), and those of wild-type plants decreased ($\sim 0.3 \mu\text{mol/g FW}$). In roots, the alanine concentration of *er-ant1* was lower than that of the wild type ($\sim 0.2 \mu\text{mol/g FW}$ versus $\sim 0.3 \mu\text{mol/g FW}$).

Histidine formation is an energy-costly process and starts with the condensation of ATP and phosphoribosyl pyrophosphate. Besides being a proteinogenic amino acid, histidine plays an essential role in metal ion homeostasis of plants. Furthermore, histidine is of high importance for the development of the embryo (Stepansky and Leustek, 2006). The histidine levels of *er-ant1* leaves are significantly higher compared to those of wild-type leaves, irrespective of whether the tissue was harvested after illumination or at the end of the dark period (Figure 3-1 H). However, the opposite applies for roots: Here, the histidine level of *er-ant1* was significantly lower ($\sim 0.03 \mu\text{mol/g FW}$) than that of the wild type ($\sim 0.06 \mu\text{mol/g FW}$).

Amino acids were also quantified in plants which were cultivated at high CO_2 conditions. In general, *er-ant1* plants showed under this condition only minor changes compared to the wild type. However, under high CO_2 *er-ant1* still accumulated more glycine in shoots and roots than the wild type (Figure 3-2 A), but the total glycine level was much lower compared to ambient CO_2 (Figure 3-1 A). Interestingly, alanine levels of illuminated *er-ant1* leaves were lower under ambient CO_2 (Figure 3-1 G), but higher under high CO_2 (Figure 3-2 B) when

compared to the wild type. While the alanine content was slightly higher in *er-ant1* roots at ambient CO₂ conditions, it resembled that of the wild type at high CO₂ (Figure 3-2 B).

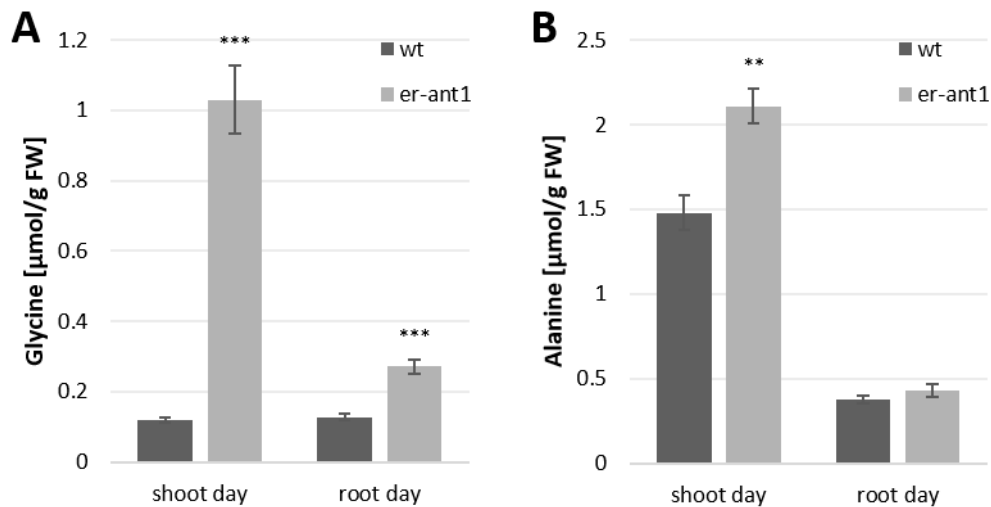


Figure 3-2: HPLC determined amino acid content in leaves and roots of *er-ant1* and wild type plants. Plants were grown hydroponically at 2000 ppm CO₂ and a light/dark cycle of 16/8 h for four weeks and five days. Samples were harvested 5 h after onset of light. Shown are mean values of five individual replicates, \pm SE. Asterisks indicate the significance level between wild-type and mutant plants according to Student's t-test (* $P < 0.05$, ** $P < 0.01$, *** $P < 0.001$). wt: wild type. FW: fresh weight.

These data demonstrate that the absence of ER-ANT1 apparently affects several pathways associated with amino acid metabolism.

3.1.2 Comparison of the amino acid profile of *er-ant1* with that of photorespiration mutants

The high glycine accumulation of *er-ant1* leaves is due to reduced activity of the glycine decarboxylase complex (GDC), which is a key enzyme in the photorespiration pathway (Hoffmann *et al.*, 2013). To see whether changes of other amino acids can also be explained by defects in photorespiration, data of this study were compared with published data of other mutants impaired in photorespiration (Table 3-1).

The comparison revealed that the amino acid pattern of *er-ant1* shows remarkable similarities to those of other mutants defective in photorespiration (Figure 3-1). However, also differences became apparent, for example, that illuminated *er-ant1* leaves did not exhibit increased glutamine and serine concentrations, which are higher in several other

photorespiration mutants. This observation suggests that many but probably not all changes in the amino acid profile of *er-ant1* result from the perturbation of its photorespiration.

Table 3-1: Comparison of selected amino acid levels in illuminated leaves of *er-ant1* and other photorespiration mutants adapted to ambient CO₂ conditions.

	<i>er-ant1</i>	<i>shm1</i>	<i>bou</i>	<i>glu1</i>	<i>pglp1</i>
Glycine	68 x	104 x	222 x	n.d.	12 x
Serine	=	3 x	2 x	n.d.	=
Arginine	8 x	28 x	3 x	8 x	3 x
Glutamate	4 x	4 x	2 x	4x	2 x
Glutamine		2 x	5 x	2x	3 x
Aspartate	8 x	5 x	3 x	3 x	=
Alanine	5 x	3 x	=	n.d.	6 x
Histidine	2 x	26 x	6 x	n.d.	n.d.

Shown are fold changes of the mutant compared to corresponding wild-type plants. Red colour highlights relative increase; blue colour indicates a decrease. '=' shows that amino acid level resembles that of the wild type. 'n.d.' indicates that corresponding information was not available. Data were extracted from different publications: *shm1*: Leaf material was harvested after three weeks cultivation at high CO₂ followed by two weeks adaption to ambient CO₂ (Collakova *et al.*, 2008). *bou*: 5-d-old seedlings (Eisenhut *et al.*, 2013). *glu1*: Leaves were harvested 4 h after onset of light from plans which were grown hydroponically (5 mM nitrate) at elevated CO₂ for 42 days and subsequently adaption to ambient CO₂ for 2 d (Potel *et al.*, 2009). *pglp1*: Leaves were harvested 5 h after onset of light from 8-week-old plants permanently cultivated at high CO₂ and then shifted for 5 h to ambient CO₂ conditions (Flügel *et al.*, 2017).

3.2 Transcriptomic analyses

Transcriptomic analyses focus on the gene expression on the level of RNA (Dong and Chen, 2013). Transcriptomics provide genome-wide information and thus allow the identification of differentially expressed genes involved within a specific biological process (Dong and Chen, 2013). Therefore, the identification of conditions under which *ER-ANT1* expression changes, as well as the differences between the *er-ant1* transcriptome and that of other photorespiration mutants, may help to understand the role of ER-ANT1 in the physiological context.

3.2.1 Influence of perturbations on *ER-ANT1* expression

The Genevestigator perturbation tool was used to identify conditions that significantly affect the expression of *ER-ANT1* (Hruz *et al.*, 2008). A high number of perturbations led to significant

alterations of *ER-ANT1* transcript levels in wild-type and mutant plants. To give a concise overview, different versions (e.g. various incubation times, cultivation methods and plant tissues) of one basic experiment, experiments including the application of multiple stressors in parallel, as well as alterations in different mutant plants, were excluded. The remaining hits were again filtered (p-value < 0.05; fold change > 1.5) to focus on the most relevant changes (Table 3-2).

The perturbation experiments revealed that several types of abiotic stressors induced *ER-ANT1* expression. For example, expression of *ER-ANT1* in leaves was induced by heat stress (37°C, 1 h) and high light exposure (Table 3-2). These two factors are tightly connected to photorespiration (Peterhansel *et al.*, 2010) and often co-occur in nature (Wang *et al.*, 2017). The transcriptional regulation apparently involves the heat stress transcription factors HsfA1a/1b. This is because the heat-dependent induction failed in the corresponding double knock-out mutants (Busch *et al.*, 2005).

Moreover, hypoxia stimulated the expression of *ER-ANT1* (Table 3-2). Hypoxic conditions can occur naturally in seeds and meristematic tissues, but may also result from environmental stresses, such as soil waterlogging (Bailey-Serres and Voesenek, 2010; Loreti *et al.*, 2016). Because ATP production in mitochondria requires oxygen, its depletion ultimately leads to an energy crisis. Thus acclimation to hypoxia involves extensive reprogramming of gene expression (Branco-Price *et al.*, 2008), which triggers *inter alia* fermentation processes (Adrover *et al.*, 2008; Loreti *et al.*, 2016).

Interestingly, *ER-ANT1* transcripts also accumulated in roots of seedlings after arsenate treatment (Table 3-2). This toxic metalloid may enter the roots accidentally via unspecific aquaporins or phosphate transporters (Abbas *et al.*, 2018). In the cell, arsenate is reduced to arsenite, which can be sequestered in vacuoles (Gupta *et al.*, 2011). This conversion is linked to the generation of dangerous reactive oxygen species and leads to the activation of antioxidative enzymes (Abbas *et al.*, 2018). Further adverse effects of arsenate are *inter alia* inhibition of root growth and root cell proliferation, fertility loss, nutrient depletion, reduced ATP synthesis, photosynthetic inhibition and chlorophyll degradation (Abbas *et al.*, 2018). Since both, hypoxia and arsenate treatment, result in ATP depletion, one might envision that the cellular energy state regulates the expression of *ER-ANT1*. However, these two

perturbations, just as light and heat lead to elevated ROS levels, which might also influence *ER-ANT1* transcription (Kumar *et al.*, 2019; Caverzan *et al.*, 2012).

Table 3-2: Genevestigator perturbation analysis of *ER-ANT1*.

ID	Source	Experiment	Tissue	Genotype	Log ₂ FC
00179	Busch <i>et al.</i> , 2005	heat	leaves	WT	3.1
00293	Mueller <i>et al.</i> , 2008	phytoprostane	cell culture	WT	1.9
00222	Mandaokar <i>et al.</i> , 2006	methyl jasmonate	stamen	<i>opr3</i>	1.7
00618	van Aken <i>et al.</i> , 2013	high light	leaves	WT	1.3
00538	Fu <i>et al.</i> , 2014	arsenate	roots	WT	1.2
00695	Albrecht <i>et al.</i> , 2010	<i>SCO3</i> disruption	seedling	<i>sco3</i> vs WT	1.2
00275	Branco-Price <i>et al.</i> , 2008	hypoxia	seedling	WT*	1.1
00217	Pesaresi <i>et al.</i> , 2009	<i>PSAD1</i> disruption	leaves	<i>psad1-1</i> vs WT	1.0
00222	Mandaokar <i>et al.</i> , 2006	OPDA	stamen	<i>opr3</i>	1.0
00490	Narsai <i>et al.</i> , 2011	germination	seeds	WT	-2.2
00466	Qin <i>et al.</i> , 2009	pollen tube growth	pollen	WT	-2.0
00681	Stotz <i>et al.</i> , 2011	<i>S. sclerotiorum</i>	leaves	WT	-1.6
00672	Zhang <i>et al.</i> , 2012	<i>L. huidobrensis</i>	leaves	WT	-1.6
00490	Narsai <i>et al.</i> , 2011	stratification	seeds	WT	-1.6
00626	Pandey <i>et al.</i> , 2013	drought	leaves	WT	-1.5
00670	Maeda <i>et al.</i> , 2014	cold	leaves	WT	-1.4
00199	Li <i>et al.</i> , 2006	3 % glucose	seedling	WT	-1.4
00696	Xiong <i>et al.</i> , 2013	TOR RNAi	seedling	<i>tor</i> RNAi vs WT	-1.1
00587	Singh <i>et al.</i> , 2012	LecRK-VI.2 Oex	leaves	OH1 vs WT	-1.1
00291	Qiu <i>et al.</i> , 2008	benzothiadiazole	whole plants	WT	-1.1
00063	Greville K., 2007 **	100 mM sucrose	seedling	WT	-1.0
00391	MacLean D., 2009 ***	methyl jasmonate	leaf	WT	-1.0

WT = wild type. * Wild type with 35S:His6FLAG-RPL18B ; ** (www.ncbi.nlm.nih.gov/geo/query/acc.cgi?acc=GSE6158);

*** www.ncbi.nlm.nih.gov/geo/query/acc.cgi?acc=GSE17464

It became apparent that *ER-ANT1* expression is associated with jasmonic acid (JA) metabolism. Phytoprostanes are structurally highly related to the JA synthesis intermediate OPDA (Mueller *et al.*, 2008). Both, phytoprostanes and OPDA, induce the expression of genes related to

detoxification, stress responses and secondary metabolism (Mueller *et al.*, 2008) as well as of *ER-ANT1* (Table 3-2). Interestingly, the volatile JA derivative methyl jasmonate (MeJA) lowers the *ER-ANT1* transcript level in wild-type plants but leads to a stimulated expression in stamen of mutant plants lacking OPDA reductase 3 (OPR3) (Table 3-2).

Also, *sco3* and *psad1-1* mutant plants showed higher *ER-ANT1* expression than the respective wild-type control (Table 3-2). The *sco3* mutant carries a missense mutation in a gene encoding the microtubule-associated peroxisomal protein SNOWY COTYLEDON 3 (SCO3) (Albrecht *et al.*, 2010) whereas the *psad1-1* mutant lacks the D-subunit of photosystem I, PsaD1 (Ihnatowicz *et al.*, 2004). These two mutants are impaired in chloroplast function and plant growth. While *psad1-1* mutants show increased photosensitivity, due to disturbed electron transfer from PSI to ferredoxin (Ihnatowicz *et al.*, 2004), *sco3* mutants exhibit photoinhibition at high CO₂ conditions (0.6%), pointing to a yet unknown role of SCO3 during photorespiration (Albrecht *et al.*, 2010).

ER-ANT1 is an ATP transport protein and therefore, it is interesting that *ER-ANT1* expression is downregulated during germination (compared to desiccated seeds) and pollen tube growth (compared to dry pollen samples). These two developmental stages are highly energy consuming. However, the origin of the ATP in the tissues is not fully understood. For ATP synthesis in germinating seeds, a pathway which oxidises malate and provides phosphoenolpyruvate as a potential substrate for ATP synthesis has been suggested (Perl, 1986). In this pathway, also alcohol dehydrogenases might be involved by the anaerobic recycling of NADH to NAD⁺ (Perl, 1986). The source of ATP during pollen tube formation is also complex and intensely discussed (Selinski and Scheibe, 2014). Although it has been shown that mitochondria are highly abundant and that mitochondrial respiration plays a role during pollen tube growth, this developmental process is rarely sensitive to inhibition of respiration (Selinski and Scheibe, 2014). Besides, it is known that also fermentation processes are involved in pollen tube growth, but it is suggested to be insufficient to fulfil the high demand for ATP (Selinski and Scheibe, 2014).

The expression of *ER-ANT1* is downregulated in seedlings by cold and drought and in seeds during stratification (Table 3-2). Both, cold and drought, are known to induce the accumulation of soluble sugars (Déjardin *et al.*, 1999). Because *ER-ANT1* expression is also

downregulated by sucrose and glucose addition, the cold- and drought-dependent repression might be caused by the corresponding sugar accumulation. In this context, it is important to mention that O₂ deficiency is associated with an almost complete sugar depletion and with increased *ER-ANT1* expression (Déjardin *et al.*, 1999).

Interestingly, treatment with the necrotrophic ascomycete *Sclerotinia sclerotiorum* and the herbivore *Liriomyza huidobrensis* led to downregulation of *ER-ANT1* expression (Stotz *et al.*, 2011; Zhang *et al.*, 2012). In *Arabidopsis*, the activation of corresponding pathogen defence mechanisms depends on JA, salicylic acid and ethylene signalling (Guo and Stotz, 2007; Zhang *et al.*, 2012). Benzothiadiazole (BTH) is a synthetic analogue of salicylic acid and mimics its function (Kouzai *et al.*, 2018). Just like the pathogens, also BTH caused downregulation of *ER-ANT1* (Table 3-2). Moreover, it was shown that *ER-ANT1* expression is reduced in plants overexpressing the L-type lectin receptor kinase-VI.2 (LecRK-VI.2) (Singh *et al.*, 2012). Interestingly, this kinase is a positive regulator of bacterial PAMP-triggered immunity and acts in MeJA-mediated stomata closure (Yekondi *et al.*, 2018).

Furthermore, *ER-ANT1* expression is lower in TOR (TARGET OF RAPAMYCIN) RNAi plants than in wild-type plants. In mammalian, the TOR kinase mediates the translational control of cell proliferation and insulin signalling and plays a role in cancer initiation and metastasis (Xiong *et al.*, 2013). The corresponding TOR kinase from plants acts as a central integrator of nutrient, energy, light and hormone signalling in the regulation of plant growth (Wu *et al.*, 2019).

3.2.2 Transcriptomic analysis of *er-ant1* mutants

It is already known that *er-ant1* exhibits alterations in various metabolites (Figure 3-1; Hoffmann *et al.*, 2013). Therefore, it was not surprising that also the transcriptome indicated that multiple pathways are affected in this mutant. Microarrays provide a high-throughput platform for the determination of gene expression on the whole genome level. For *Arabidopsis*, a comprehensive collection of reference expression data from different mutants, tissues and treatments is publicly available. This enables to identify possible similarities of own data to already described effects (Rensink and Buell, 2005). Therefore, the transcriptome of *er-ant1* mutants that were adapted to ambient CO₂ conditions was compared with that of corresponding wild-type plants. In total, 2501 transcripts were at least

2-fold increased and 2148 transcripts were at least 2-fold decreased in *er-ant1* plants compared to the wild type (Figure 3-3 A).

PANTHER gene ontology (GO) analyses were performed to figure out whether the differentially expressed genes are characteristic for specific pathways (Thomas *et al.*, 2003). The upregulated transcripts clustered in 50 key GO terms such as 'response to biotic stimuli', 'cellular response to hypoxia', 'abscisic acid', 'ethylene stress', 'salt stress', 'responses to hydrogen peroxide' and 'leaf senescence' (data not shown). The downregulated transcripts accumulated in 69 clusters, including 'purine ribonucleoside salvage', 'chlorophyll biosynthetic processes', 'protein import into the chloroplast', 'photosynthesis', 'water transport', 'jasmonic acid biosynthetic processes', 'phloem transport', 'response to red light' and many more (data not shown).

The connection between the lack of ER-ANT1 and its photorespiratory phenotype is entirely unknown. It is likely that the photorespiratory phenotype is due to secondary/pleiotropic effects induced by the missing ER-ANT1 protein. Therefore, it was interesting to test whether it is possible to dissect transcriptional changes caused by the photorespiratory defect from those not associated with photorespiration. For that, the *er-ant1* mutant transcriptome was compared with publicly accessible data from other photorespiration mutants. Eisenhut *et al.* analysed the whole-genome expression of wild-type and photorespiration mutant plants exposed to ambient air (Eisenhut *et al.*, 2017). Within the study, the investigators compared a mutant lacking the peroxisomal glycerate dehydrogenase (HPR), which shows a weak photorespiratory phenotype, and three strong photorespiration mutants, lacking either plastidial 2-phosphoglycolate phosphatase (PGLP), mitochondrial serine hydroxymethyltransferase (SHMT) or D-glycerate 3 kinase (GLYK). Microarray data of *er-ant1* were compared with the RNAseq data of the photorespiration mutants analysed by Eisenhut *et al.*, 2017 to identify genes differentially expressed in the *er-ant1* mutant exclusively (Figure 3-3 B, C).

44 % of the genes higher expressed in *er-ant1* plants compared to wild-type plants are also upregulated in all strong photorespiration mutants (Figure 3-3 B). Furthermore, 79 % of all upregulated genes are at least also induced in one photorespiration mutant (Figure 3-3 B). When comparing the *er-ant1* transcriptome to the transcriptome of every single mutant,

er-ant1 rather resembles the strong photorespiration mutants than the weak *hpr1* mutant. Among the strong photorespiration mutants, *er-ant1* is most similar to the *shm1* mutant, which shares 68 % of all upregulated genes in *er-ant1* (Figure 3-3 B).

The same analysis was performed with genes which expression was relatively downregulated in *er-ant1*. Here, 24 % are also downregulated in all strong photorespiration mutants, while 72 % are downregulated at least in one of the photorespiration mutants used for comparison (Figure 3-3 C). Just like observed for the upregulated genes, *er-ant1* showed more similarity to the expression profile of the strong photorespiration mutants with the highest similarity to *shm1*, while only 4 % of downregulated genes in *er-ant1* were also downregulated in the weak photorespiration mutant *hpr1* (Figure 3-3 B).

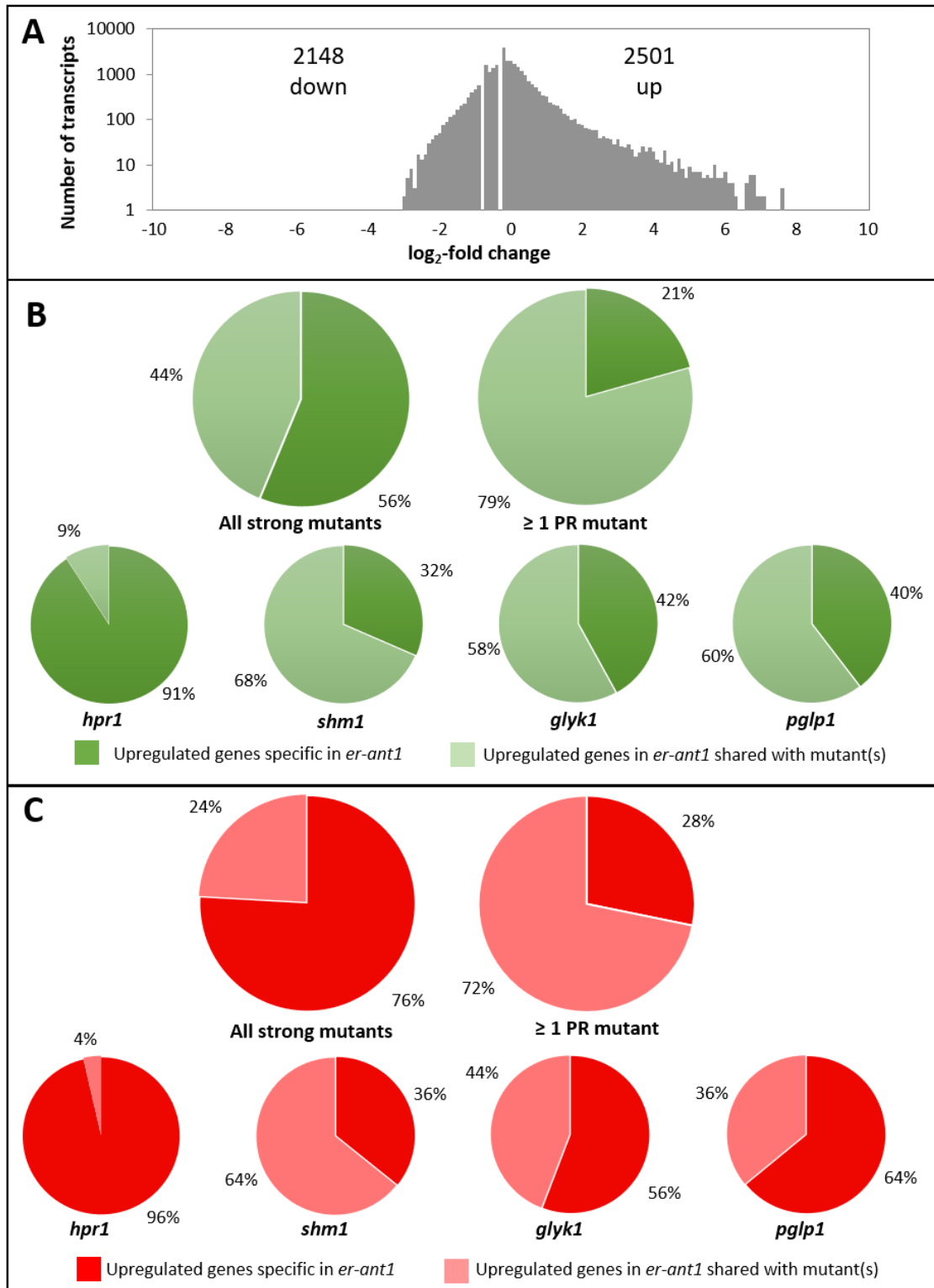


Figure 3-3: Transcriptome of *er-ant1* after the shift from high to ambient CO₂ and comparison with other photorespiration mutants. (A) Global transcriptional response of *er-ant1* towards shift from high to ambient CO₂ conditions. All changes are given as log₂-fold values compared to wild type. (B) Overlap of upregulated genes and (C) downregulated genes between *er-ant1* and photorespiration (PR) mutants. Presented are shares (in %) between *er-ant1* and all strong mutants (*shm1*, *glyk1*, *pglp1*), at least one PR mutant, single PR mutants and mutant-specific responses. *er-ant1* data: Microarray, 4d shift, this study. Other PR data: RNA-seq, 8h shift, (Eisenhut *et al.*, 2017).

Next, an in-depth gene ontology analysis was conducted with those genes differentially regulated in *er-ant1* but not in other strong photorespiration mutants (for details see 6.1 in the appendix). The obtained results were useful to assign transcriptional responses of *er-ant1* to the general defective photorespiration and to identify changes specific to *er-ant1*.

3.2.3 The interplay between CO₂ assimilation and nitrate metabolism in *er-ant1*

Both nitrate and CO₂ assimilation depend on the provision of reducing equivalents. It is well known that elevated CO₂ levels stimulate carbon fixation in the Calvin cycle and by this the consumption of plastidic NADPH, whereas low CO₂ decreases photosynthetic carbon fixation and the corresponding need for NADPH in the chloroplast stroma (Bloom, 2015). Consequently, photorespiratory conditions increase the availability of stromal NADPH. Excess reducing power can leave the plastid via the malate valve and fuel cytosolic nitrate reduction with NADH. The elevated NADPH availability in the stroma is not only beneficial for nitrate but also nitrite reduction. This is because a high stromal NADPH/NADP ratio slows down the consumption of reduced ferredoxin by the ferredoxin-NADP reductase (Bloom, 2015). The resulting higher level of reduced ferredoxin supports the transfer of reducing power to the ferredoxin-nitrite reductase (NIR1), which exhibits a lower affinity than the ferredoxin-NADP reductase (Bloom, 2015). Interestingly, low CO₂ levels do stimulate not only the reduction processes involved in nitrate assimilation but also the translocation of nitrite (NO₂⁻) from the cytosol into the stroma (Bloom, 2015). This is because the plastidic import of both, CO₂ and NO₂⁻, relies on the proton gradient across the chloroplast envelope. Consequently, a reduced passage of CO₂ leads to a higher proton gradient, which can drive NO₂⁻ import more efficiently (Bloom, 2015).

Arginine accumulates in illuminated *er-ant1* leaf tissues as well as in other photorespiration mutants (Table 3-1). This amino acid has the highest nitrogen/carbon ratio and plays a key role in nitrogen metabolism (Slocum, 2005). Since CO₂ fixation and nitrogen assimilation are competitive processes in plants (Blume *et al.*, 2019), the arginine accumulation of *er-ant1* might be indicative for a decreased carbon assimilation capacity compared to the wild type. Therefore, microarray data of *er-ant1* and wild-type plants were compared, and possible alterations in the expression of Calvin cycle genes were visualised with the software MapMan (Version 3.6.0RC1, Thimm *et al.*, 2004) (Figure 3-4). In *er-ant1*, the expression of Calvin cycle

genes was either not affected or downregulated when compared to the wild type (Figure 3-4). Several genes associated with the RuBisCO protein (RuBisCO small subunits RBCS-1B, RBCS-2B, RBCS-3B and the chaperonins for RuBisCO assembly CPN60A1, CPN60B1) showed much lower expression in *er-ant1* than in the wild type. Moreover, expression of the ATP-consuming phosphoglycerate kinase and of the NADPH-consuming glyceraldehyde-3-phosphate dehydrogenase was markedly reduced in *er-ant1*. These data imply that in *er-ant1*, the observed arginine accumulation may result from its decreased CO₂ assimilation capacity. In C₃ plants, exposure to low CO₂ is known to decelerate the Calvin cycle and to cause the corresponding arginine accumulation (Blume *et al.*, 2019). In *er-ant1*, however, these metabolic responses are already visible under ambient CO₂ conditions.

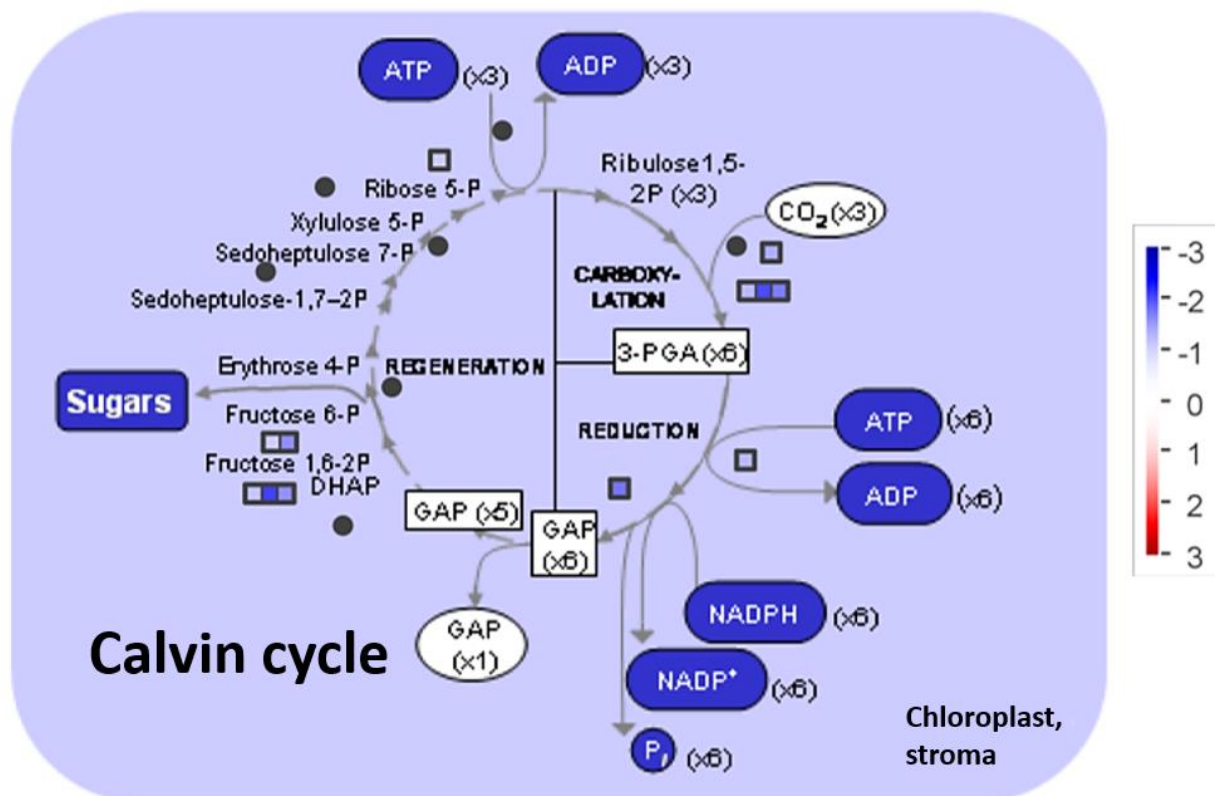


Figure 3-4: MapMan analysis of the Calvin cycle with *er-ant1* transcriptome data (\log_2 -fold change ≥ 1 ; ≤ -1). Blue boxes indicate lower gene expression in *er-ant1* compared to the wild type. The scale (right) describes the change in gene expression of *er-ant1* versus wild type (\log_2 -fold change).

Elevated cellular arginine levels are often associated with a downregulation of genes involved in its synthesis and upregulation of genes for its catabolism. When *er-ant1* is cultivated under ambient CO₂, its metabolism resembles that of wild-type plants exposed to low CO₂ at least in terms of CO₂ fixation and arginine accumulation (Hoffmann *et al.*, 2013). Therefore, it was

interesting to check whether the expression of genes involved in arginine metabolism in ambient-air-exposed *er-ant1* plants mimics the low-CO₂-induced status of wild-type plants.

In wild-type plants, transcript levels of genes associated with ornithine biosynthesis and ornithine to arginine conversion are substantially downregulated by low CO₂ (Figure 3-5). A corresponding downregulation was not visible in *er-ant1* exposed to ambient air. Therefore, elevated arginine levels do not affect the expression of arginine synthesis genes in *er-ant1*. However, low CO₂-induced alterations in the expression of genes involved in arginine degradation of the wild-type plants highly resemble the situation in *er-ant1* cultivated at ambient air.

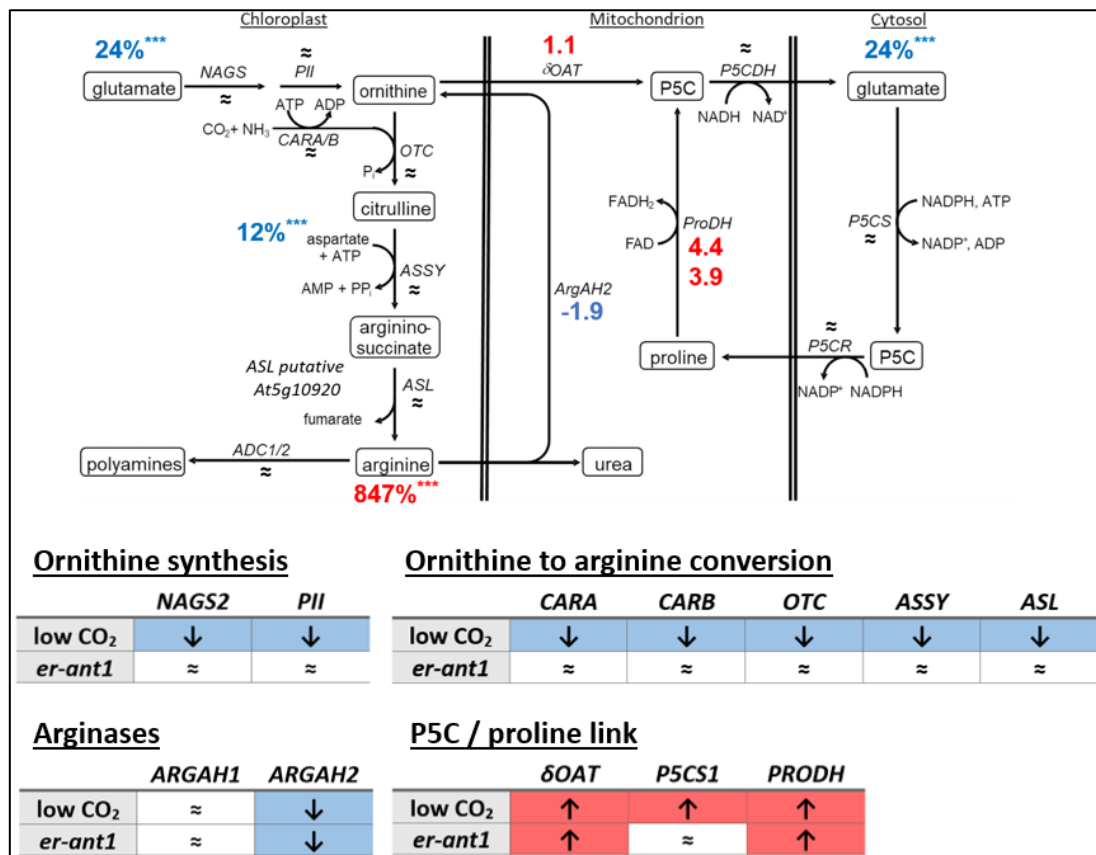


Figure 3-5: Comparison of gene regulation of wild-type plants cultivated at low CO₂ (Blume *et al.*, 2019) and *er-ant1* cultivated at ambient CO₂. Gene regulation and metabolites involved in ornithine synthesis and degradation. The picture was adapted from Blume *et al.*, 2019 (“Fig 1. Overview on ornithine synthesis and degradation.”). Blue colours and arrows downwards indicate a decrease, red colours and arrows upwards indicate an increase. Values without unit are expression log₂ fold changes in the microarray of *er-ant1* mutants grown at ambient air conditions for four days compared to corresponding wild-type plants. Percentage values refer to the percentage of metabolites in *er-ant1* grown at ambient CO₂ conditions for five days compared to corresponding wild-type plants. *ARGAH*, arginase; *ASL*, argininosuccinate lyase; *ASSY*, argininosuccinate synthetase; *CARA*, carbamoyl phosphate synthetase A; *CARB*, carbamoylphosphate synthetase B; *NAGS2*, N-acetyl-L-glutamate synthase 2; *δOAT*, ornithine- δ -aminotransferase; *OTC*, ornithine transcarbamylase; *Pii*, Pii protein; *P5CDH*, pyrroline-5-carboxylate dehydrogenase; *P5CR*, pyrroline-5-carboxylate reductase; *P5CS1*, pyrroline-5-carboxylate synthetase; *PRODH*, proline dehydrogenase.

Arginine degradation requires its transport into mitochondria (Winter *et al.*, 2015) where arginases catalyse the hydrolysis of arginine to urea and ornithine. Two arginases exist in *Arabidopsis*, and *ARGAH2* represents the major isoform expressed in leaves. Interestingly, expression of *ARGAH2* is downregulated in the wild type by low CO₂ as well as in the *er-ant1* mutant at ambient air. However, it remains unaffected in other strong photorespiration mutants (Brownfield *et al.*, 2008; Eisenhut *et al.*, 2017).

3.2.4 Jasmonate synthesis is affected in *er-ant1*

Analyses of the nitrate metabolism in *er-ant1* revealed downregulation of *ARGAH2* and thus of arginine degradation. Interestingly, *ARGAH2* expression is induced by jasmonate (Brownfield *et al.*, 2008). Jasmonic acid (JA) is an important signalling molecule in plant defence and metabolic regulation and has an essential function in plants male fertility (Caarls *et al.*, 2017; Thines *et al.*, 2013). The observed downregulation of *ARGAH2* (Figure 3-5) might thus be indicative for a reduced JA level in *er-ant1*. It is important to keep in mind that the other photorespiration mutants do not show a correspondingly reduced *ARGAH2* expression (Eisenhut *et al.*, 2017). Therefore, it was checked whether the expression of JA synthesis-related genes is downregulated in *er-ant1* and whether this does not apply to other photorespiration mutants (Figure 3-6).

JA biosynthesis begins in the plastid with the release of α -linolenic acid from galactolipids of chloroplast membranes by phospholipase 1 (PLA1) (Wasternack and Hause, 2013). The expression of *PLA1* was downregulated in *er-ant1* but not in other strong photorespiration mutants. The following oxygenation of α -linolenic acid is catalysed by 13-lipoxygenases (13-LOXs). In *er-ant1*, three out of four genes encoding the 13-LOXs were differentially regulated. While expression of *LOX4* is upregulated in *er-ant1* and other strong photorespiration mutants, *LOX2* and *LOX6* are exclusively downregulated in *er-ant1*. The latter two encode LOX proteins which are responsible for the wound-induced synthesis of JA in leaves (*LOX2*) and roots (*LOX6*) (Chauvin *et al.*, 2016; Grebner *et al.*, 2013). In contrast, *LOX4*, just as *LOX3*, is only expressed in vascular tissues and was shown to be important for JA controlled male fertility (Caldelari *et al.*, 2011).

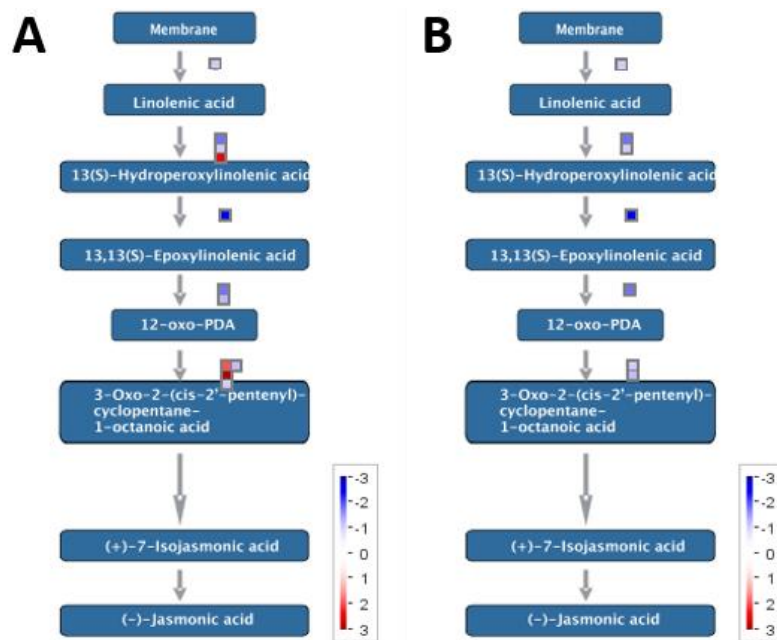


Figure 3-6: MapMan analysis of differentially expressed genes in *er-ant1* related to jasmonic acid synthesis. A: Differentially expressed genes in *er-ant1* grown at ambient CO₂ compared to corresponding wild-type plants. B: Differentially expressed genes in *er-ant1* but not in other strong photorespiration mutants (comparison with transcriptomic data of *shm1*, *pglp1* and *glyk1* Eisenhut *et al.*, 2017). (\log_2 -fold change ≥ 1 ; ≤ -1). Blue boxes indicate lower gene expression in *er-ant1* compared to the wild type; red boxes indicate higher expression in *er-ant1*. The scales (right) describes the change in gene expression of *er-ant1* versus wild type (\log_2 - fold change).

JA biosynthesis continues with the conversion of (13S)-hydroperoxy linoleic to an unstable allene epoxide catalysed by allene oxide synthase (AOS). AOS is encoded by a single gene in *Arabidopsis* (Laudert *et al.*, 1996). Defects in AOS function result in impaired JA biosynthesis and cause male sterility. The corresponding gene expression is downregulated exclusively in *er-ant1*.

Allene oxide cyclases (AOC) catalyse the next step of JA synthesis, which is the cyclisation of allene epoxide to 12-oxo-phytodienoic acid (OPDA). The expression of three of the four AOC isoforms (*AOC1*, 3 and 4) was downregulated in *er-ant1* but not in other photorespiration mutants. Expression of *AOC1* is even upregulated in the strong photorespiration mutants (Eisenhut *et al.*, 2017).

The generated OPDA is transported to peroxisomes, where it is reduced to 3-oxo-2-(cis-2'-pentenyl)-cyclopentane-1-octanoic acid by the OPDA reductase 3 (OPR3) (Nguyen *et al.*, 2017). The expression of *OPR3* was downregulated in *er-ant1*, whereas in other strong photorespiration mutants, *OPR3* expression has shown to be even increased (Eisenhut *et al.*, 2017). Mutant plants completely lacking OPR3 are male sterile (Stintzi and Browse, 2000). The

Arabidopsis genome encodes two further characterised OPRs (OPR1 & OPR2) and three yet uncharacterised putative OPRs (OPR4, OPR5 & OPR6) (Beynon *et al.*, 2009). Expression of *OPR1* and *OPR4* was upregulated in *er-ant1* as well as in the strong photorespiration mutants, whereas *OPR6* expression was downregulated in *er-ant1* exclusively. In this context, it is important to note that these OPRs are not associated with JA biosynthesis or apparently play a minor role in this process. For example, OPR1 is predicted to be located to the cytosol and may detoxify explosive 2,4,6-trinitrotoluene (TNT) as well as probably other xenobiotics in roots (Beynon *et al.*, 2009). In *er-ant1*, the expression of genes involved in the final steps of JA biosynthesis was unaltered when compared to the wild type.

This analysis demonstrates that in *er-ant1*, the expression of JA biosynthesis genes is downregulated at different positions but remains comparatively unaffected in the typical photorespiration mutants.

3.2.5 Analysis of serine-metabolism in *er-ant1* leaves

Serine is required for the biosynthesis of proteins and several other biomolecules involved in various pathways (Ros *et al.*, 2014). Plants can use three different pathways for serine production (Figure 3-7) (Ros *et al.*, 2014). The glycolate pathway takes place in mitochondria and uses glycolate from the photorespiratory pathway as a precursor for serine production. Therefore, this pathway occurs in photosynthetic tissues, where it is the dominating route for serine biosynthesis (Douce *et al.*, 2001). The resulting serine can be distributed via long-distance transport throughout the whole plant. The phosphorylated pathway of serine biosynthesis (PPSB) is located in plastids and is of importance in cell types not conveniently connected to the vasculature (e.g. embryo or pollen grains) or during dark periods, when photorespiration is inactive (Ros *et al.*, 2014). The same is true for the glycerate pathway in the cytosol, which is, in general, less explored.

Although serine metabolism is tightly connected with photorespiration, *er-ant1* differs in this context from other photorespiration mutants. Illuminated leaves of photorespiration mutants, such as *shm1* and *bou*, were shown to exhibit elevated serine contents (Eisenhut *et al.*, 2013; Collakova *et al.*, 2008), whereas those of *er-ant1* are at wild-type level (Figure 3-1 B;

Hoffmann *et al.*, 2013). However, *er-ant1* contained higher serine levels than the wild type in leaves during the night or in roots (Figure 3-1 B).

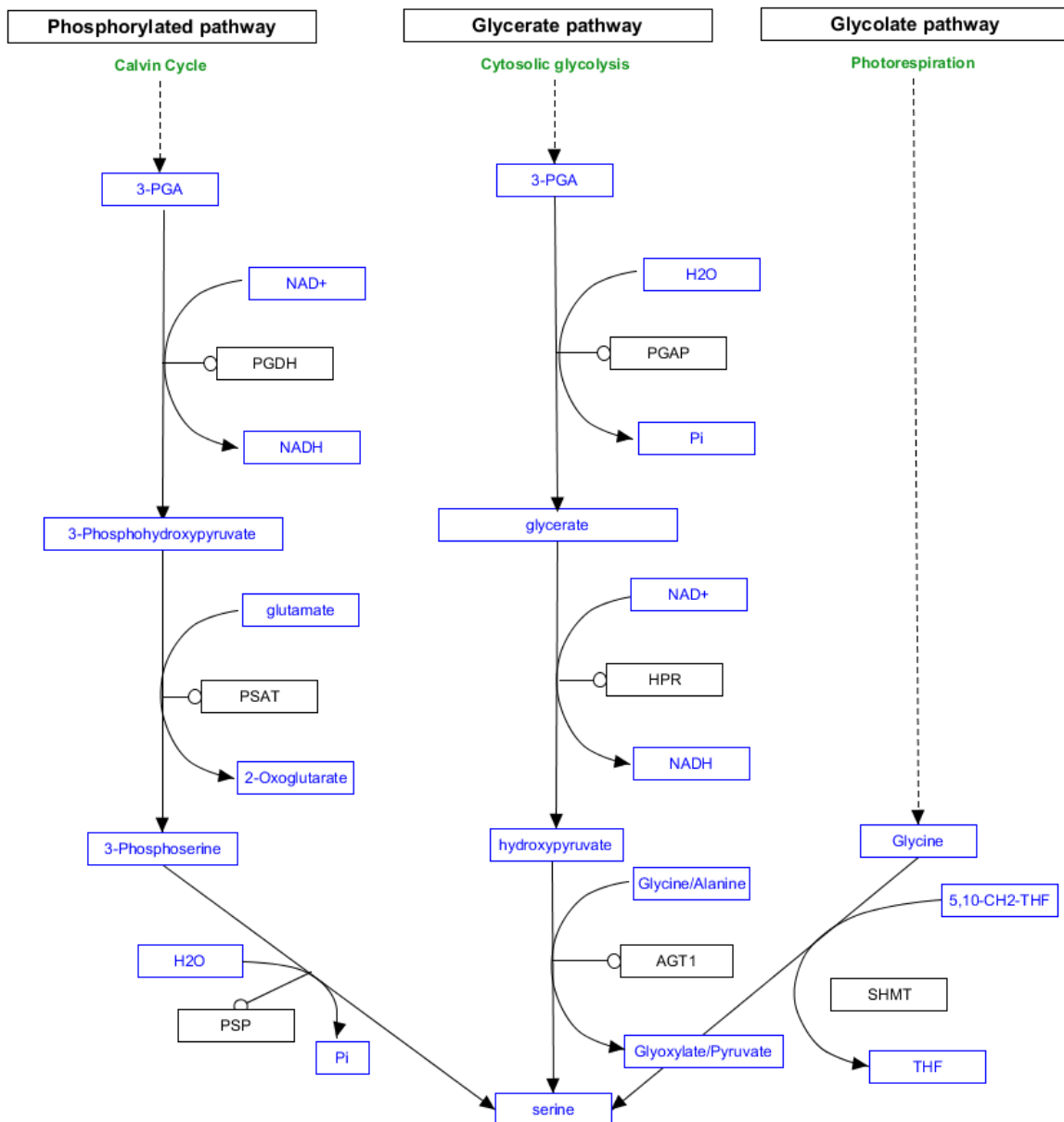


Figure 3-7: Serine biosynthesis in plants. PGDH: 3-phosphoglycerate dehydrogenase; PSAT: 3-phosphoserine aminotransferase; PSP: 3-phosphoserine phosphatase; PGAP: 3-phosphoglycerate phosphatase; HPR: Glycerate dehydrogenase (hydroxypyruvate reductase); AGT1: Serine-glyoxylate aminotransferase; SHMT: serine hydroxymethyltransferase. Picture adapted from Ros *et al.*, 2014.

Analyses of transcriptome data revealed increased expression of several important PPSB genes in the leaves of the strong photorespiratory mutants (Eisenhut *et al.*, 2017). In *er-ant1*, the expression of the major 3-phosphoglycerate dehydrogenase, *PGDH1* (Ros *et al.*, 2014), is similar to the wild type whereas *shm1*, *glyk1* and *pglp1* show increased transcription of the

corresponding gene (Table 3-3). Expression of *PGDH2* was higher in the strong photorespiration mutants as well as in *er-ant1*. However, in contrast to *PGDH1*, *PGDH2* appears to be of minor importance and whether it actually plays a role in serine biosynthesis is not clarified yet (Benstein *et al.*, 2013).

The *Arabidopsis* genome encodes two phosphoserine aminotransferases (PSATs). PSATs generally mediate the amino group transfer from glutamate to 3-phosphohydroxypyruvate (Ros *et al.*, 2014). The isoform PSAT1 was shown to be part of the PPSB in which it catalyses the second step of serine synthesis (Wulfert and Krueger, 2018). However, whether PSAT2 is of any importance in the PPSB is not known. The generally weaker expression of *PSAT2* compared to *PSAT1* as well as its inability to complement the loss of PSAT1 function, rather point to no or a comparatively minor relevance in serine biosynthesis (Wulfert and Krueger, 2018). Expression *PSAT1* was up- and that of *PSAT2* was downregulated in the strong photorespiration mutants but remained at wild-type level in *er-ant1* (Table 3-3). Expression of the final enzyme of the PPSB, the 3-phosphoserine phosphatase, was not altered in any of the tested mutants.

Table 3-3: Expression of genes involved in the PPSB in *er-ant1* and strong photorespiration (PR) mutants.

Name	ID	<i>er-ant1</i>	Strong PR mutants
PGDH1	AT4G34200	---	up
PGDH2	AT1G17745	up	up
PGDH3	AT3G19480	---	---
PSAT1	AT4G35630	---	up
PSAT2	AT2G17630	---	down
PSP	AT1G18640	---	---

3.2.6 Analysis of the S-adenosylmethionine metabolism in *er-ant1* leaves

The serine synthesised by the PPSB can directly act as a precursor for the tryptophan, cysteine and homocysteine production in the plastid (Okamura and Hirai, 2017). In the chloroplast, as

well as after transfer to the cytosol, homocysteine is converted into methionine. This reaction is catalysed by methionine synthetases (MS) and involves a folate-mediated one-carbon transfer. In tetrahydrofolate metabolism, the single carbon units are supposed to originate also from the serine provided by the PPSB (Wulfert and Krueger, 2018). The PPSB is stimulated in photorespiration mutants but not in *er-ant1*, and thus it was of interest to compare their transcriptome data regarding methionine biosynthesis.

The *Arabidopsis* genome encodes two cytosolic MS isoforms (MS1 and MS2) and one plastidic (MS3) (Ravanel *et al.*, 2004). The expression of *MS1* and *MS2* is downregulated in *er-ant1*, *glyk1* and *pglp1* but not in *shm1* (Table 3-4, Eisenhut *et al.*, 2017). *MS3* expression was neither affected in *er-ant1* nor in one of the strong photorespiration mutants (Table 3-4). Therefore, the cytosolic conversion of homocysteine to methionine might be reduced in *er-ant1* but also in *glyk1* and *pglp1*.

Table 3-4: Gene expression of methionine synthases in *er-ant1* and strong photorespiration mutants.

Name	localisation	ID	<i>er-ant1</i>	<i>shm1</i>	<i>glyk1</i>	<i>pglp1</i>
MS1	cytosol	AT5G17920	down	---	down	down
MS2	cytosol	AT3G03780	down	---	down	down
MS3	chloroplast	AT5G20980	---	---	---	---

Interestingly, only about 20 % of the plant methionine is incorporated into proteins, whereas 80 % are activated to S-adenosylmethionine (SAM). SAM represents one of the most abundant cofactors. Amongst its other functions, it is required for one-carbon group transfer to different acceptor molecules and is involved in various metabolic processes. SAM production takes place in the cytosol. Here, SAM synthetases (SAMs) catalyse the adenosyl-group transfer from ATP to methionine (Sauter *et al.*, 2013; Hesse *et al.*, 2004).

Arabidopsis possesses four SAMs (SAM1-SAM4). *SAM1*, *SAM2* and *SAM4* are expressed in most tissues (Chen *et al.*, 2016). Analyses of corresponding mutant plants demonstrate the importance of the cofactor in plant metabolism: For example, double mutants lacking *SAM2* and *SAM4* are nonviable and double mutants lacking *SAM1* and *SAM4* or *SAM1* and *SAM2*

exhibit a dwarf phenotype (Mao *et al.*, 2015; Meng *et al.*, 2018). Moreover, the absence of functional SAM4 results in highly reduced SAM levels and lower DNA and histone methylation. Therefore, it has been suggested that SAM is also involved in the modulation of the epigenetic status (Meng *et al.*, 2018). The chloroplast located isoform SAM3 is expressed predominantly in pollen (Chen *et al.*, 2016) and plays a specific role during pollen germination and tube growth.

Interestingly, when compared to the wild type, the expression of three out of four SAMs was downregulated in *er-ant1* but remained unaltered in other photorespiratory mutants (Table 3-5; Eisenhut *et al.*, 2017). In *er-ant1*, only the expression of SAM1 is at wild-type level, however, it is upregulated in *pglp1*.

Table 3-5: Gene expression of S-adenosylmethionine synthases in *er-ant1* and strong photorespiration mutants.

Name	ID	<i>er-ant1</i>	<i>shm1</i>	<i>glyk1</i>	<i>pglp1</i>
SAM1	At1G02500	---	----	----	up
SAM2	At4G01850	down	----	----	----
SAM3	At2G36880	down	----	----	----
SAM4	At3G17390	down	----	----	----

SAM represents one of the most abundant cofactors. Therefore, it is not surprising that its synthesis consumes high amounts of methionine and adenine nucleotides. The previous analyses revealed that the phosphatase pathway of serine biosynthesis is upregulated in the strong photorespiration mutants but not in *er-ant1*. This might decrease the availability of PPSB derived serine and thus also of methionine in *er-ant1*. It is imaginable that the limited substrate availability causes downregulation of SAM synthesis, particularly in *er-ant1*. On the other hand, one may envision that perturbations in SAM metabolism or related processes might affect the biosynthesis and thus provision of the corresponding substrates.

3.2.7 The *er-ant1* plants show alterations in the cellular redox state

It is known that *er-ant1* mutants contain higher levels of reactive oxygen species (ROS) than the wild type (Hoffmann *et al.*, 2013). Moreover, in *er-ant1*, the total amount of reduced (GSH) and oxidised (GSSG) glutathione, as well as the GSH/GSSG ratio, is increased (Hoffmann *et al.*, 2013). These facts point towards a generally elevated cellular redox state in *er-ant1*. Interestingly, the transcriptomic analysis revealed that expression of three out of five genes coding for alternative oxidases (AOXs) is upregulated in *er-ant1* (Table 3-6). Correspondingly higher activity of AOXs implies that the use of reducing equivalents is shifted from oxidative phosphorylation to energy dissipation without ATP production. This mechanism allows preventing over-energisation of the respiratory chain and ROS formation in mitochondria (Vishwakarma *et al.*, 2014).

With regard to the defective photorespiration in *er-ant1*, particularly the upregulation of *AOX1A* expression is interesting. This is because the corresponding protein is of importance for balancing the NAD(P)H/ATP ratio and optimising photosynthesis in response to changing CO₂ and light conditions (Vishwakarma *et al.*, 2014; Dahal and Vanlerberghe, 2018). The upregulation of AOXs is in line with a generally increased redox state of *er-ant1* (Hoffmann *et al.*, 2013).

Table 3-6: Expression of genes encoding alternative oxidases in *er-ant1*.

Name	ID	Description	log ₂ FC
AOX1A	AT3G22370	alternative oxidase 1A	5.4
AOX1B	AT3G22360	alternative oxidase 1B	1.4
AOX1C	AT3G27620	Alternative oxidase 1C	0
AOX1D	AT1G32350	alternative oxidase 1D	8.4
AOX2	AT5G64210	Alternative oxidase 2	0.7

Another possibility to counteract over-energisation in mitochondria is the action of rotenone-insensitive type II NAD(P)H dehydrogenases. These non-pumping enzymes can bypass complex I by transferring electrons from NAD(P)H to ubiquinol (Michalecka *et al.*, 2003). The

type II NAD(P)H dehydrogenases NAD1 and NAD2 reside at the matrix-facing surface of the mitochondrial inner membrane, whereas NDB1-NDB4 are present at the cytosolic side.

Having seen that three *AOX* transcripts were upregulated in *er-ant1*, it was of interest to check whether also the expression of type II NAD(P)H dehydrogenase genes is differentially regulated in this mutant. The expression of all corresponding genes, except for *NDB1*, was upregulated in *er-ant1* (Table 3-7). Therefore, at least two processes for removal of reduction power (*AOX* and NAD(P)H dehydrogenases) without concomitant ATP production are apparently stimulated in *er-ant1*.

Table 3-7: Altered type II NAD(P)H dehydrogenase gene transcripts in *er-ant1* plants.

ID	Name	Description	log₂ FC
NDA1	AT1G07180	NAD(P)H dehydrogenase A1	2.0
NDA2	AT2G29990	NAD(P)H dehydrogenase A2	1.6
NDB1	AT4G28220	NAD(P)H dehydrogenase B1	0.1
NDB2	AT4G05020	NAD(P)H dehydrogenase B2	3.5
NDB3	AT4G21490	NAD(P)H dehydrogenase B3	2.9
NDB4	AT2G20800	NAD(P)H dehydrogenase B4	5.3

The mitochondrial malate dehydrogenase (mMHD) is involved in the maintenance of low NADH concentrations in the matrix (Bykova *et al.*, 2014). Particularly during photorespiration, mMHD activity is of importance, since the GDC is feedback-inhibited by NADH. The catalytic activity of mMHD consumes NADH and releases NAD⁺ and by this guarantees high fluxes through the GDC (Bykova *et al.*, 2014). Interestingly, when compared to wild-type plants, in *er-ant1* expression of both *mMDH* is downregulated (Table 3-8). While the transcript level of *mMDH1* is reduced in *er-ant1* exclusively, that of *mMDH2* is also lower in *shm1* and *pglp1* (Eisenhut *et al.*, 2017). At first glance, this regulation might imply that particularly in *er-ant1*, the NADH/NAD ratio in the mitochondrial matrix is rather too low than too high. However, it is also imaginable that misregulation of the mMHD in the mitochondrial matrix results in an

elevated mitochondrial NADH level which inhibits GDC activity and causes the photorespiratory phenotype.

Table 3-8: Gene expression of mitochondrial malate dehydrogenases in *er-ant1*.

Name	ID	<i>er-ant1</i>	<i>shm1</i>	<i>glyk1</i>	<i>pglp1</i>
mMDH1	AT1G53240	down	---	---	---
mMDH2	AT3G15020	down	down	---	down

3.2.8 Expression signature of genes encoding mitochondrial proteins in *er-ant1*

It has been proposed that AOXs fulfil an overall role in the reprogramming of the cellular metabolism in response to changing environments from which plants cannot escape (Clifton *et al.*, 2006). Clifton *et al.* investigated AOX responses to different treatments. Furthermore, they clustered expression profiles of 670 genes encoding mitochondrial proteins in response to 219 treatments. Based on this, the corresponding list of candidate genes was used for Genevestigator signature studies to identify a possible re-programming also in *er-ant1*.

In the *er-ant1* transcriptome, 142 of the 670 genes encoding mitochondrial proteins (Clifton *et al.*, 2006) were differentially regulated. This list of genes was used together with the corresponding log₂ FC values to run the Genevestigator signature tool (Zimmermann *et al.*, 2004; Hruz *et al.*, 2008), which allows for identifying mutations and conditions that induce similar gene expression patterns.

More than 50 mutations and conditions highly related to those occurring in *er-ant1* could be identified (Figure 3-8). The perturbation hits revealed a comparatively high number of herbicides inhibiting the acetolactate synthase (ALS) (Table 3-9).

Dataset: 3282 perturbations from data selection: AT_AFFY ATH1-0
 Showing 142 measure(s) of 142 gene(s) on selection: AT-0

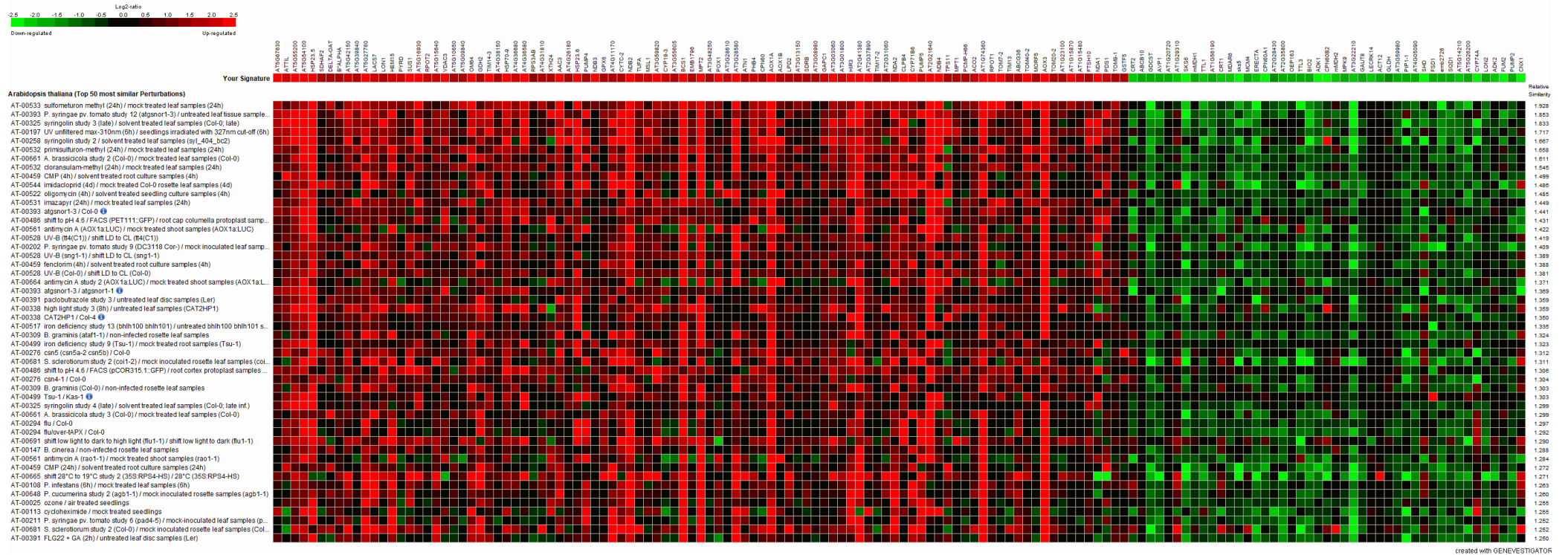


Figure 3-8: Expression signature of genes encoding mitochondrial proteins in *er-ant1*. Shown are the expression signature of 142 genes which encode mitochondrial proteins and are differentially regulated in *er-ant1* (first line) and identified conditions which cause most similar expression signatures. Green colour indicates downregulation; red colour indicates upregulation. Genes were considered as differentially regulated when log₂ fold change was lower than -1 or higher than 1.

Table 3-9: Identified herbicide experiments provoking expression signatures similar to *er-ant1*.

Experiment ID	Source	Perturbation	Mode of action
AT-00533	Das <i>et al.</i> , 2010	Sulfometuron methyl	ALS (Brown, 1990)
AT-00532	Das <i>et al.</i> , 2010	Primisulfuron methyl	ALS (Brown, 1990)
AT-00532	Das <i>et al.</i> , 2010	Cloransulam methyl	ALS (Pline <i>et al.</i> , 2002)
AT-00531	Das <i>et al.</i> , 2010	Imazapyr	ALS (Muhitch <i>et al.</i> , 1987)

ALS catalyses two reactions in the branched-chain amino acid biosynthesis (BCAA) pathway: In one reaction, it converts two pyruvate molecules to 2-acetolactate, which is subsequently used for leucine and valine production. Moreover, ALS synthesises 2-acetohydroxybutyrate for isoleucine production from pyruvate and 2-ketobutyrate (Zhou *et al.*, 2007).

ALS-inhibitors and glyphosate (GLP) are two classes of herbicides which specifically inhibit one enzyme in either branched chain (ALS-inhibitors) or aromatic (GLP) amino acid synthesis (Zulet *et al.*, 2015). Interestingly, it has been shown that both herbicides reduce ATP production by induction of fermentation and alternative respiration (Zulet *et al.*, 2015).

3.2.9 Fermentation in *er-ant1*

The alternative respiratory pathway and ALS-related responses are apparently induced in *er-ant1* (Table 3-6, Table 3-7, Table 3-9). Therefore, it was interesting to check whether also the expression of fermentation-related genes is upregulated in *er-ant1*. During fermentation, pyruvate can be converted via the pyruvate decarboxylases (PDC1 and PDC2) and alcohol dehydrogenase (ADH) into ethanol or alternatively via the lactate dehydrogenase into lactate (Figure 3-9; Tadege, 1999; Mithran *et al.*, 2014).

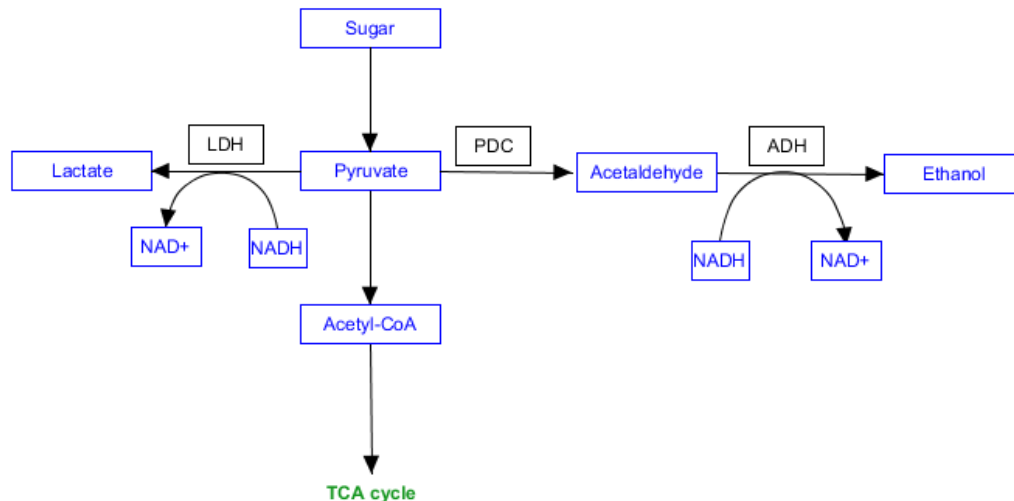


Figure 3-9: Metabolic routes of lactic acid and ethanolic fermentation in plants.

Interestingly, the expression of several fermentation-associated genes was upregulated in *er-ant1* as well as in the strong photorespiration mutant *shm1* (Table 3-10). Most of these transcripts are also elevated in *glyk1* and *pglp1* with the exception of *PDC2*, which was not increased in *pglp1*, and *ADH1*, which was neither increased in *glyk1* nor in *pglp1*. Moreover, also the expression of *HB1*, a marker gene for hypoxic stress (Giuntoli *et al.*, 2017), was upregulated only in *er-ant1* and *shm1*. Therefore, fermentation processes appear to be induced in *er-ant1* and *shm1* as well as to a lesser extent in the remaining two mutants.

Table 3-10: Expression of genes associated with fermentation in *er-ant1* and strong photorespiration mutants.

Name	ID	<i>er-ant1</i>	<i>shm1</i>	<i>glyk1</i>	<i>pglp1</i>
PDC1	AT4G33070	up	up	up	up
PDC2	AT5G54960	up	up	up	---
ADH1	AT1G77120	up	up	---	---
LDH1	AT4G17260	up	up	up	up
ALAAT2	AT1G72330	up	up	up	up
HB1	AT2G16060	up	up	---	---

3.2.10 Hypoxia-associated reprogramming in *er-ant1*

Oxygen deficiency in plants occurs naturally, for example, in seeds and meristematic tissues, and due to environmental stress as soil waterlogging (Bailey-Serres and Voeselek, 2010; Loreti *et al.*, 2016). Since oxygen is required for mitochondrial ATP production, hypoxia ultimately leads to a decrease in the cellular energy state (Loreti *et al.*, 2018). As a consequence, an extensive reprogramming of gene expression is triggered in which fermentative metabolism, and by this also ATP production during glycolysis, is stimulated (Loreti *et al.*, 2016). Although this mechanism only marginally compensates for the missing oxidative phosphorylation in mitochondria, it apparently guarantees survival under hypoxic conditions (Loreti *et al.*, 2018).

It has been shown that when *Arabidopsis* plants experience hypoxia, the expression of a set of 49 core genes is induced for a limited period of time (Mustroph *et al.*, 2009). It became evident that the expression of genes involved in fermentation, including the hypoxic stress marker *HB1*, is upregulated in *er-ant1* (Table 3-10). Therefore, it was of interest to analyse a putative oxygen deficiency in *er-ant1* in more detail. In fact, 19 out of the 49 hypoxia marker genes were also among the upregulated transcripts in *er-ant1* (Table 3-11). Here, it is necessary to mention that the experimental conditions used by Mustroph *et al.* are not directly comparable with the study of this thesis. They used younger plants grown on agar plates at $80 \mu\text{mol photons m}^{-2} \text{s}^{-1}$ and harvested them in the dark, after application of hypoxia by argon gassing for 2 h.

Three of the 49 hypoxia-induced core genes are downregulated in *er-ant1* (Table 3-11). Moreover, expression of two of these genes was downregulated in *er-ant1* but not in the other strong photorespiration mutants *shm1*, *glyk1* and *pglp1*. One of these two genes (AT3G17860) encodes the protein JAZ3 (Jasmonate-zim-domain protein 3). Jasmonate-zim-domain proteins are transcriptional repressor proteins, which interact with various transcription factors. JAZ3 is an inhibitor of the transcription factor MYC2, which positively regulates wounding response and negatively regulates pathogen response (Du *et al.*, 2017).

Table 3-11: Hypoxia core genes differentially expressed in *er-ant1* compared to respective expression in strong photorespiration mutants.

Name	ID	<i>er-ant1</i>	<i>shm1</i>	<i>glyk1</i>	<i>pglp1</i>
PI4KG5	AT1G26270	up	---	up	up
F3N23.14	AT1G72940	up	up	up	up
CML38	AT1G76650	up	up	up	up
ADH1	AT1G77120	up	up	---	---
AHB1	AT2G16060	up	up	---	---
ERF071	AT2G47520	up	up	up	up
LBD41	AT3G02550	up	---	---	---
AT3G23170	AT3G23170	up	up	up	up
FLZ2	AT4G17670	up	---	up	---
ACR7	AT4G22780	up	up	up	up
T19F6.9	AT4G24110	up	up	up	up
F27G19.50	AT4G27450	up	---	---	up
PDC1	AT4G33070	up	up	up	up
CYP707A3	AT5G45340	up	up	up	up
FLZ1	AT5G47060	up	---	---	---
RBOHD	AT5G47910	up	up	up	up
PDC2	AT5G54960	up	up	up	---
TIL	AT5G58070	up	up	up	up
SRO5	AT5G62520	up	up	up	up
JAZ3	AT3G17860	down	---	---	---
PFK6	AT4G32840	down	down	down	---
F9D12.12	AT5G26200	down	---	---	---

3.3 Effect of vitamin B₆ on *er-ant1*

The *er-ant1* mutant shows numerous alterations in amino acid levels and gene expression compared to the wild type and to other photorespiration mutants (Figure 3-1; Chapter 3.2; Hoffmann *et al.*, 2013; Eisenhut *et al.*, 2017). Interestingly, *er-ant1* specific changes affect quite different pathways. A cofactor needed for various reactions of different pathways is pyridoxal 5'-phosphate (PLP).

Vitamin B₆ is the generic term for the substances pyridoxine (PN), pyridoxal (PL) and pyridoxamine (PM), which are all subject to phosphorylation (Mooney and Hellmann, 2010). The phosphorylated form of PL, PLP, is the major active form within organisms and acts as a cofactor in more than 140 enzymatic reactions involved in a variety of processes (Colinas *et al.*, 2016). In *Arabidopsis*, 64 proteins contain a domain characteristic for PLP dependent enzymes (Retrieved from <https://www.ebi.ac.uk/interpro/entry/IPR001926>, 2019, March 29). In plants, PLP is, for example, important during amino acid metabolism and chlorophyll biosynthesis (Parra *et al.*, 2018).

In photorespiration, PLP plays crucial roles, too. For example, it is a component of the GDC P protein. Moreover, the within photorespiration to GDC connected SHMT is a PLP-dependent enzyme (Heldt and Piechulla, 2012; Kandoth *et al.*, 2017). Using a mathematical model of mitochondrial GDC and SHMT, Nijhout *et al.* have shown that PLP deficiency correlates with linearly increasing glycine levels while serine levels are only minor affected (Nijhout *et al.*, 2009). Furthermore, *Arabidopsis* mutant plants with decreased Vitamin B₆ levels accumulate, just as *er-ant1*, glycine and arginine (Leuendorf *et al.*, 2010).

Moreover, *er-ant1* mutant plants show elevated levels of reactive oxygen species (ROS) (Hoffmann *et al.*, 2013). Connected to that, vitamin B₆ was shown to suppress oxidative stress by directly scavenging of ROS, chelating metal ions and increasing synthesis of reduced glutathione (Bilski *et al.*, 2000; Chetyrkin *et al.*, 2008; Adrover *et al.*, 2008; Cheng *et al.*, 2016).

These observations led to the assumption that PLP availability might be insufficient in *er-ant1*. Therefore, it was tested whether exogenous supplementation of vitamin B₆ can restore the *er-ant1* phenotype. For this, PN instead of PLP was used because only the non-phosphorylated vitamers can enter the cell and uptake of exogenous PN has already been shown to complement defective PLP synthesis in the *Arabidopsis* mutant *pdx1.3* (Titiz *et al.*, 2006). After

uptake, PN can be phosphorylated to PNP by the pyridoxal kinase SOS4 and subsequently converted into PLP by the action of the oxidase PDX3 within the PLP salvage pathway (Rueschhoff *et al.*, 2013; Colinas *et al.*, 2016).

Feeding of increasing PN concentrations stimulated the growth of *er-ant1* mutant plants (Figure 3-10 A). The determination of the fresh weight supported this observation: The fresh weight of *er-ant1* mutants was higher the more PN was added (Figure 3-10 B). By contrast, wild-type plants were not or even negatively affected by supplementation of PN. The highest PN concentration led to a decrease in fresh weight of the wild type (Figure 3-10 B).

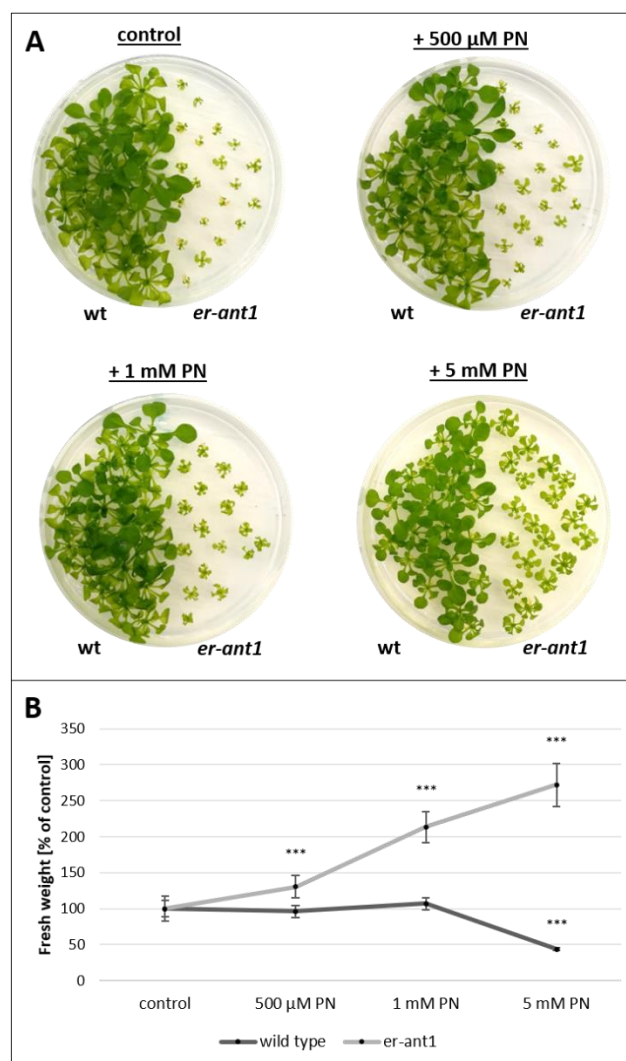


Figure 3-10: Effect of pyridoxine feeding on growth of *er-ant1* and wild-type plants. Plants were cultivated on agar plates ($\frac{1}{2}$ MS including GA5 vitamins, 0.8 % agar) at ambient CO₂ conditions (10 h light/14 h dark) for 25 days. (A) wild type and *er-ant1* on agar plates without additional pyridoxine (PN) (control) and with different concentrations of additional PN. (B) Fresh weight of *er-ant1* and the corresponding wild-type plants grown on agar plates containing different concentrations of PN in the percentage of control fresh weight. Shown are mean values of \geq five individual plates, \pm SE. Asterisks indicate the significance level between wild-type and mutant plants according to Student's t-test (*P < 0.05, **P < 0.01, ***P < 0.001).

3.4 Identification of *er-ant1* suppressor mutants

The aim of this study was to identify proteins acting in pathways not yet known to be associated with the function of ER-ANT1. To achieve this goal, an EMS-based suppressor screen was conducted.

For this, *er-ant1* seeds (M_0) were mutagenised with ethyl methanesulfonate (EMS) which results in an M_1 generation composed of plants with random point mutations (Figure 3-11 D). *A. thaliana*, as a diploid plant, underlies the principles of heredity/dominance. Because dominant mutant phenotypes are much less common than recessive phenotypes in *Arabidopsis* (Meinke, 2013), the M_1 generation was not analysed for possible suppressor mutants. Instead, pools of each 500 M_1 plants were cultivated at high CO_2 (2000 ppm) conditions to ensure proper plant growth and seed development. The most apparent phenotype of *er-ant1* plants is their reduced growth when cultivated under ambient air conditions. Plants of the M_2 Generation were grown under ambient CO_2 conditions and plants with increased size compared to the original *er-ant1* mutant were considered as suppressor mutants (Figure 3-11 A, B).

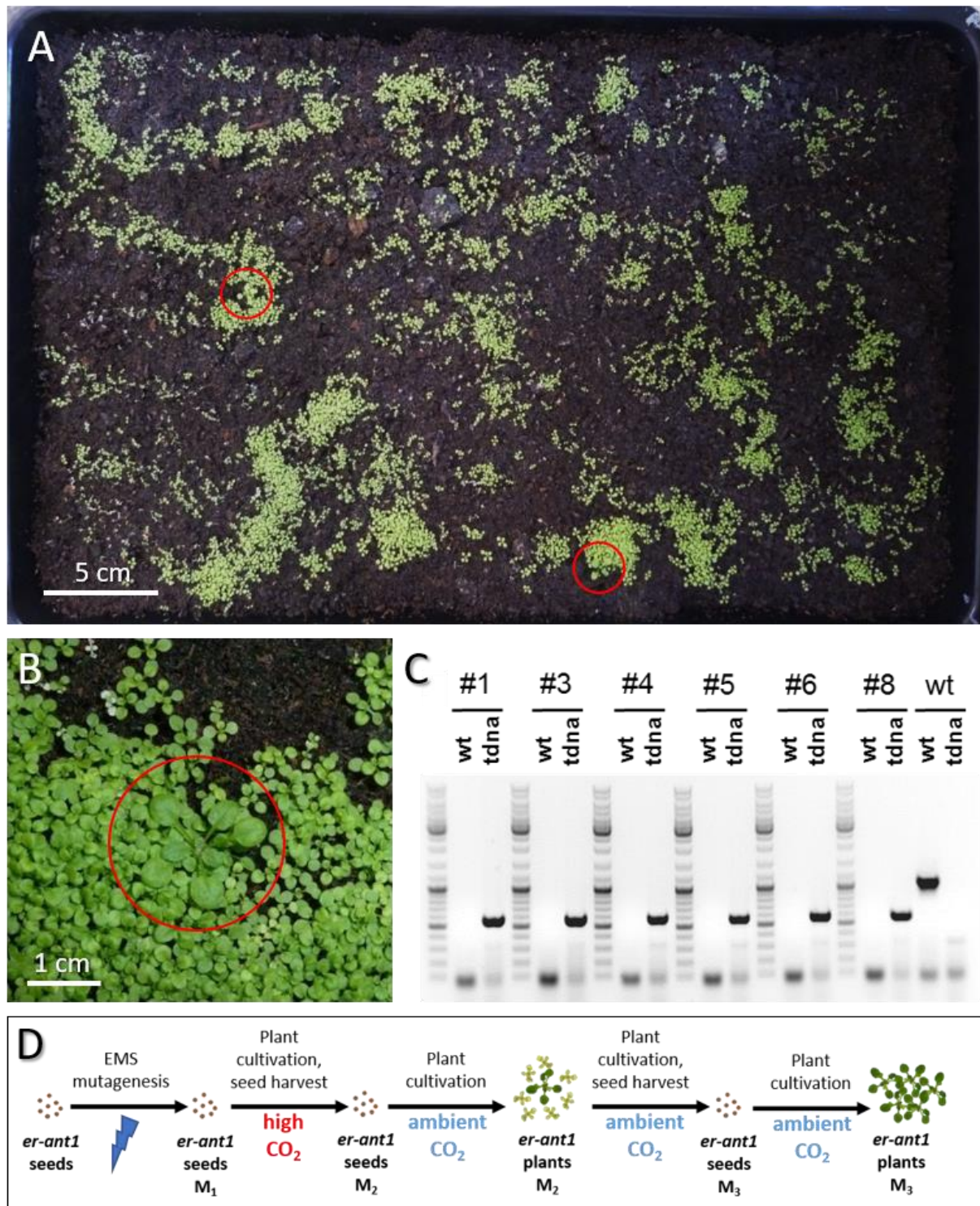


Figure 3-11: EMS suppressor screen. (A, B) EMS re-mutagenised plants of the M₂ generation grown under ambient air conditions. Red circles indicate *er-ant1* EMS suppressor mutant plants. (C) Verification of the T-DNA insertion in individual suppressor plants with T-DNA mutant-specific primer combination (~550bp). Primer combination specific for wild-type sequence resulted only in the wild-type control in a PCR-product of ~1000bp. (D) Overview EMS mutagenesis and isolation of putative suppressor mutant M₃ lines. A, B and C provided by Sebastian Hassler (TUK).

Suppressor mutants were isolated, and the *er-ant1* specific T-DNA insertion was verified by PCR (Figure 3-11 C) to ensure that the selected plants maintained their homozygosity for the recessive *er-ant1* mutant allele. The following experiments were conducted with the individuals of the M₃ generation, all showing the suppressor phenotype.

3.5 Characterisation of *er-ant1* suppressor mutants

First of all, the different suppressor mutant lines were characterised morphologically. This included the determination of the chlorophyll content, which is low in *er-ant1* (Hoffmann *et al.*, 2013). Next, it was tested whether the suppressor mutants still accumulate glycine. Moreover, photosystem II performance, the assembly of the photosynthetic complexes and the chloroplast ultrastructure was analysed.

The dwarf phenotype and glycine accumulation of *er-ant1* mutants do not occur when the mutant plants are cultivated at high CO₂ conditions (2000 ppm). For this reason, all experiments were performed with plants adapted several days to ambient CO₂ conditions as well as with plants grown permanently at high CO₂ conditions as a control. If not declared otherwise, remaining conditions as light intensity, light quality, duration of light, temperature and humidity remained the same. The experiments were conducted five days after the splitting up.

3.5.1 Morphology of M₃ *er-ant1* suppressor plants

Plants of the M₃ generation were generally bigger and had more leaves compared to *er-ant1* plants but were still smaller than the wild type (Figure 3-12). Furthermore, they differed among each other in their appearance. While, for example, plants of line 1.3 showed only slighter growth enhancement compared to *er-ant1*, line 16.2 almost reached the size of the wild type. Moreover, the leaves of line 16.2 were more toothed in comparison to the leaves of the wild type and *er-ant1*. The leaves varied in their colour: Leaves of line 4.2 were generally paler, line 5.4 showed yellow cotyledons whereas younger leaves of line 6.3 showed an increased green colouring compared to wild-type plants. All in all, the appearance of the suppressor mutants suggests that different genetic variations may be responsible for their respective phenotypes.

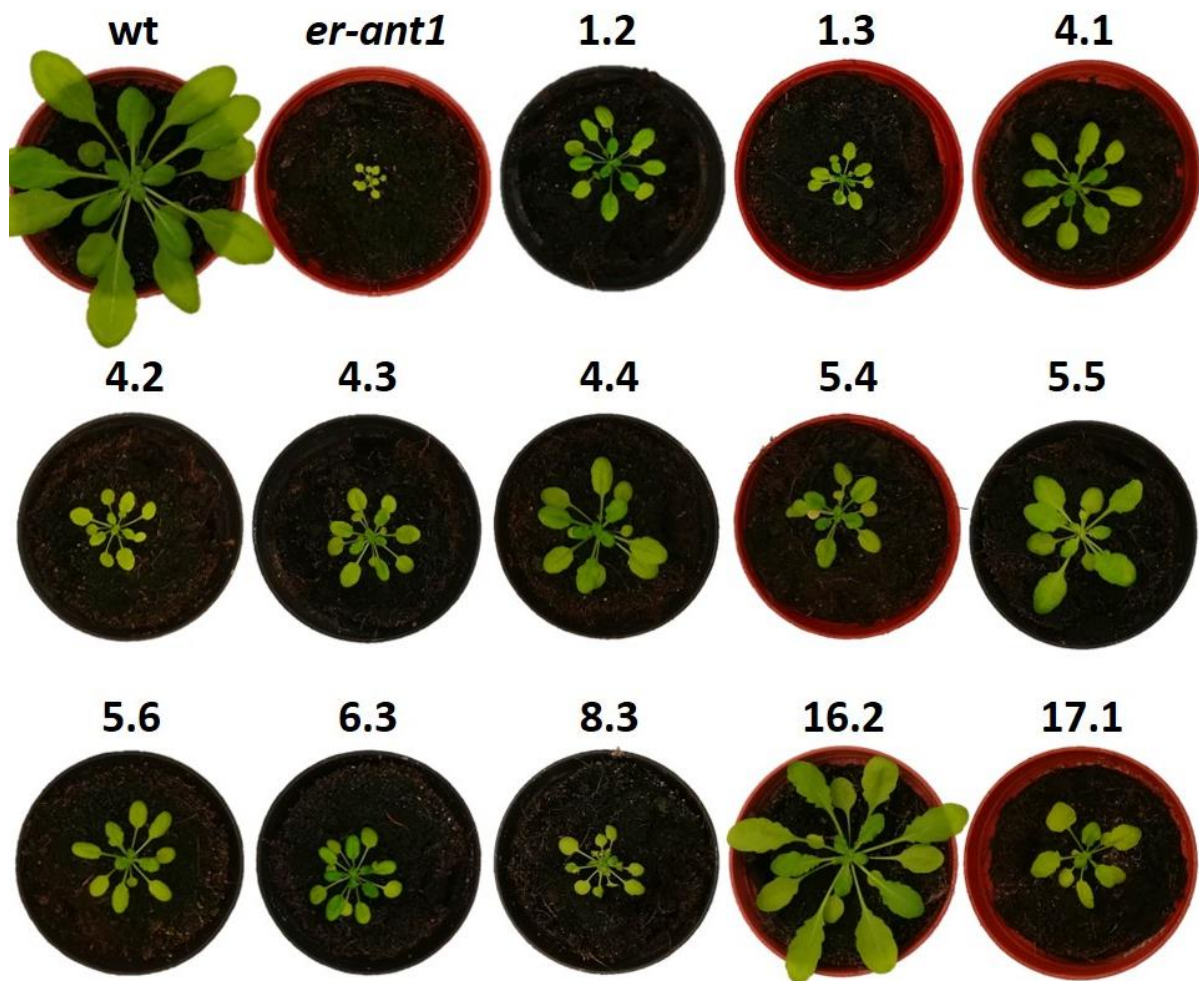


Figure 3-12: Morphology of *er-ant1* suppressor plants. 24-days-old wild type, *er-ant1* and selected *er-ant1* M₃ suppressor mutants grown at ambient CO₂ and a light/dark cycle of 10/14 h.

3.5.2 Chlorophyll content of suppressor plants

Original *er-ant1* mutants possess a decreased chlorophyll content, which is reflected in pale green leaf colour (Leroch *et al.*, 2008). Interestingly, *er-ant1* M₃ suppressor plants showed differences in leaf colour compared to original *er-ant1* (3.5.1). The total chlorophyll amount was determined to convert this subjective observation to measurable data.

All suppressor mutant leaves had a higher chlorophyll concentration than the *er-ant1* leaves (Figure 3-13). Among the suppressor mutants, the lowest chlorophyll amount was detected in line 1.3 (~ 1.6 mg/g fresh weight (FW)). The highest amount (~ 3.4 mg/g FW) was measured in leaves of line 16.2 plants, which were also the largest suppressor mutant plants.

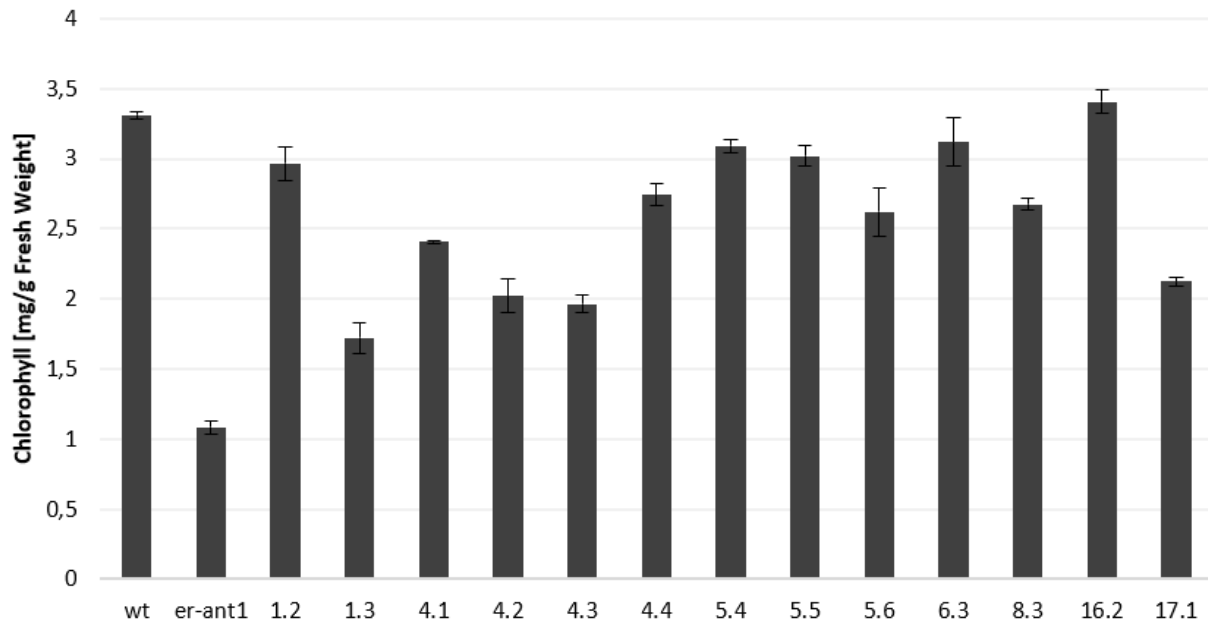


Figure 3-13: Total chlorophyll content in leaves of *er-ant1* and *er-ant1* M₃ suppressor plants relative to wild type. Wild-type, *er-ant1* and selected *er-ant1* M₃ suppressor mutant plants were grown at ambient CO₂ and a light/dark cycle of 10/14 h. Leaf samples were taken from 6-weeks-old plants, 5 h after onset of light. Shown are mean values of three individual replicates, \pm SE.

3.5.3 Glycine quantification in the suppressor plants

Another striking characteristic of *er-ant1* mutants is their high leaf glycine content (Hoffmann *et al.*, 2013). Since the growth of M₃ plants was partly rescued (3.5.1), it was of interest whether this is also reflected by a decreased glycine level.

The glycine HPLC quantification revealed that some M₃ suppressor plants showed a slight reduction in glycine when compared to *er-ant1* (Figure 3-14). However, the glycine content of all suppressor mutants was still substantially higher. The glycine content of the lines 1.2, 5.6 and 8.3 was approximately 50-fold higher and of the lines 4.2, 5.4, 5.5 and 16.2 28-fold to 36-fold higher than that of the wild type. Lines 4.1, 4.3 and 6.3 even showed glycine levels similar to *er-ant1* (~ 70-fold of wild type).

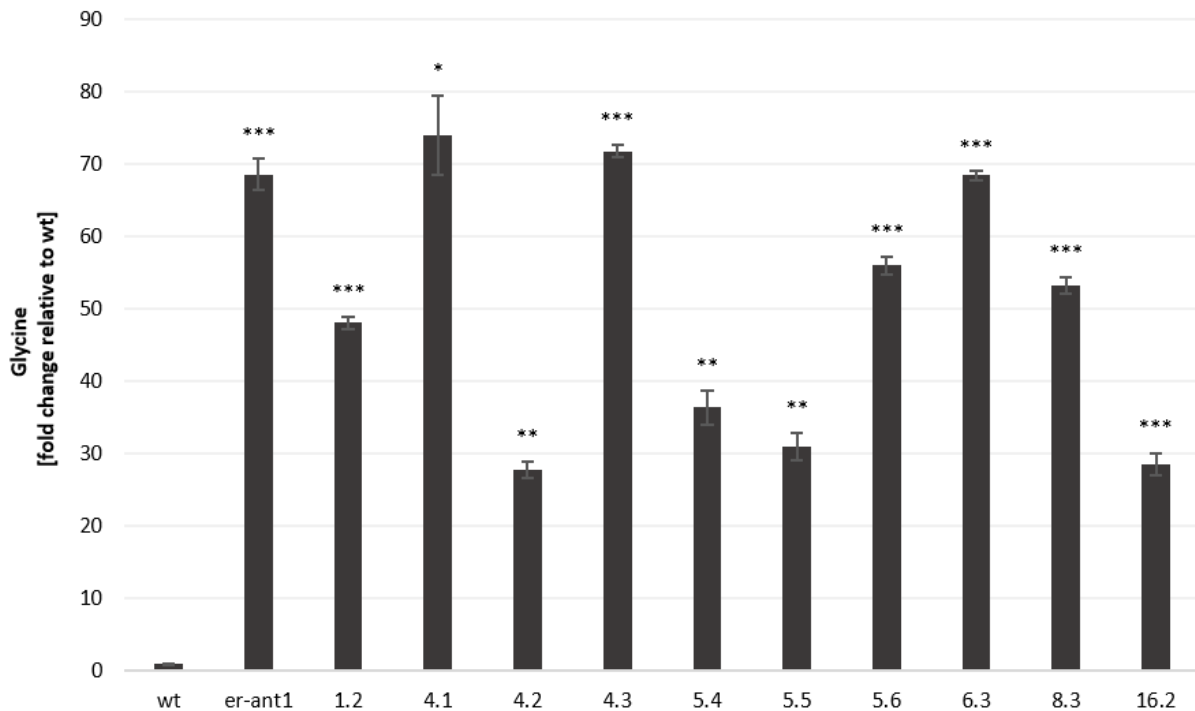


Figure 3-14: Glycine content in leaves of *er-ant1* and *er-ant1* M₃ suppressor plants relative to wild type. Plants were grown under 2000 ppm CO₂ and a light/dark cycle of 16/8 h for four weeks and subsequently shifted to ambient air. Samples were taken after 5 d of adaptation, 5 h after onset of light. Shown are mean values of five individual replicates, ± SE. Asterisks indicate the significance level between wild-type and mutant plants according to Student's t-test (*P < 0.05, **P < 0.01, ***P < 0.001). wt: wild type.

3.5.4 Photosystem II performance of suppressor mutants

The measurement of chlorophyll fluorescence is a non-invasive method to investigate the activity of photosystem II (PSII). Chlorophyll molecules absorb light energy, which can drive photosynthesis (photochemistry), be emitted as heat or emitted as light (fluorescence). These three processes compete with each other. Thus emitted fluorescence gives information about the quantum efficiency of photochemistry and heat dissipation (Murchie and Lawson, 2013).

The value F_v/F_m correlates to the maximum quantum yield of PSII photochemistry. If plants are unstressed, this value equals ~ 0.83 (Björkman and Demmig, 1987). Prolonged exposure to ambient air conditions reduces the maximum quantum yield of PSII (F_v/F_m) of *er-ant1* leaves mutants probably caused by increasing damage of the photosynthetic machinery (Hoffmann *et al.*, 2013).

Therefore, it was studied whether the transfer from high CO₂ to ambient CO₂ also affects F_v/F_m of *er-ant1* suppressor mutants.

All tested plants had an F_v/F_m value of ~ 0.83 when permanently cultivated at high CO_2 conditions (Figure 3-15 A). Five days adaption to ambient CO_2 did not change the F_v/F_m in wild-type plants, but led to a decreased value (~ 0.74) in *er-ant1* (Figure 3-15 B). The *er-ant1* suppressor mutants also exhibited significantly decreased F_v/F_m values. However, the reduction in line 1.2 (~ 0.8) and 8.3 (~ 0.8) was lower than that of *er-ant1* mutants.

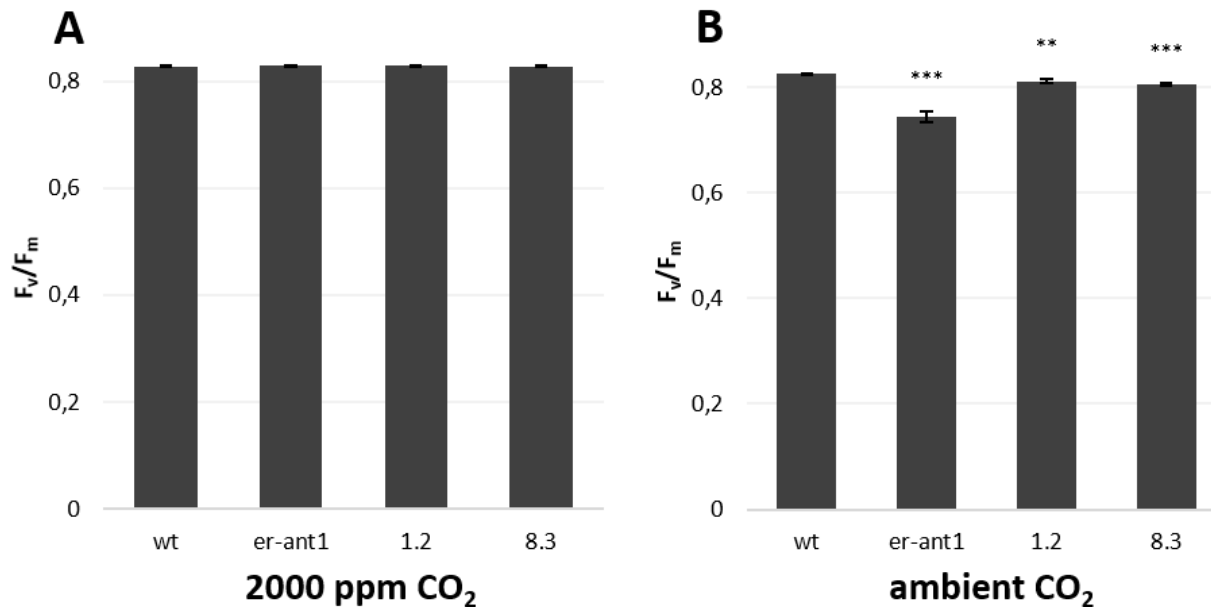


Figure 3-15: Maximum quantum yield of PSII (F_v/F_m). Wild-type, *er-ant1* and selected *er-ant1* M₃ suppressor mutant plants were grown under 2000 ppm CO_2 and a light/dark cycle of 10/14 h for four weeks and plants for ambient samples were subsequently shifted to ambient air. Samples were taken after 5 d split, 2.5 h after onset of light followed by 15 min dark-adaption. Shown are mean values of seven individual replicates, \pm SE. Asterisks indicate the significance level between wild-type and mutant plants according to Student's t-test (* $P < 0.05$, ** $P < 0.01$, *** $P < 0.001$). wt: wild type.

Determination of the effective quantum yield of PSII ($Y(II)$) and the non-photochemical quenching (NPQ) after exposure to increasing light intensities allowed more profound insights into the functionality of the photosynthetic system. In principle, $Y(II)$ may vary between the values 0 and 1. The value 0.5 would mean that 50 % of the absorbed quanta are converted into chemically fixed energy by charge separation in PSII, whereas the other 50 % dissipate into fluorescence and heat (Baker *et al.*, 1989).

When cultivated permanently at high CO_2 conditions, wild-type plants exhibited a slightly higher $Y(II)$ in response to increasing light intensities than *er-ant1* and corresponding suppressor mutants (Figure 3-16 A). No differences between *er-ant1* and the suppressor mutant lines were detectable. However, when plants were adapted to ambient CO_2 conditions

(Figure 3-16 B), Y(II) of *er-ant1* and the two suppressor lines was decreased compared to the wild type. Nevertheless, Y(II) values of suppressor plants were higher than that of *er-ant1*.

The NPQ is a measure of non-photochemical fluorescence quenching. This process acts as a 'safe' mechanism as it dissipates excess excitation energy by heat and thereby prevents the likelihood of singlet oxygen formation. On the one hand, a high NPQ indicates an excessive photon flux density. On the other hand, a high NPQ shows that the plant retained physiological mechanisms to protect itself.

When cultivated at high CO₂, no NPQ differences were detectable between the tested genotypes until exposure to the higher light intensities: Beginning at PAR (photosynthetically active radiation/ light intensity) 219, the NPQ of *er-ant1* and suppressor mutants was higher than the wild-type NPQ at all following measuring points (Figure 3-16 C). The NPQ values of suppressor mutants resembled at the beginning of the experiment the NPQ values from *er-ant1*. After exposure to PAR 535, differences between the mutant lines occurred: The highest NPQ values were obtained for *er-ant1*, followed by line 8.3 and finally line 1.2 and the wild type.

After adaption to ambient air, wild-type NPQs were only slightly changed compared to the high CO₂ conditions (Figure 3-16 D). The suppressor mutants showed NPQ graphs similar to under high CO₂ conditions, but the NPQ values increased much stronger in response to increasing light intensities than NPQ values of wild-type plants. Compared to that, the *er-ant1* NPQ graph shows no similarities, neither to that of *er-ant1* determined at high CO₂ conditions nor to those of the other tested genotypes at ambient conditions. Almost no non-photochemical quenching was observed after exposure to the first light intensity (73). From here on, the slope of the graph of the *er-ant1* NPQ became linear. After exposure to PAR 219, the NPQ of *er-ant1* was higher than in wild-type plants. The measured NPQ decreased relative to the wild type after the next light intensity (534). After exposure to the highest light intensity (1290), NPQ of *er-ant1* was slightly higher when compared to the NPQ of wild-type plants.

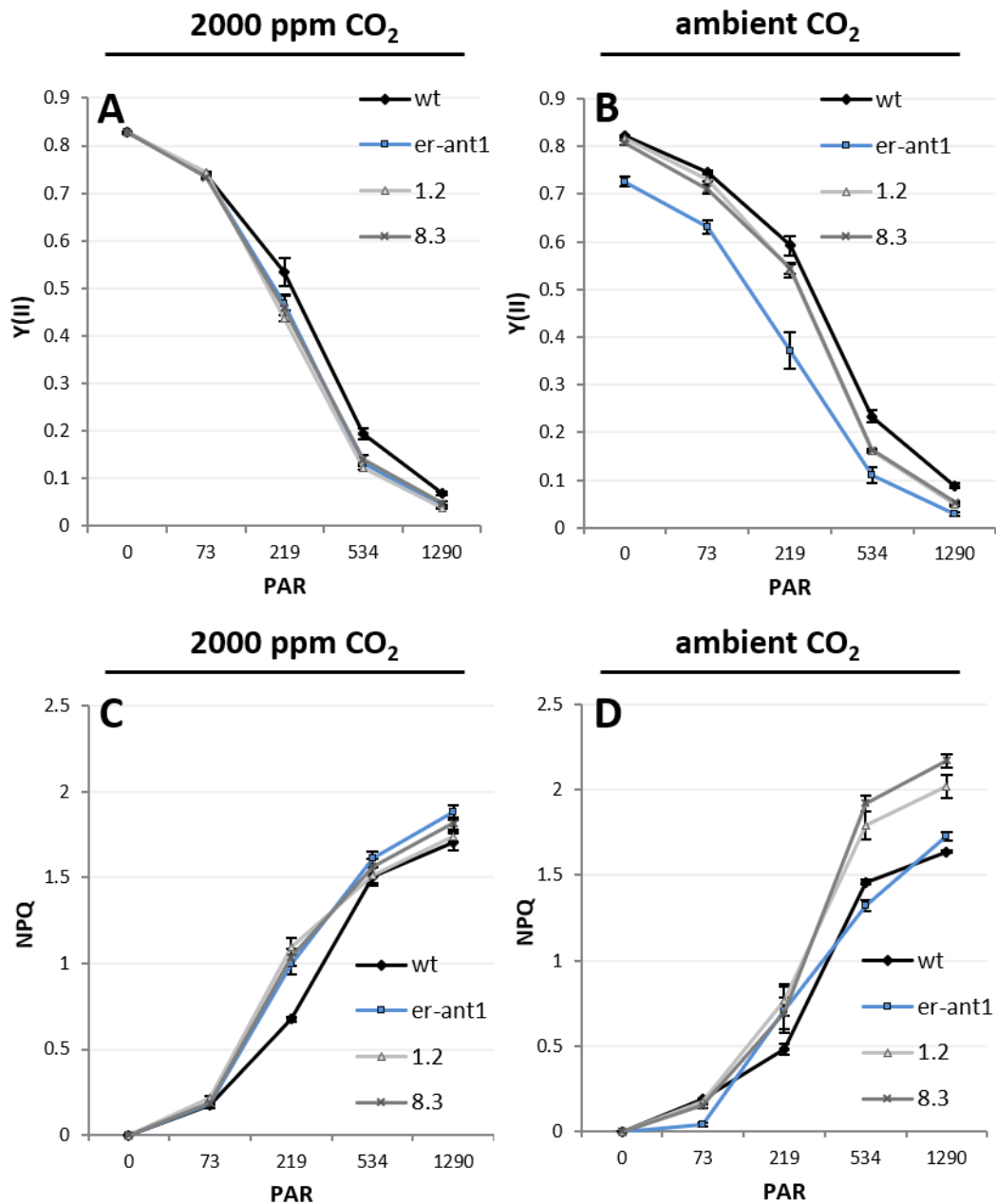


Figure 3-16: Effective quantum yield of PSII (Y(II): A, B) and non-photochemical quenching (NPQ: C, D) after exposure to increasing light intensities. Wild-type, *er-ant1* and selected *er-ant1* M₃ suppressor mutant plants were grown under 2000 ppm CO₂ and a light/dark cycle of 10/14 h for four weeks. Plants for ambient samples were subsequently shifted to ambient air. Samples were taken after further cultivation in each condition for five days. Samples were 15 min dark-adapted and then exposed to actinic light at different light intensities (photosynthetically active radiation (PAR)) for 5 min each. Shown are mean values of four individual replicates, \pm SE.

3.5.5 Assembly of photosynthetic complexes

To get further insights into the photosynthetic machinery of *er-ant1* and its suppressor mutants a 2D Blue Native (BN)/SDS-PAGE approach was used to investigate the assembly of photosynthetic complexes. No differences in the assembly of photosynthetic complexes were

detectable, neither between genotypes nor between plants exposed to high CO₂ or ambient air (Figure 3-17).

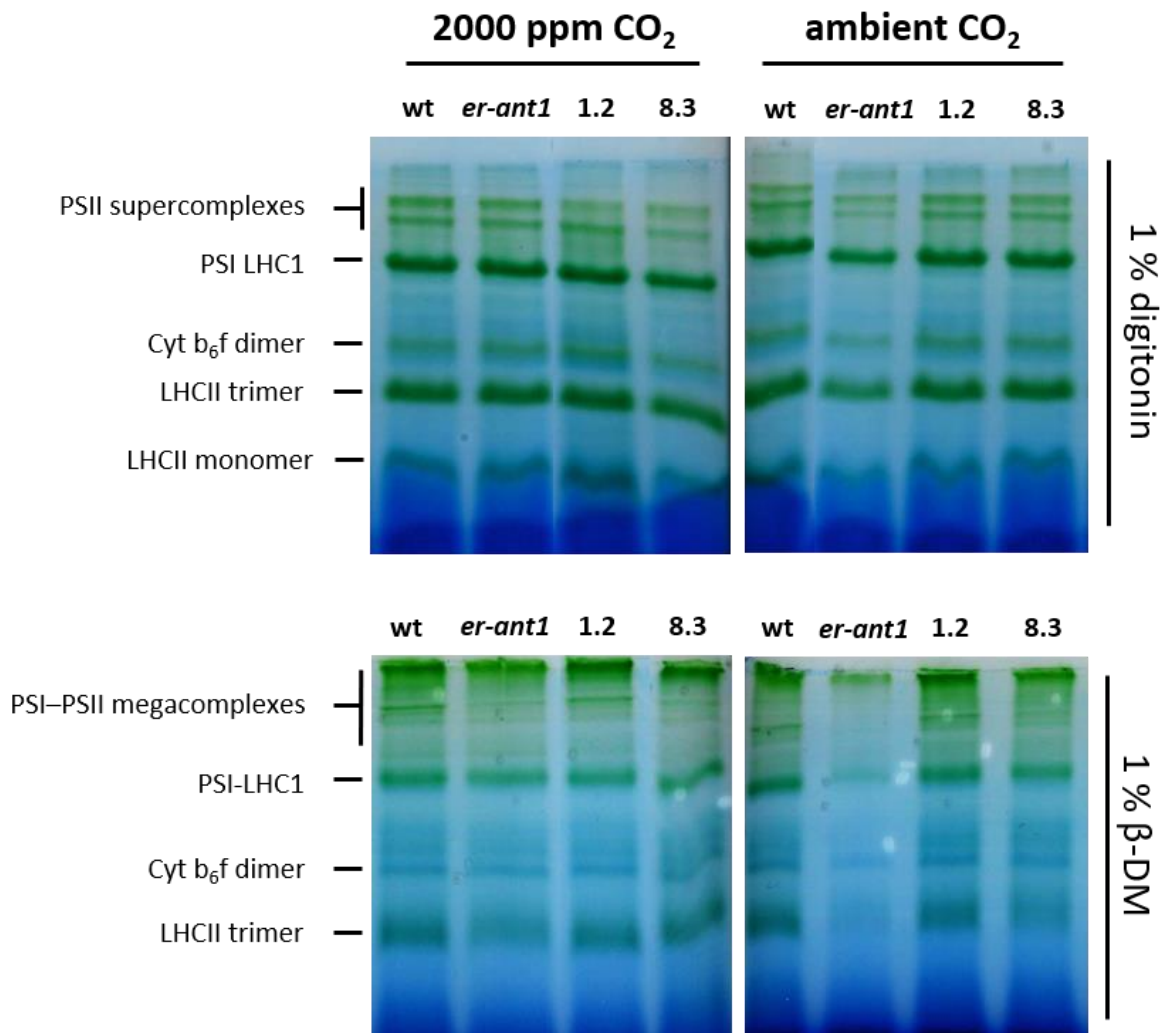


Figure 3-17: BN-PAGE analysis of thylakoid membrane complexes of wild type, *er-ant1* and *er-ant1* suppressor mutants. Wild-type, *er-ant1* and selected *er-ant1* M₃ suppressor mutant plants were grown under 2000 ppm CO₂ and a light/dark cycle of 10/14 h for four weeks. Plants for ambient samples were subsequently shifted to ambient air. Samples were taken after further cultivation in each condition for five days. Thylakoid fractions equivalent to 10 µg of chlorophyll were treated either with 1 % digitonin or 1 % β-DM. Bands representing protein complexes are indicated.

The run of the SDS-PAGE in the second dimension revealed that proteins of higher molecular weight formed more complexes when plants were grown at high CO₂ conditions permanently (Figure 3-18 A-D). When plants were shifted to ambient CO₂ conditions for five days, more proteins were apparently associated in complexes of lower molecular weight. Furthermore,

line 1.2 formed more protein complexes than the corresponding wild type when adapted to ambient conditions (Figure 3-18 C)

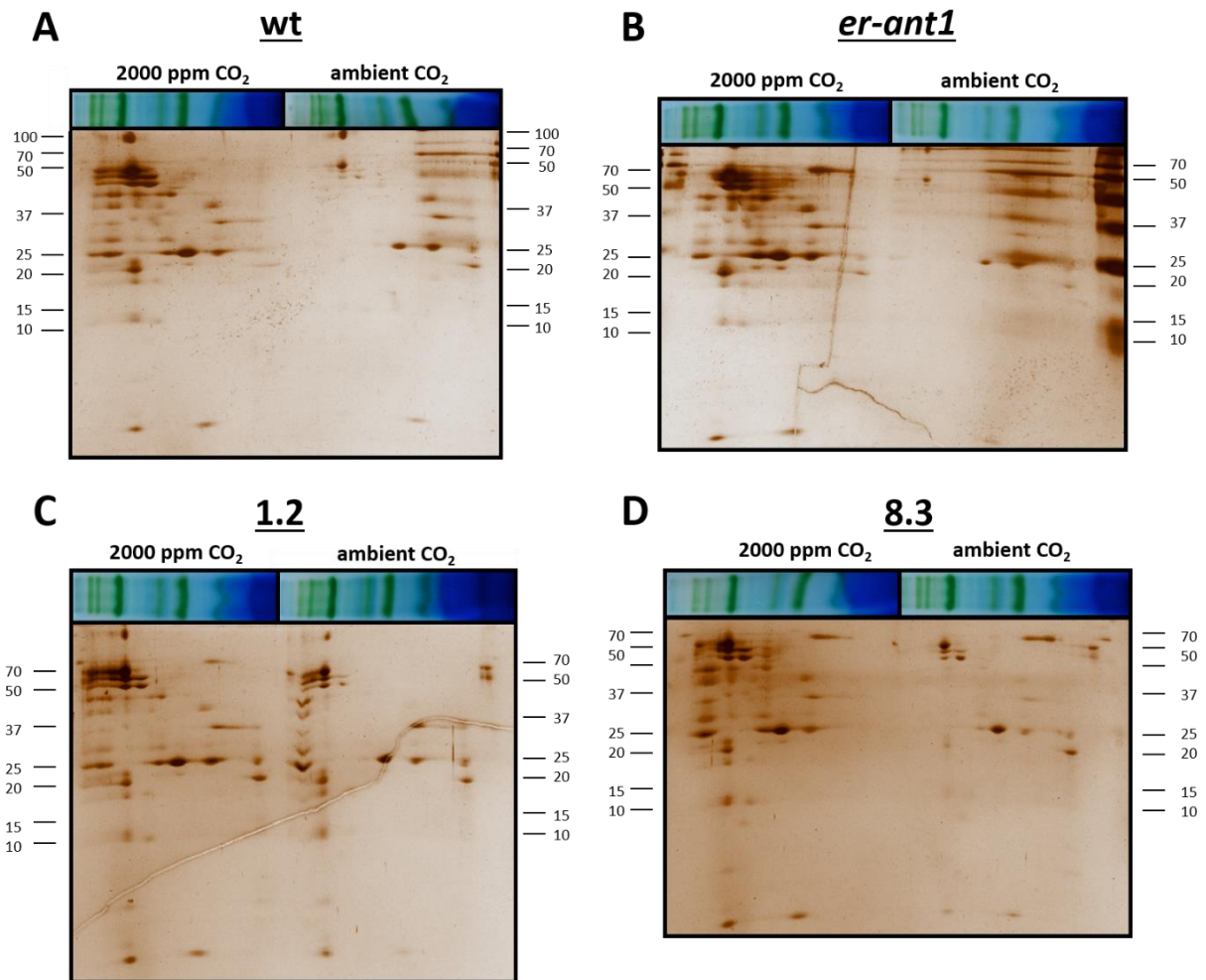


Figure 3-18: Silver staining of 2D-PAGE of thylakoid fractions from wild type, *er-ant1* and *er-ant1* suppressor mutants. BN-PAGE strips are shown on top of the 2D-PAGE, illustrating the position of oligomeric complexes.

3.5.6 Ultrastructure of *er-ant1* suppressor mutant chloroplasts

The determination of PSII performance revealed differences between *er-ant1* and its suppressor mutants. To check whether this is due to morphological alterations in the ultrastructure of the chloroplasts, transmission electron microscopy (TEM) of the cells was conducted. The chloroplast ultrastructure of *er-ant1* and *er-ant1* suppressor mutants did not markedly differ from that of wild-type chloroplasts (Figure 3-19 A, B). However, a substantial accumulation of starch granules in line 8.3, regardless of the CO₂ cultivation condition, became apparent.

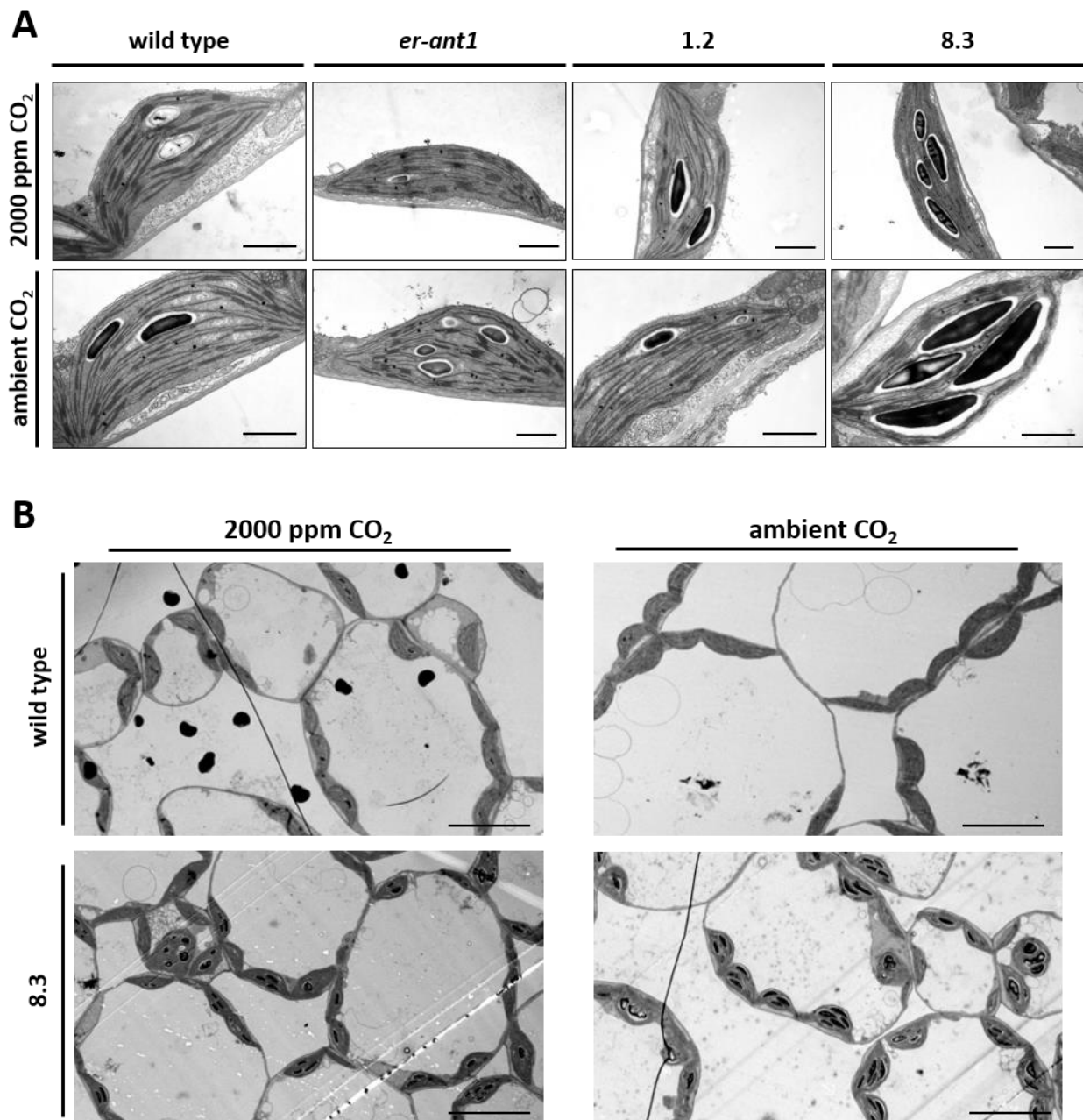


Figure 3-19: TEM micrographs of ultrathin sections of leaves from wild type, *er-ant1* and *er-ant1* suppressor mutants. A: Single chloroplasts from plants cultivated at high CO₂ and ambient CO₂ conditions. Scale bar = 1 μm B: Cells of the wild type and the *er-ant1* suppressor line 8.3 cultivated at high and ambient CO₂ conditions. Pictures provided by Anurag Sharma (UCPH). Scale bar = 10 μm

The thylakoid membranes within a single chloroplast form a continuous network. Within this network, the grana stacks are interconnected by the stroma lamellae (Shimoni *et al.*, 2005). Grana stack height and diameter were determined because these factors are important for plants state transition ability (Figure 3-20).

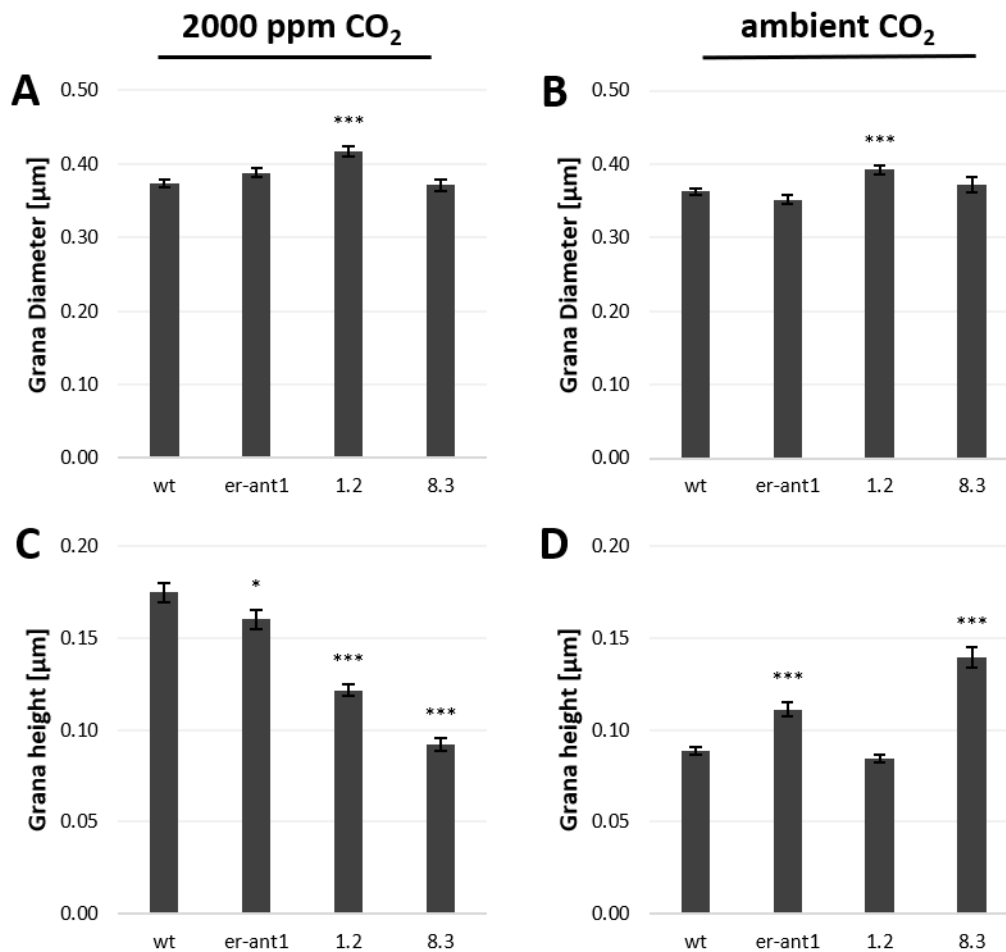


Figure 3-20: Diameter and height of grana stacks in the wild type, *er-ant1* and *er-ant1* suppressor mutants. Shown are mean values of >100 grana stacks, \pm SE. Asterisks indicate the significance level between wild type and mutant according to Student's t-test (* $P < 0.05$, ** $P < 0.01$, *** $P < 0.001$). Grana heights and diameters were measured by Anurag Sharma (UCPH).

Plants of the suppressor mutant line 1.2 exhibited a slightly larger grana stack diameter at both cultivation conditions than plants of the remaining genotypes (Figure 3-20 A, B). When plants were grown at high CO₂ conditions, the grana stack height of *er-ant1* was slightly, and that of the two suppressor mutants was markedly decreased compared to the wild type (Figure 3-20 C, D). Grana stacks of line 1.2 were approximately 0.05 μm smaller than corresponding wild-type stacks, while the height of line 8.3 is even reduced to 50%. When plants were cultivated under ambient CO₂, the height of wild-type grana stacks was decreased to approximately 0.09 μm . Compared to that, *er-ant1* possessed significantly higher grana stacks (0.11 μm). The highest grana stacks were visible in the *er-ant1* suppressor mutant line 8.3 (0.14 μm), whereas the other suppressor mutant showed no difference regarding grana stack height compared to the wild type.

3.6 Identification and verification of suppressor candidate genes

After the identification of *er-ant1* suppressor mutants and the observation of interesting phenotypic characteristics, it was essential to identify the mutations causative for the suppression. This required the initial identification of single nucleotide polymorphisms (SNPs) which are exclusively occurring in the DNA of a respective suppressor mutant, but not in the original *er-ant1* T-DNA insertion line.

Different approaches can be used to identify the suppression causing SNPs; each method has its own advantages and disadvantages. The initial use of a more traditional chromosomal mapping approach (Alonso-Blanco *et al.*, 1998) turned out to be too laborious and time-consuming and thus not feasible in the course of this PhD thesis (for details and initial results see 6-2 in the appendix). Therefore, a modern approach based on Next-Generation Sequencing was followed for the identification of mutations causative for the suppression phenotypes.

3.6.1 Identification of suppressor candidates using Next-Generation Sequencing

The identification of the suppression-causing mutation was performed by a combination of bulked segregant analysis (BSA) and Next-generation sequencing (NGS).

For this, individual M₃ plants were crossed with the original *er-ant1* T-DNA insertion line (Figure 3-21 A). Since always both plants, *er-ant1* and the respective suppressor mutant, were homozygous for the *er-ant1* T-DNA insertion, this also applied to all individuals of the backcross (BC₁) F₁ generation. Within the BC₁F₁ generation, the 13 lines used for sequencing exhibited *er-ant1* like phenotypes (Figure 3-21 B).

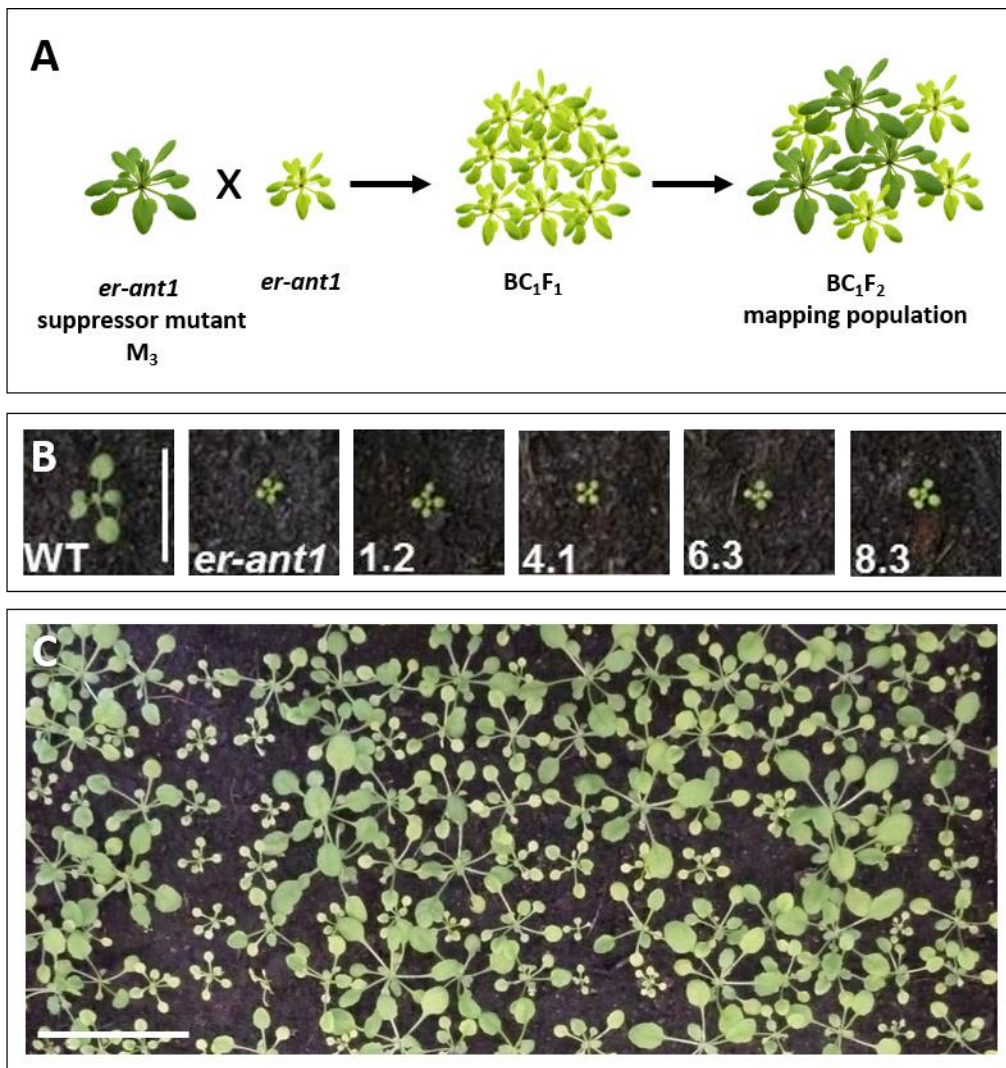


Figure 3-21: Generation of mapping population (BC_1F_2) used for NGS sequencing. (A) Performed crosses for the generation of a mapping population. (B) 16-days-old plants, cultivated in ambient air conditions. Wild-type, *er-ant1* and selected BC_1F_1 plants. Scale = 1 cm. (C) Example of a typical mapping population after five weeks of cultivation at ambient air conditions (BC_1F_2 , line 4.1). Scale = 5 cm.

By PCR it was confirmed that also the individuals of the following BC_1F_2 generation (mapping population) were still homozygous for the *er-ant1* T-DNA insertion. Due to segregation, traits of the suppressor mutant also became homozygous, resulting in plants showing partial complementation of the *er-ant1* dwarf phenotype (Figure 3-21C).

3.6.2 Bulked segregant Next-Generation Sequencing analysis

In total, 13 mapping populations, each composed of larger plants (suppressor phenotype) and small plants (original *er-ant1* phenotype) were analysed for mutations causative for their respective mutations. Detailed information of the procedure, definitions and brief

explanations of the different steps are given in 2.2.20. Briefly, gDNA was pooled from 50 bigger plants (homozygous for the suppressor mutation, from here on called **positive pool**) and 50 plants with *er-ant1* phenotype (heterozygous or do not contain suppressor mutation at all; from here on called **negative pool**) of each mapping population (Figure 3-22).

Then, the pooled gDNA samples of the 13 mapping populations and pooled gDNA of 50 original *er-ant1* mutant plants were used for whole genome resequencing (Figure 3-22). After the quality control of the raw sequencing data, reads were mapped to the reference genome (TAIR 10).

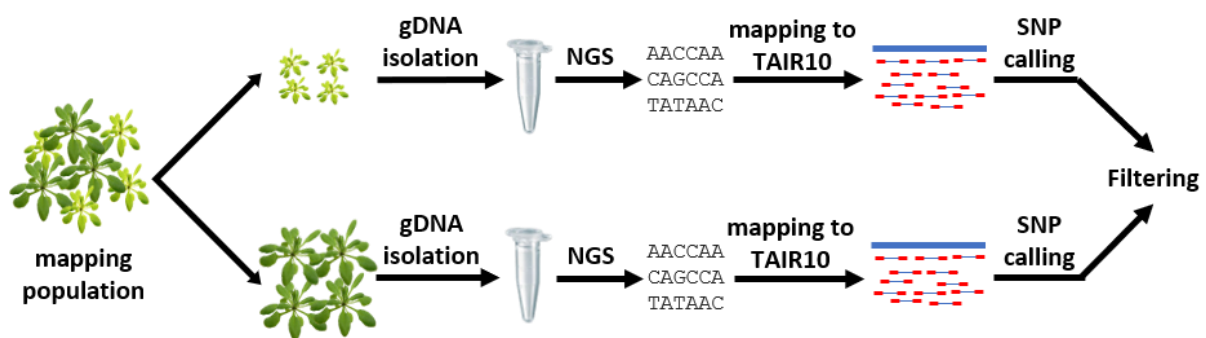


Figure 3-22: Workflow for bulked segregant Next-Generation Sequencing analysis.

For TAIR 10 (119 667 750 bp), the mapping rate of the samples ranged from 92.22 % to 98.64 %. The average depth on the reference genome was in the range of 41.63x to 56.45x. Moreover, 99.96 % of the genome was covered at least 4x. The full statistics are shown in the appendix (Table 6-7). This demonstrates that the sequencing procedures were successful and, therefore, were evaluated as highly reliable.

3.6.3 Identification of single nucleotide polymorphisms

A single nucleotide polymorphism (SNP) refers to a variation of a single nucleotide which may occur at a specific position in the genome, including transition and transversion of a single nucleotide. The goal was to identify G/C to A/T transitions because EMS mutagenesis primarily results in this type of exchange (Maple and Møller, 2007). Prior identification of mutations causative for the suppression phenotypes, SNPs within the sequences were detected and annotated. After quality control (2.2.20.5), 12 030 SNPs were detected in the sequencing data

of the *er-ant1* T-DNA insertion line. The number of SNPs of the sequenced mapping populations ranged from 12 182 SNPs to 13 749 SNPs (Figure 3-23).

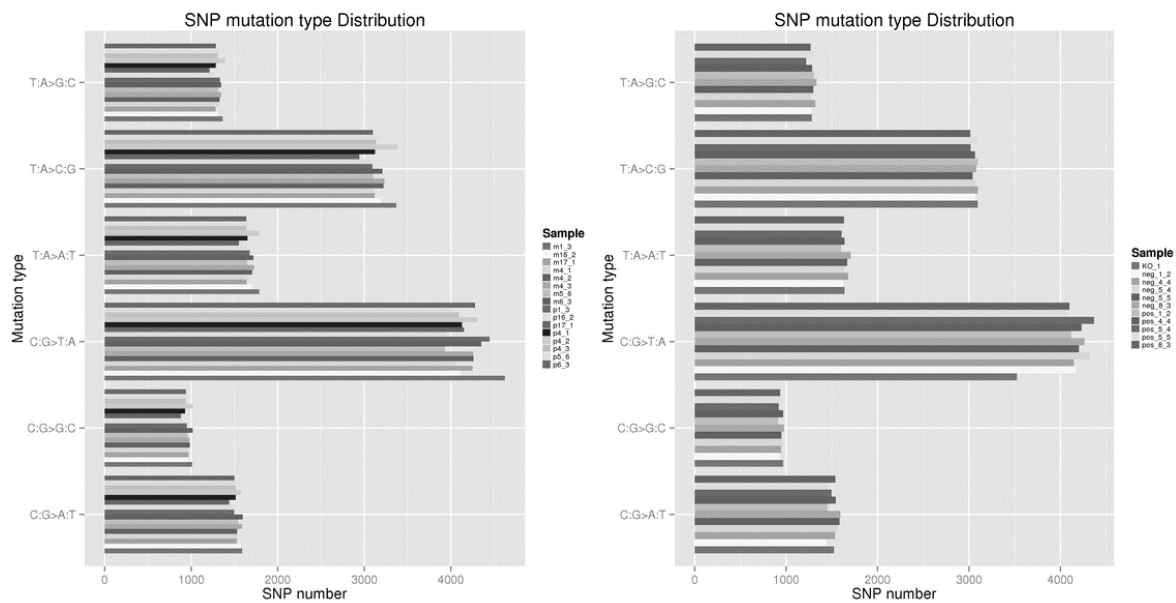


Figure 3-23: Number and type of SNPs in the sequenced gDNA pools. Pictures provided by Novogene.

3.6.4 Identification of candidate suppressor mutations

The following section contains only the most relevant intermediate results using the example of one analysed line (line 6.3). More detailed information of the procedure, definitions and brief explanations of the different steps are given in 2.2.20.6.

To visualise the localisation of SNPs on chromosomes and to get information about the effects each SNP has on the genetic information, the software CandiSNP was used (Etherington *et al.*, 2014).

On chromosome 2, an accumulation of SNPs with high allele frequencies became visible (Figure 3-24). Such an accumulation indicates that a corresponding sequence region is essential for the phenotype used for selection. Accordingly, there was a high probability that the SNP causative for the suppression could be found within this chromosomal region.

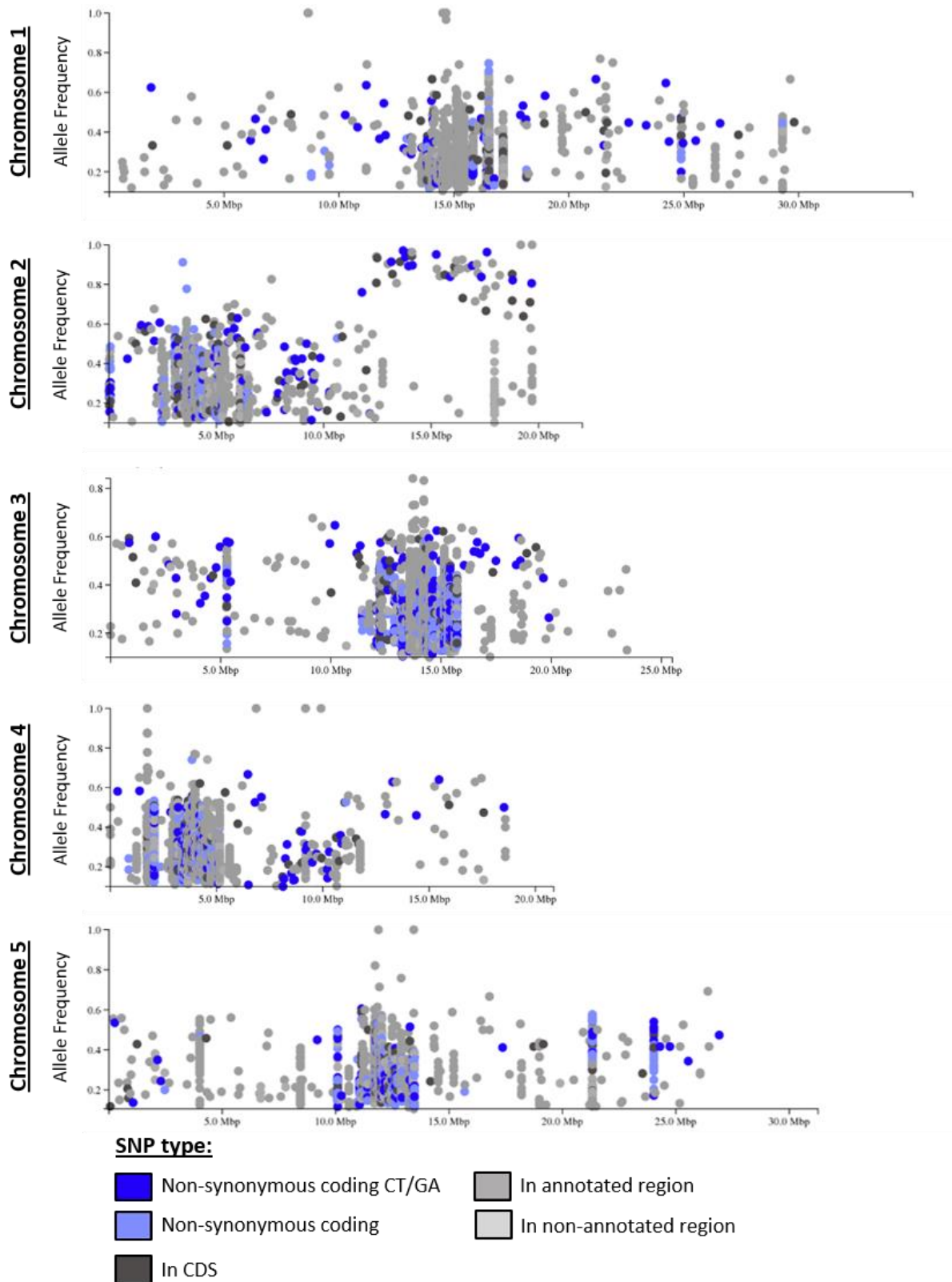


Figure 3-24: Adapted CandiSNP visualisation output file. SNPs with respective allele frequency and chromosomal position are visualised as dots. Shown are 12 730 SNPs in the positive pool of line 6.3. Different colours indicate different types of SNPs (see colour legend below picture).

The implementation of all filtering steps revealed ten promising candidate SNPs for line 6.3. Most of these identified SNPs resulted in an amino acid exchange (Table 3-12). The only exception was an identified SNP in AT2G33255 (Haloacid dehalogenase-like hydrolase (HAD) superfamily protein) which changed a triplet coding for glutamine into a stop codon. A preliminary stop codon in a coding sequence leads to a truncated protein and presumably results in its loss of function.

Table 3-12: Candidate SNPs identified in *er-ant1* suppressor line 6.3.

TAIR ID	AF	Change	Entrez Gene Description
AT2G32250	0.97	R/C	FAR1-related sequence 2 (FRS2)
AT2G42240	0.96	A/V	RNA-binding (RRM/RBD/RNP motifs) family protein
AT2G33010	0.96	T/I	Ubiquitin-associated (UBA) protein
AT2G36350	0.95	S/L	Protein kinase superfamily protein
AT2G33255	0.94	Q/*	Haloacid dehalogenase-like hydrolase (HAD) superfamily protein
AT2G32480	0.94	G/D	chloroplastic membrane metallo proteases (ARASP)
AT2G30880	0.91	R/H	Pleckstrin homology (PH) domain-containing protein (SWAP70)
AT2G33340	0.90	G/R	MOS4-associated complex 3B (MAC3B)
AT2G40490	0.89	S/F	Uroporphyrinogen decarboxylase (HEME2)
AT2G32870	0.89	G/E	TRAF-like family protein

Interestingly, candidate SNPs in AT2G33255 could also be identified in other *er-ant1* suppressor mutant lines (Table 3-13).

Table 3-13: Identified SNPs in AT2G33255 of different *er-ant1* suppressor mutant lines.

Line	AF	Max AF	SNP Position	Change
8.3	0.86	0.88	14098898	G→D
4.1	0.97	1	14099659	G→E
4.2	0.83	0.94	14099659	G→E
4.4	1	1	14099659	G→E
6.3	0.94	0.97	14099679	Q→*
5.6	0.86	0.92	14100204	G→E
17.1	0.98	0.98	14100204	G→E

Shown are allele frequencies of the SNP in AT2G33255 (AF), highest allele frequency among all candidate SNPs in the respective line (Max AF), AT2G33255 SNP position on chromosome two (SNP position), and the respective SNP caused amino acid change (Change). Lines are sorted by SNP position (5'→3'). Redundant lines are highlighted by identical colours.

Some of the SNPs identified in AT2G33255 had identical chromosomal positions: the sequences of the lines 4.1, 4.2 and 4.4 exhibited a non-synonymous SNP at position 14099569, leading to an amino acid exchange from glycine to glutamic acid. Lines 5.6 and 17.1 shared an SNP at position 14100204, also changing glycine to glutamic acid (Table 3-13; Figure 3-25). Furthermore, an SNP resulting in an exchange of glycine to aspartic acid was identified in the sequence of line 8.3.

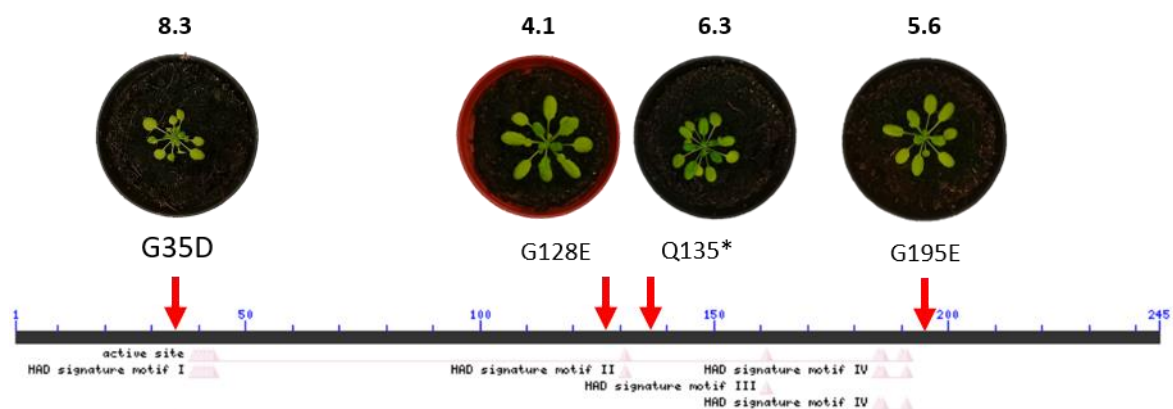


Figure 3-25: Position of SNP induced changes in AT2G33255 gene product.

Because SNPs in AT2G33255 were not only found in various *er-ant1* suppressor mutant lines but also occurred at different chromosomal positions and thus caused different changes in the corresponding protein, the SNPs in this gene were considered as very promising suppressor candidates.

3.6.5 Confirmation of candidate SNPs via Sanger sequencing

Since NGS is not free from errors (Fox *et al.*, 2014), the chosen candidate SNPs were confirmed in the individuals of the respective M₃ generation via “Sanger”-sequencing prior to further analyses. For line 6.3, the candidate SNP in AT2G33255 was verified in all tested individuals (Figure 3-26).

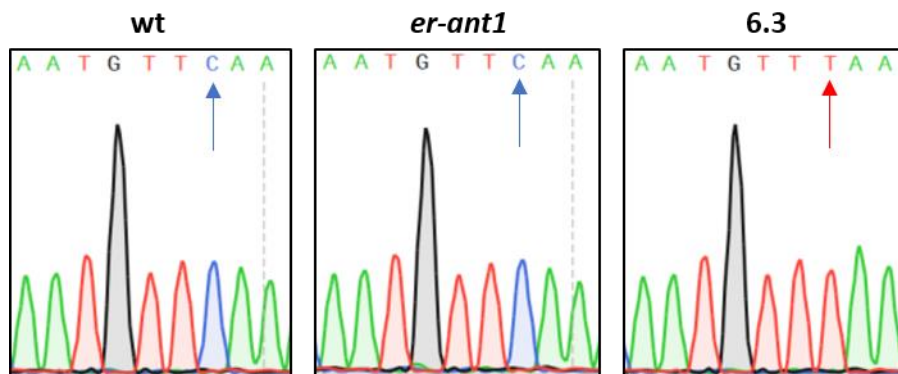


Figure 3-26: Confirmation of candidate SNP in AT2G33255 via Sanger sequencing of wild-type, *er-ant1* and *er-ant1* line 6.3 suppressor M₃ plant gDNA. Blue arrows highlight nucleotides identical to the reference genome TAIR10. The red arrow highlights the confirmed candidate SNP.

Furthermore, it was confirmed that the corresponding region of wild-type and *er-ant1* gDNA sequences was not modified when compared to the public reference genome information TAIR 10 and line 6.3.

3.7 Confirmation of the AT2G33255 suppressor mutation

The SNP in line 6.3 leads to a preliminary stop codon within the AT2G33255 coding sequence. Accordingly, the resulting amino acid sequence would lack 110 amino acids of its C-terminus and might thus be functionally inactive. So, the next goal was to confirm that the loss of function of the protein encoded by AT2G33255 was causative for the observed suppressor

phenotype in line 6.3. This was achieved by crossing AT2G33255 T-DNA insertion lines with the original *er-ant1* mutant and subsequent analysis for complementation. Since AT2G33255 was annotated as a “Haloacid dehalogenase-like hydrolase (HAD) superfamily protein”, the corresponding transcript and protein are called from now on “*HAD*” and “HAD”, respectively, for simplicity.

3.7.1 Isolation of *had* T-DNA insertion mutants

To follow the reverse genetic approach, a respective *had* knockout mutant had to be identified, first. For this, three different exonic T-DNA insertion lines (*had-1*, *had-2* and *had-3*) were analysed. After isolation of homozygous T-DNA insertion plants, the resulting *had-1*, *had-2*, *had-3* and *er-ant1* plants were used for the determination of *HAD* expression via qRT-PCR relative to wild-type plants (Figure 3-27).

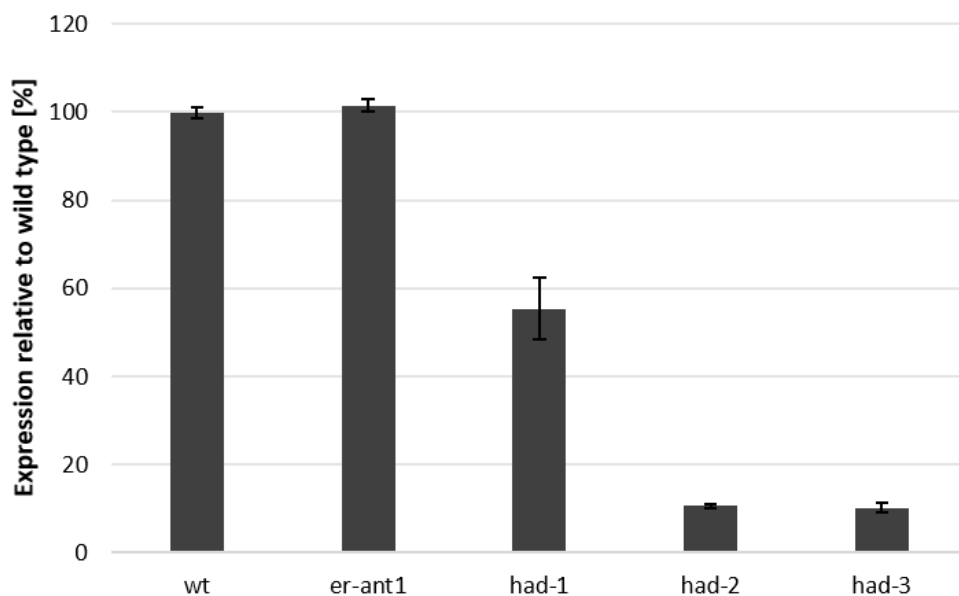


Figure 3-27: *HAD* expression level of *er-ant1* and three *had* T-DNA insertion lines relative to wild type. Expression levels were determined via qRT-PCR. RNA for cDNA synthesis was extracted from leaves of 3-week-old plants. Data were normalised to the SAND housekeeping gene. Shown are mean values of >four plants, \pm SE.

The *HAD* expression level of *er-ant1* was similar to the wild type. It was markedly reduced in *had-1* but still remarkably higher (55 % relative to wild type) than in *had-2* and *had-3* (~ 10 % relative to wild type). According to this, the independent knockout lines *had-2* and *had-3* were selected for the following experiments. Nevertheless, line *had-1* was kept for future tests in which a knockdown of HAD might be useful.

3.7.2 Morphology of *had-2* and *had-3* plants

No information exists about the characterisation of *had* knockout plants. Therefore, they were initially analysed for morphologic phenotypes. No apparent differences between plants of the *had-2* or *had-3* genotype and the wild type were observed when plants were grown under ambient air conditions (Figure 3-28).

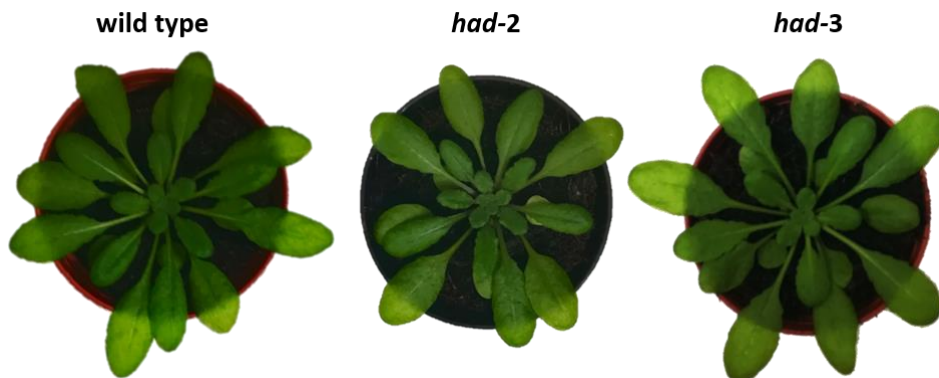


Figure 3-28: 4-week-old plants grown at ambient CO₂ conditions (10h light/14 h dark).

3.7.3 Crossing of *er-ant1* with *had-2*

To confirm that knocking out *HAD* in the *er-ant1* background is causative for the observed suppressor phenotype in the *er-ant1* suppressor mutant line 6.3, *had-2* was crossed with the original *er-ant1* mutant. Segregating plants exhibited either the original *had-2* morphology (wild-type morphology), the original *er-ant1* morphology (dwarfs) or an intermediate size remarkably bigger than *er-ant1* plants but still smaller than *had-2* plants (semi size) (Figure 3-29 A and B).

To test whether the intermediate size was due to a homozygous T-DNA insertion in both, *er-ant1* and *had-2*, corresponding T-DNA screens were performed. This analysis revealed that exclusively the semi-sized plants were homozygous for both T-DNA insertions (Data not shown). To confirm the *had-2 x er-ant1* double knockout, *ER-ANT1* and *HAD* transcript levels were quantified in wild-type, *er-ant1*, *had-2* and homozygous *had-2 x er-ant1* F₃ plants by qRT-PCR (Figure 3-29 C). In *had-2 x er-ant1*, the *ER-ANT1* and *HAD* transcript levels resembled the transcript levels of the respective single mutants. Thus, this mutant can be considered as a true knockout.

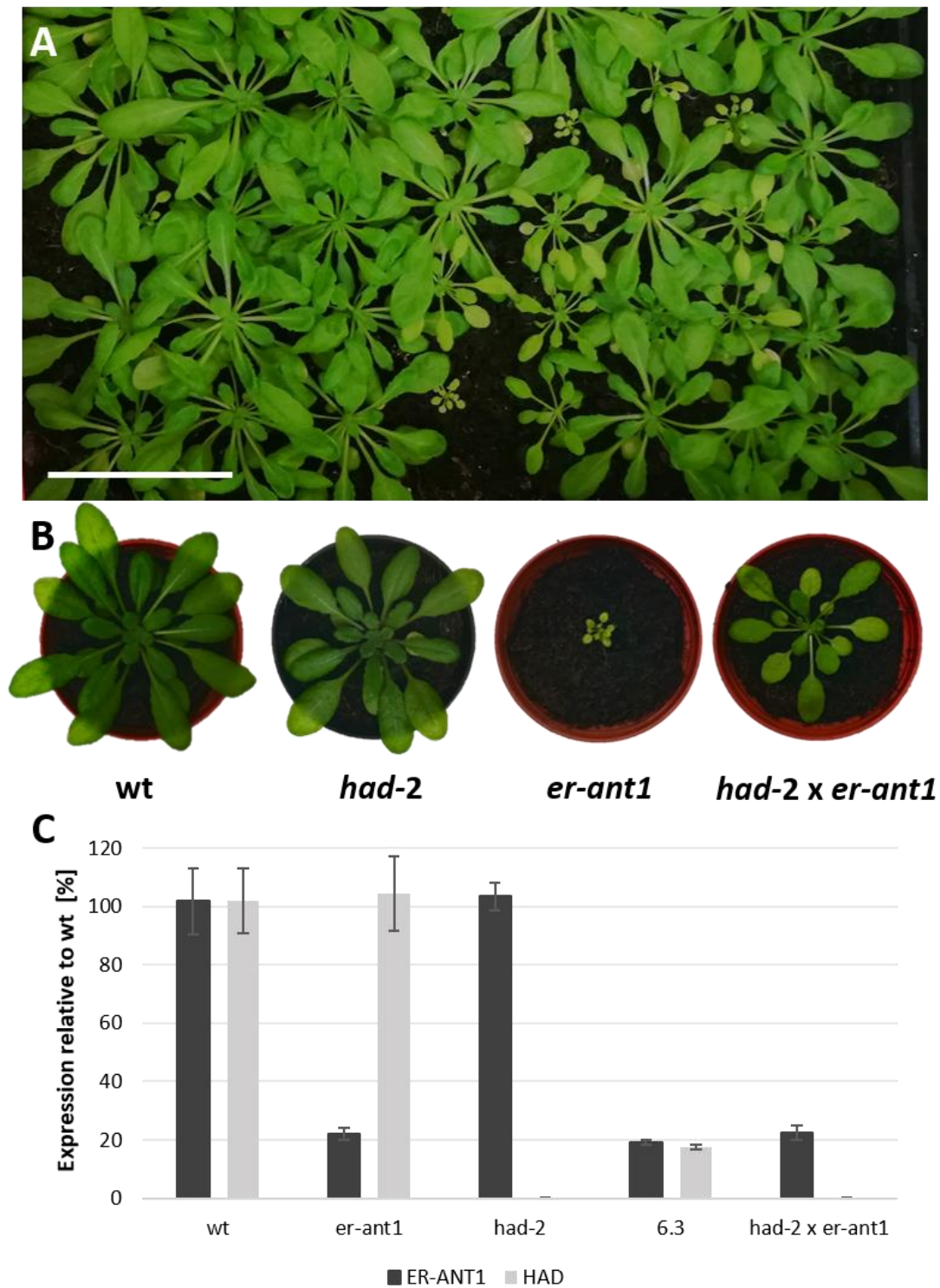


Figure 3-29: Complementation of the dwarf phenotype by *had-2 x er-ant1* crossing. (A) Population of F₂ *had-2 x er-ant1* plants after four weeks cultivation at ambient CO₂ conditions. Scale = 5 cm. (B) Phenotypic comparison of 4-week-old plants grown under ambient CO₂ conditions. (C) Transcript levels of *ER-ANT1* (dark grey) and *HAD* (light grey) determined by qRT-PCR. RNA for cDNA synthesis was extracted from leaves of 3-week-old plants. Data were normalised to the SAND housekeeping gene. wt: wild type. Shown are mean values of 3 plants, ± SE.

3.7.4 Amino acid content in *had* knockout mutants and *had-2 x er-ant1*

The glycine content of line 6.3 M₃ suppressor plants was similar to that of *er-ant1* (3.5.3). To check whether this is also true for the *had-2 x er-ant1* mutant, its glycine level was quantified. Moreover, other amino acids known to be altered were quantified in *had* and *er-ant1* single knockout plants as well as in *had-2 x er-ant1*.

In general, Amino acid contents in *had-2* and *had-3* were not significantly changed compared to wild-type plants. When compared to the wild type, *er-ant1* showed much lower levels of aspartate, glutamate and alanine, substantially increased histidine and arginine levels and a remarkably high accumulation of glycine (Table 3-14). Except for glycine, which remained high, all other amino acid levels were restored to almost wild-type level by the additional absence of functional HAD (Table 3-14).

Table 3-14: HPLC determined amino acid contents of *had-2*, *had-3*, *er-ant1* and *had-2 x er-ant1* relative to wild-type plants.

Amino acid	<i>had-2</i>	<i>had-3</i>	<i>er-ant1</i>	<i>had-2 x er-ant1</i>
Aspartate	95 %	98 %	12 % ^{***}	93 % [*]
Glutamate	104 %	93 %	24 % ^{***}	82 % [*]
Glycine	158 %	102 %	6847 % ^{***}	6363 % ^{***}
Histidine	125 %	108 %	219 % ^{***}	137 % [*]
Alanine	115 %	104 %	20 % ^{***}	96 %
Arginine	109 %	122 %	847 % ^{***}	124 %

Plants were grown at 2000 ppm CO₂ and a light/dark cycle of 16/8 h for four weeks and subsequently shifted to ambient air. Samples were taken after 5 d of adaptation, 5 h after onset of light. Shown are the mean values of four individual replicates. Asterisks indicate the significance level between wild-type and mutant plants according to Student's t-test (*P < 0.05, **P < 0.01, ***P < 0.001).

3.8 Characterisation of HAD

In general, there was very little information published about HAD. Thus, various analyses have been performed to elucidate its function and to understand why its lack positively affects the development of *er-ant1*.

3.8.1 Expression analysis *in silico*

Knowledge about the expression of a particular gene at different developmental stages can provide information which helps to unravel the function of the corresponding protein. Therefore, expression of *HAD* at different developmental stages of *A. thaliana* was analysed *in silico* with the Genevestigator development tool (Zimmermann *et al.*, 2004; Hruz *et al.*, 2008). This tool summarises the expression of genes during the organism's life cycle based on information of several publicly available microarray data sets. The result is shown in Figure 3-30.

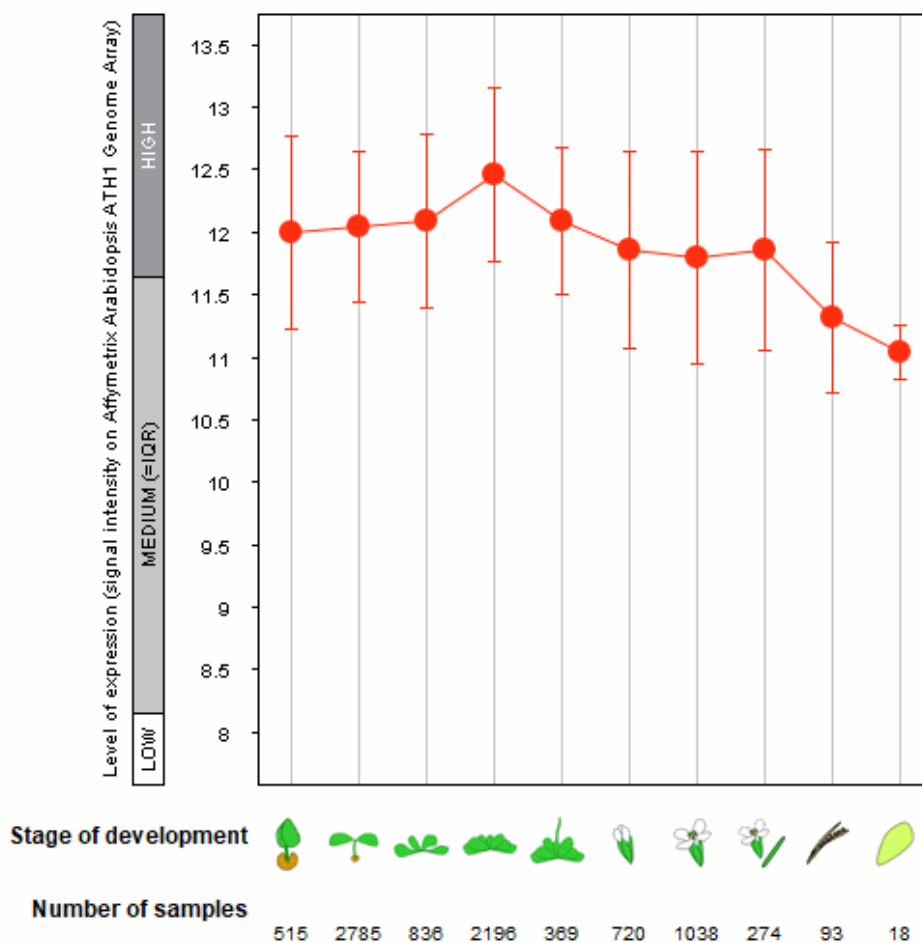


Figure 3-30: Result of Genevestigator development expression analysis. The expression value indicated for a given stage of development is the average expression of all samples annotated as such. IQR= interquartile range.

HAD expression is already high in germinated seeds and reaches a maximum in fully developed rosettes (Figure 3-30). With the begin of bolting, expression of *HAD* decreases but remains on an overall high level until silique development. *HAD* expression is lower in mature siliques and

therefore belongs to the 50 % of medium-expressed genes. The expression of *HAD* is only lower in senescent leaves, but it is still in the interquartile range.

3.8.2 Promotor activity of *HAD* *in vivo*

To analyse the promoter activity, a GUS study was conducted. This method allows a more detailed view on the promoter activity, for example, on specific regions of plant organs and tissues. For this, the putative promoter region (1166 bp) of *HAD* was inserted into the vector pBGWFS7 upstream of the β -glucuronidase gene. After plant transformation, GUS activity was determined by histochemical staining.

Within this study, germinating seeds, young germlings (two-leaf-stage), 14-days-old plants 18-days-old plants, 3-weeks-old plants, stems, flowers and siliques were tested. Although positive results have been expected within all stages (3.8.2), blue GUS staining could only be observed in young plants (Figure 3-31).

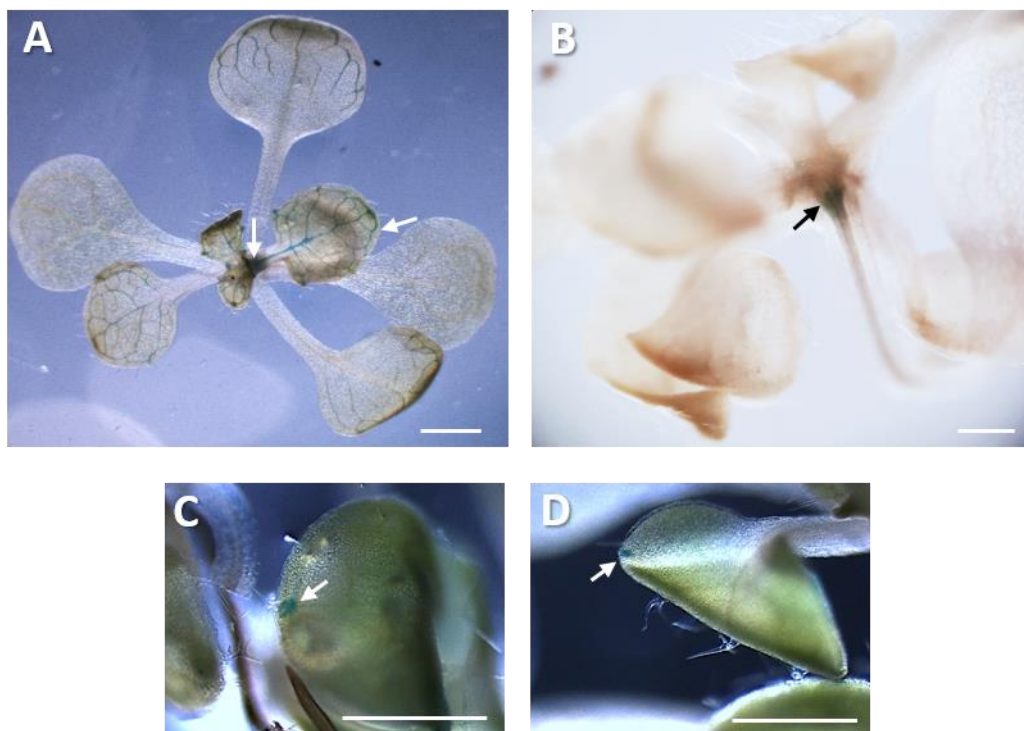


Figure 3-31: Histochemical localisation of GUS Expression under the control of the *HAD* promoter in *Arabidopsis* Col-0 plants. (A) 3-weeks-old plant. (B) 2-weeks-old plant. (C, D) 18-days-old plants. Arrows indicate stained structures.

After three weeks of growth, blue staining was visible in leaf vascular tissue of younger leaves and the apical meristem (Figure 3-31, A). In 2-weeks-old plants, blue colouring was visible in

the shoot apical meristem (Figure 3-31, B). When plants were 18 days old, blue staining at the hydathodes was observed (Figure 3-31, C; D).

The staining was generally very low, which contrasts the expectations based on the expression data. Until now, it cannot be ruled out, that the selected sequence does not represent the complete promotor and that a longer sequence is required. However, a longer sequence would include the exon region of the HAD or cover the adjacent AT2G33250 gene not only partially, but almost complete.

3.8.3 Subcellular localisation of HAD

Different organelles are involved in diverse physiological tasks within a cell. Information on subcellular localisation can contribute towards the understanding of a protein's function and its biological relationships. Therefore, it was essential to know in which subcellular structure HAD is expressed. To achieve this goal, the localisation of HAD was predicted *in silico* first. Secondly, GFP localisation studies were performed.

3.8.3.1 HAD subcellular localisation analysis *in silico*

SUBA is a central resource for *Arabidopsis* protein subcellular location data. For the analysis, the algorithm takes predictive and experimental data into account (Hooper *et al.*, 2017). For the predictive data, SUBA uses the information of 16 different prediction programmes. Nine of these programmes, including for example TargetP, predicted HAD to be localised in mitochondria. ChloroP and three other prediction software programmes suggested a plastidial localisation. The three remaining programmes predicted HAD to be located either in the plasma membrane, vacuole or cytosol.

On the experimental side, SUBA compiles information of published proteomic, GFP localisation and protein-protein interaction datasets. In case of HAD, underlying data was minimal, since SUBA did not find information regarding protein-protein interaction or GFP studies. Nevertheless, SUBA compiled three published proteome datasets which identified HAD in the mitochondria, plastids and multivesicular bodies, respectively. Within these datasets, the reliability of the identified HAD localisation was evaluated. Senkler *et al.*, 2017 identified HAD by label-free quantitative shot-gun proteomics in purified mitochondria

extracts separated by 1D Blue Native PAGE. Here, they could detect seven unique HAD peptides. Another study identified HAD peptides within multivesicular bodies, but the authors evaluated this finding as not significant (Heard *et al.*, 2015). Furthermore, Zybailov *et al.*, 2008 identified two unique HAD peptides in the chloroplast. Based on all experimental and predictive data, the SUBA consensus algorithm finally predicted that HAD is located to mitochondria.

3.8.3.2 GFP subcellular localisation study HAD

The HAD amino acid sequence comprises the HAD-like superfamily domain and an N-terminal extension (approximately 50 residues). To clarify the subcellular localisation of HAD *in vivo*, tobacco and *Arabidopsis* protoplasts were transiently transformed with two different HAD-GFP fusion constructs. Protoplast transformation with HAD with C-terminal GFP resulted in green fluorescence signals weakly surrounding chloroplasts and quite strong signals in the centre of the chloroplasts (Figure 3-32). However, when GFP was attached to the N-terminus of HAD, the corresponding signal resulted in the visualisation of diffuse structures distributed throughout the cell.

These data suggest that the N-terminal GFP masks the targeting sequence and by this hinders the transit into the chloroplast. The GFP analysis is indicative for a chloroplastidial rather than for a mitochondrial localisation.

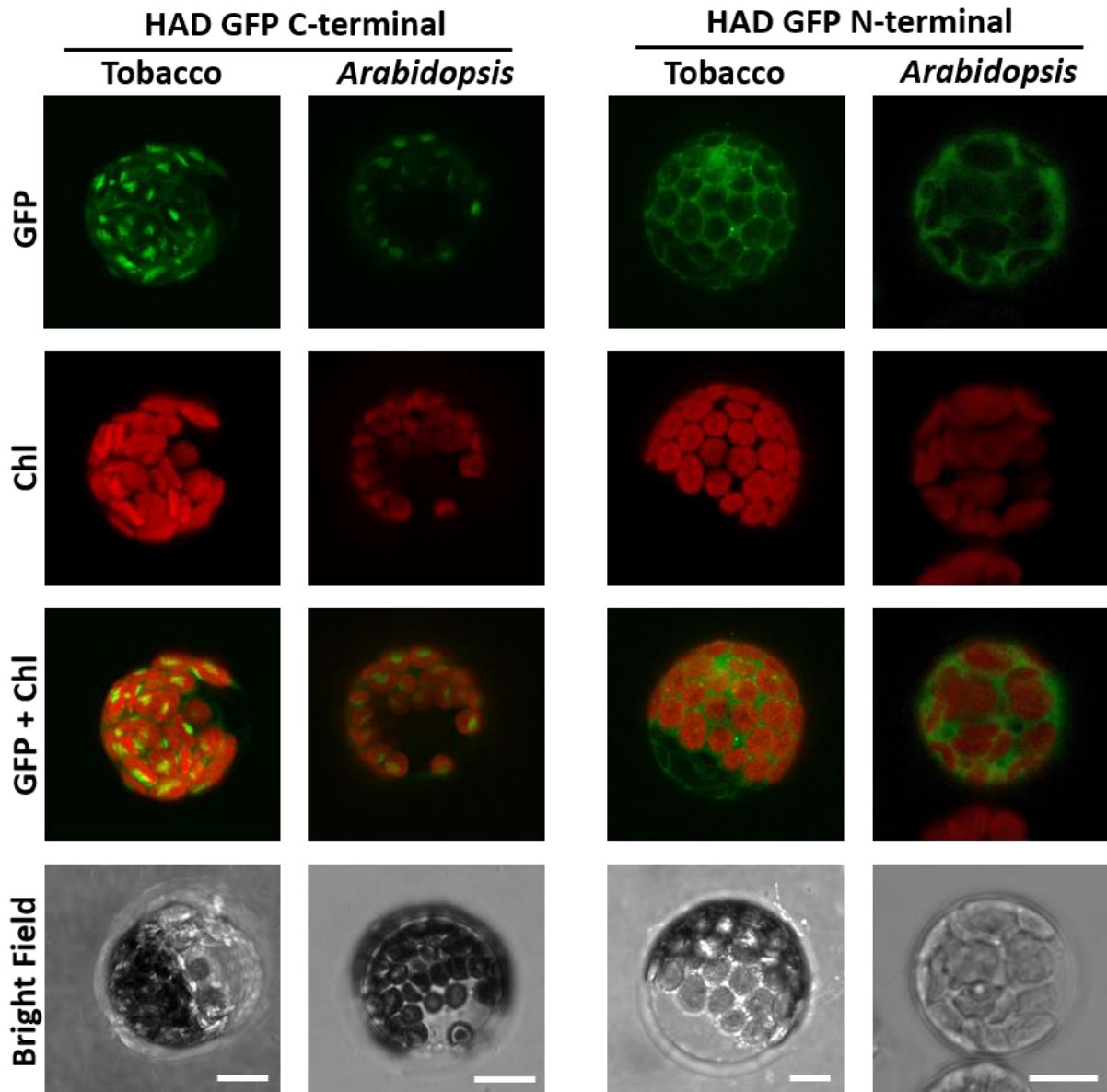


Figure 3-32: HAD-GFP localisation in transiently transformed tobacco and *Arabidopsis* protoplasts. Pictures were taken 16 h after transformation with a confocal laser microscope (Leica TCS SP5 2). Scale bar = 10 μ m

3.8.4 Haloacid dehalogenase-like hydrolase superfamily

HAD belongs to the Haloacid dehalogenase-like hydrolase (HAD-like) superfamily (HADSF). Members of this family share a conserved α/β -domain. This domain is called hydrolase fold and has similarity to the Rossmann fold (Burroughs *et al.*, 2006). Despite its name, this superfamily consists predominantly of phosphatases (~ 79 %) and ATPases (~ 20 %) and also includes members which are phosphonates, phosphomutases, phosphomannomutases and dehalogenases (Koonin and Tatusov, 1994; Kuznetsova *et al.*, 2015).

The HADSF represents the largest superfamily of phosphatases in all organisms (Kuznetsova *et al.*, 2015). In Databases, the superfamily (Interpro IPR036412) is represented by 725 780 sequences of proteins which are involved in a variety of cellular processes (Mitchell *et al.*, 2019).

In *Arabidopsis*, 156 genes coding for HAD-like proteins (excluding splice variants) could be identified in the InterPro database (Mitchell *et al.*, 2019).

3.8.5 Conserved domains of HAD

NCBI CD-Search (Conserved Domain-Search) was used to identify conserved domains in the HAD amino acid sequence. It is a web-based tool for the detection of conserved domains in protein sequences and uses RPS-BLAST to compare query protein sequences against conserved domain models. If CD-Search finds a specific hit, there is high confidence in the association between the protein query sequence and a conserved domain (Marchler-Bauer *et al.*, 2017; Marchler-Bauer and Bryant, 2004).

Figure 3-33 shows the CD-Search concise results display output, including the best scoring domain models. The CD-Search identified the four highly conserved sequence motifs of the HADSF within the HAD query sequence and confirmed HAD as a member of this superfamily. In addition, CD-Search found a specific hit carrying the information that the HAD protein belongs to the HADSF subfamily IA-v1.

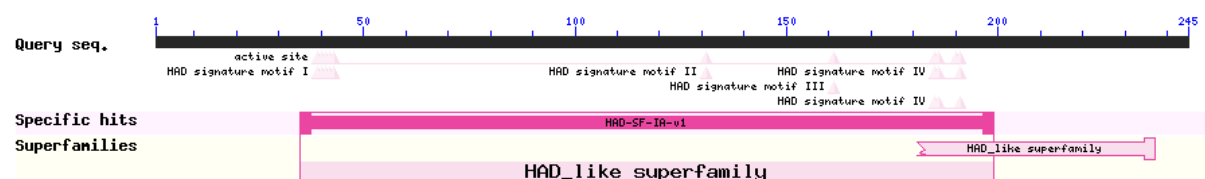


Figure 3-33: Result of the NCBI CD-Search. Blue Numbers above query sequence (black bar) indicate amino acid position. Small triangles beneath query sequence indicate amino acids involved in conserved sites. Specific hit is visualised as a bright pink bar. Superfamilies to which specific hit belongs to is shown in pastel pink colour.

HAD members of the subfamily I are characterised by a small α -helical cap between loop 1 and loop 2 of the core domain. According to TIGRFAM, subfamilies IA and IB are separated based on an apparent phylogenetic bifurcation. The “v1” is short for “variant 1” and describes that the third motif fits the variant form hhhhsDxxx(x) where “s” refers to a small amino acid

and “h” do a hydrophobic one. In *Arabidopsis*, HADSF subfamily IA is currently represented by 19 proteins (IPR006439, Mitchell *et al.*, 2019, Krishnakumar *et al.*, 2015). Eight of these 19 members are characterised more or less in detail, yet. The characterised proteins, their molecular functions, corresponding GO biological processes and literature are shown in Table 3-15.

Table 3-15: Characterised members of the HADSF subfamily 1A in *Arabidopsis*.

Gene symbol	TAIR ID	Molecular function	GO process	Literature reference
SOQ1	AT1G56500	-	light harvesting efficiency	Brooks <i>et al.</i> , 2013
FHY1	AT1G79790	Flavin mononucleotide hydrolase	Riboflavin biosyn-thesis	Rawat <i>et al.</i> , 2011
FHY	AT4G21470	Bifunctional riboflavin kinase/FMN phosphatase	Riboflavin biosyn-thesis	Sandoval and Roje, 2005
GPP1	AT4G25840	Glycerol-3-phosphatase	glycerol biosynthetic process	Caparrós-Martín <i>et al.</i> , 2007
GPP2	AT5G57440	Glycerol-3-phosphatase	glycerol biosynthetic process	Caparrós-Martín <i>et al.</i> , 2007
CBBY	AT3G48420	xylulose-1,5-bisphosphate (XuBP) phosphatase	-	Bracher <i>et al.</i> , 2015
SGPP	AT2G38740	phosphosugar phosphatase	-	Caparrós-Martín <i>et al.</i> , 2013
PYRP2	AT4G11570	5-amino-6-(5-phospho-D-ribitylamino)uracil phosphatase	Riboflavin biosynthesis	Sa <i>et al.</i> , 2016

Although the relationship between protein homology and function is complex, proteins with homologue sequences and thus similar structure often have similar features. HAD was described as a homologue to GPP1 and GPP2 before (Caparrós-Martín *et al.*, 2013). GPP1 (glycerol-3-phosphatase 1) is localised in mitochondria and was shown to dephosphorylate glycerol-3-phosphate and 5-amino-6-ribitylamino-2,4(1H,3H) pyrimidinedione 5'-phosphate (ARPP) *in vitro* (Caparrós-Martín *et al.*, 2007; Sa *et al.*, 2016). Moreover, the authors assert that in HAD and GPPs the folding of the predicted cap domains is remarkably similar (Caparrós-Martín *et al.*, 2013).

Although Caparrós-Martín *et al.* described HAD as a homologue of GPP1 and GPP2, the pairwise sequence alignment resulted in a calculated sequence identity of only 17.6 % between HAD and GPP1. HAD and GPP2 share with 18.1 % only slightly more identity (for details see 6.4 in the appendix). However, the findings that HAD belongs to the same HADSF subfamily IA and has conserved residues besides the HADSF motifs might point to a possible role of HAD as a phosphatase.

3.8.6 HAD comparison to characterised PLP phosphatases

The HADSF also includes members which are described as pyridoxal 5'-phosphate phosphatases (PLPPs). An example is the human PDXP (HADSF IIA), which, to a lesser extent, also dephosphorylates PNP and PMP (Jang *et al.*, 2003). Recently, a new PLPP has been identified and characterised in tobacco (NtPLPP1; HADSF IIA) and thereby in plants for the first time (ShuoHao *et al.*, 2019). ShuoHao *et al.* have stated that NtPLPP1 exhibits high homology to human PDXP and another PLPP from mouse, thereby forming a phylogenetic group, leaving other related plant phosphatases on another branch. The authors suggested a chloroplastidial localisation based on GFP localisation studies. Furthermore, they have measured the maximum catalytic activity for recombinant NtPLPP in *E. coli* with PLP as substrate at pH 7.5 and showed that NtPLPP requires divalent ions for activity, preferential Mg^{2+} . Although NtPLPP sequence shares only ~ 35 % homology with the human PDXP, properties as pH optimum, metal requirement, the substrate and inhibitors of purified NtPLPP were similar to PDXP. However, the measured NtPLPP K_m value of 0.45 mM was much higher than K_m values of human PDXP (1.5 -2.5 μM) (ShuoHao *et al.*, 2019; Jang *et al.*, 2003).

Because *er-ant1* mutants showed increased biomass production on agar plates containing pyridoxine (PN; Figure 3-10), one might envision that HAD acts in vitamin B₆ metabolism, and more precisely in the dephosphorylation of the vitamers.

Pairwise sequence alignments were performed to investigate if the HAD protein sequence shares similarities with the recently identified PLP phosphatase from tobacco (ShuoHao *et al.*, 2019).

The alignment demonstrates that PLPP from *N. tabacum* lacks the HADSF motif I (DxD) (Figure 3-34). Furthermore, it was not possible to align motifs II, since motif II is represented

in HAD by a threonine (T) and in PLPP by a serine (S). Motif IV is not highlighted as the program alignment failed due to the general difference of the two sequences. In summary, the alignment of these two protein sequences resulted in an identity of only 13.4 %, which was even lower than the percent identity of HAD to GPPs.

```

                *           20           *           40           *           60
PLPP_N.t. : MIGRCVSAQSSKPNELKFQTLNGIQEIAETRRFKAWFLDQFGVLDHGKQYPYGAISTLEKIAT : 63
At2g33255 : -----MTFLLSRTEFISITLRPSCSTSMAN----- : 24

                *           80           *           100          *           120
PLPP_N.t. : YGAKMVTIVSNSSFRASTTIEKTRSLGFLPSIFIGAITSGEITHTQYLQFRDLAWEASTGRSCHI : 126
At2g33255 : -----LITNAKTRLRGVVFLMDGTLTVEVIDEFAAMYRAVLGEDAYKRRIKAESPFGIDILHHI : 81

                *           140          *           160          *           180
PLPP_N.t. : MTWSDRCAISLPSLGLIEVVENAQGADFILAHGTEALGLSSGAALEMKLLDLEKILEQCCKTKI : 189
At2g33255 : ESWSP----DKQCKAYEIIADYE-----KQGIDKIQIMPGLAEICGFLDSKKIKRGLITRNV : 134

                *           200          *           220          *           240          *
PLPP_N.t. : FMVVANPDFVTVFVRALRVMPGTLAATYEKLGGEVQWVGKPKTIYKSAMKMAAEDASDCIAT : 252
At2g33255 : QKATD-----IFHQRFEVIFSEALGRETRPYK-----PNPDELIHICST--WLIQPNVVMV : 184

                260           *           280           *           300           *
PLPP_N.t. : GDSLHHDIKGANFAGIASAFITTCGIHATELGLLKFGEVADDNSIHALALQNNAHPTVYVIPSFT : 315
At2g33255 : GDSIKDEIACGKFAQAFTCLLLETGRYGPDLFVSVSGLQDFKVDLSLSKIQLNLLLETNEDINP-- : 245

```

IV

Figure 3-34: ClustalW alignment of the predicted amino acid sequences of PLPP from *N. tabacum* (NtPLPP1) and HAD (AT2G33255). Residues identical or with similar properties among sequences are indicated by black shading. Residues not identical are highlighted by different shading (grey/white). The red box marks the conserved HADSF motifs IV (E/DD, GDxxxD, or GDxxxxD). Dashes represent introduced gaps for alignment improvement. Numbers on the right indicate amino acid positions.

Beside the beforementioned characterised PLPP enzymes, another member of the HADSF from yeast has been shown to exhibit phosphohydrolase activity against PLP (Kuznetsova *et al.*, 2015). This protein, YOR131C, is still annotated as a putative uncharacterised hydrolase (UniProt Q12486) (The UniProt Consortium, 2019). Although YOR131C shares 30 % sequence identity with the yeast phosphoglycolate phosphatase PHO13 and only 20 % identity to human PDXP, it clearly uses PLP and not phosphoglycolate as substrate (Kuznetsova, 2009; Kuznetsova *et al.*, 2015). YOR131C exhibits a higher affinity for PLP than NtPLPP1 (K_m : 70 versus 450 μ M) but lower affinity than human PDXP (1.5 - 2.5 μ M) (ShuoHao *et al.*, 2019; Jang *et al.*, 2003).

All in all, YOR131C seems to function analogous to the PLPPs from human, mouse and tobacco. Therefore, it was reasonable to analyse whether HAD might show similarities to YOR131C. For that, a pairwise sequence alignment was performed, and percent sequence identity was calculated with EMBOSS Needle.

The pairwise sequence alignment of HAD and YOR131C already displays higher similarity than the HAD alignments with PLPP from *N. tabacum* (3.8.6) or GPPs from *A. thaliana* (3.8.5) (Figure 3-35). This observation is supported by the calculated 32.1% sequence identity between HAD and YOR131C.

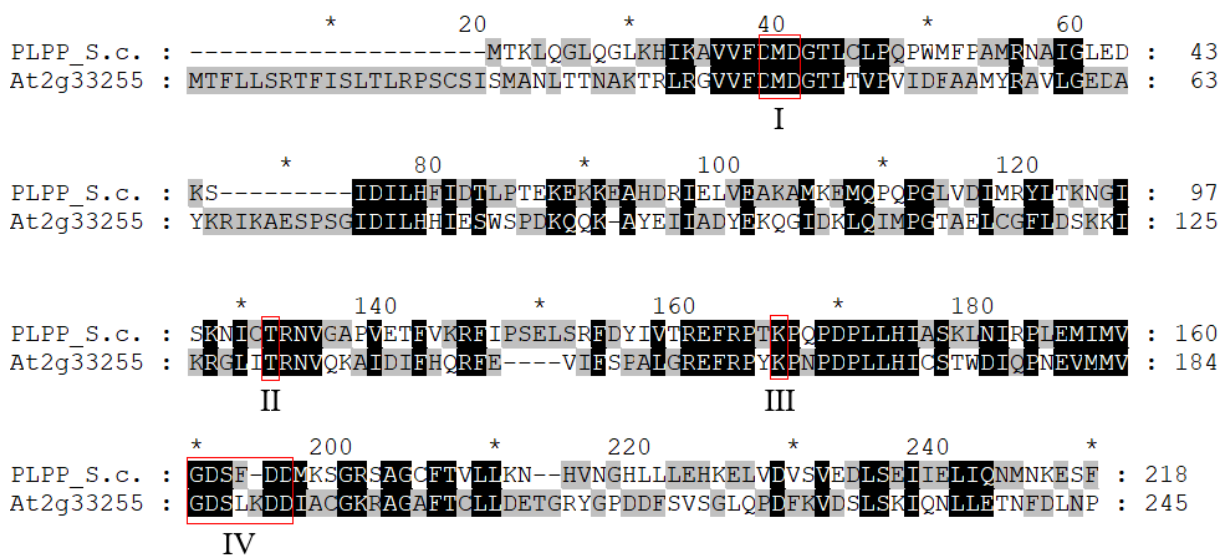


Figure 3-35: ClustalW alignment of the predicted amino acid sequences of PLPP from *S. cerevisiae* (YOR131C) and HAD (AT2G33255). Residues identical or with similar properties among sequences are indicated by black shading. Residues not identical are highlighted by different shading (grey/white). Red boxes mark conserved HADSF motifs I-IV (I: Dx/D; II, T/S; III: K/R; IV: E/DD, GDxxx/D, or GDxxxx/D). Dashes represent introduced sequenced gaps for alignment improvement. Numbers on the right indicate amino acid positions.

3.8.7 Heterologous expression and purification of the recombinant HAD

Next, it was necessary to test, whether HAD acts as a phosphatase and particularly whether it uses PLP as substrate. For this, the HAD was expressed in the heterologous *E. coli* system, purified and used for enzyme activity tests. This approach was already successfully applied for the characterisation of other HADSF members (Caparrós-Martín *et al.*, 2013).

The HAD coding region was inserted into the pET16b vector in frame with the 10x histidine-tag (His-Tag) coding sequence. The His-Tag allows analysing heterologous HAD expression by immunostaining and protein purification via IMAC. Next, the expression construct was

transformed into competent *E. coli* Rosetta cells. In pET16b, protein expression is under the control of the *lacI*-promoter and thus inducible by IPTG. Expression was induced during the exponential growth phase cells. About 12 hours post induction, cells were harvested and disrupted. A possible formation of inclusion bodies was analysed by centrifugation of non-soluble proteins and SDS-PAGE.

The high amount of proteins in lane 1 (Figure 3-36) demonstrates that a large proportion of the recombinant protein formed insoluble aggregates. However, for functional analysis, the soluble HAD was required. Therefore, the fraction of soluble proteins was applied to the IMAC. By this procedure, the small amount of soluble HAD could be separated from the remaining soluble *E. coli* proteins (Figure 3-36).

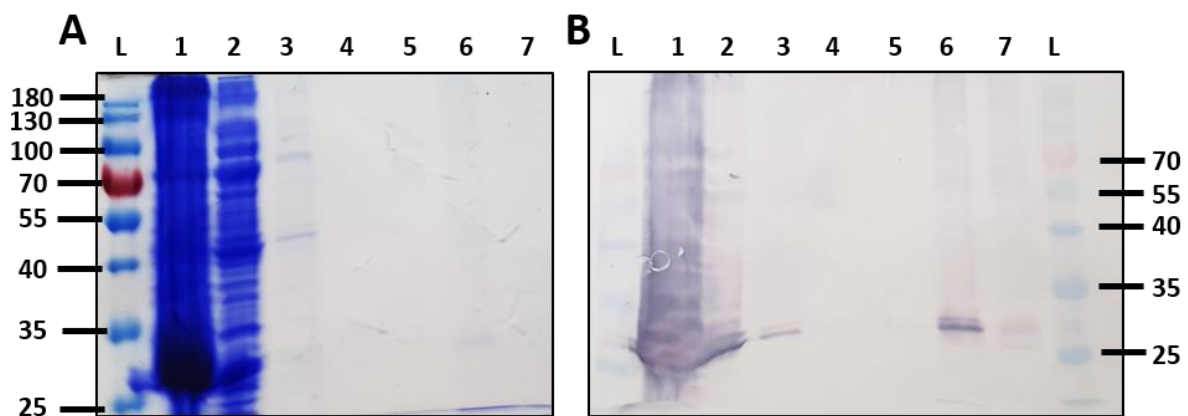


Figure 3-36 Purification of HAD after heterologous expression in *E. coli* Rosetta cells. (A) Separation of IPTG-induced *E. coli* cells before and after purification via SDS-PAGE. (B) Protein blot analysis of IPTG-induced cells before and after purification using anti-His-tag antibody (1st antibody) and anti-mouse antibody (2nd antibody) followed by NBT/BCIP staining. Numbers at image border indicate the molecular weight of the protein (kDa). L: Protein Ladder (PageRuler); 1: Lysed pellet of IPTG-induced *E. coli* cells; 2: flow through; 3: binding buffer 1; 4: binding buffer 2; 5: wash buffer; 6: 1st eluate; 7: 2nd eluate.

Immune-staining detected one major band of a molecular weight between 25 and 35 kDa in the inclusion-body fraction, as well as in the flow through, first washing and the eluate of the IMAC (Figure 3-36 B; line 6). The calculated molecular weight of HAD with His-tag is ~ 30 kDa. This demonstrates that recombinant HAD was expressed and successfully purified.

3.8.8 Substrate specificity of HAD

A previous study analysed HAD as a homologue of GPP1 and GPP2. Although GPP substrates could be identified, HAD did not show activity with any of the applied substrates

(Caparrós-Martín *et al.*, 2013). To investigate whether the recombinant and purified HAD acts as a phosphatase, enzyme activity assays were performed with different putative substrates, including also several of the study performed by Caparrós-Martín *et al.* The enzyme assay was stopped directly, to determine possible free phosphate already in the reaction mixture, and after one hour. The free phosphate in the solution was analysed colourimetrically.

For most tested substrates, no phosphate release could be detected (Table 3-16).

Table 3-16: Hydrolytic activity of HAD on different substrates.

Tested substrate	Phosphate release
6-phosphogluconic acid	-
D-fructose-6-phosphate	-
D-fructose-1,6-bisphosphate	-
D-glucose-6-phosphate	-
α -D-glucose-1-phosphate	-
glyceraldehyde 3-phosphate	-
dihydroxyacetone-phosphate	-
phosphoenolpyruvate	-
adenosine triphosphate	-
pyridoxal 5'-phosphate	+

(+) indicates released phosphate, (-) indicates no released phosphate after 1 h dark incubation at 23° C. Assays were performed with 10 mM substrate and 25 μ g purified HAD protein per ml.

However, for PLP substantial increase in colour intensity (1 h, Figure 3-37) became visible within the phosphate determination test.

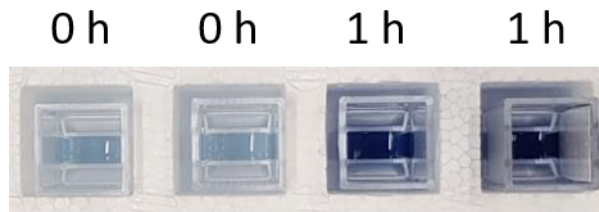


Figure 3-37: Appearance of phosphate determination test solution in cuvettes after HAD phosphatase activity assay. For the 0 h samples, the phosphatase activity assay was stopped with perchloric acid directly after starting. For 1 h samples, the assay was stopped after 1 h dark incubation at 23°C. The assay was performed with 10 mM PLP as substrate and 25 μ g purified HAD protein per ml.

Next, a control experiment was conducted to verify that the increased colour intensity after one hour was due to HAD phosphatase activity against PLP. For that, the phosphatase activity of the purified HAD protein was determined before and after heat inactivation. Because weak blue staining was already visible when the reaction was directly stopped (0 h Figure 3-37), two further control samples were included, to identify the source of the free phosphate in the samples. The released phosphate was quantified photometrically. Since the colour of the phosphate determination samples after one hour was very intense, the reactions in this experiment were already stopped after ten minutes.

Approximately 12 nmol free phosphate was quantified in samples which contained HAD and 2mM PLP. By contrast, only 1 nmol of free phosphate was measured in samples which contained the boiled HAD protein plus PLP or PLP alone, but not in samples with purified HAD protein without substrate (Figure 3-38). This clearly demonstrates that PLP hydrolysis is due to the enzymatic activity of the HAD. Moreover, the PLP is contaminated with traces of phosphate.

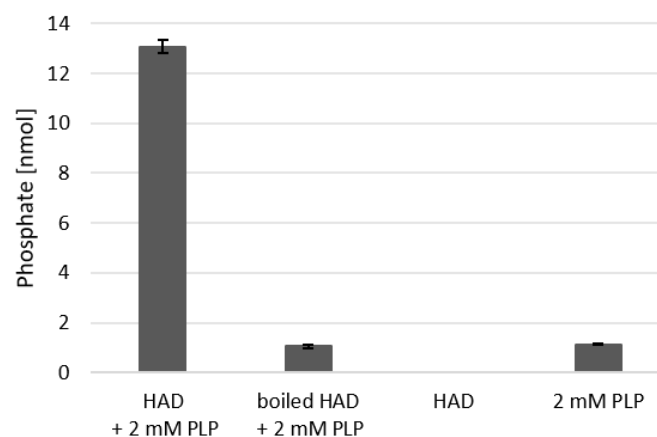


Figure 3-38: Photometrically determined free phosphate of different enzyme activity approaches. All reactions were stopped with perchloric acid 10 min after starting enzyme activity assay. 200 μ l of the assay was used for colourimetric phosphate approach. Free phosphate was measured photometrically as an increase in absorbance at 705 nm. Shown are mean values of four replicates, \pm SE (HAD + 2mM PLP; boiled HAD + 2mM PLP) and two replicates (HAD; 2mM PLP).

The HADSF members, except 2-haloacid dehalogenases, use magnesium as a cofactor during catalysis (Peeraer *et al.*, 2004). This is also true for YOR131C from yeast, which shows phosphatase activity against PLP (Kuznetsova *et al.*, 2015). Therefore it was tested, whether PLP phosphatase activity of HAD is also Mg^{2+} -dependent. An enzyme assay with and without the addition of Mg^{2+} was conducted, and the time-dependent release of phosphate was determined photometrically (Figure 3-39). A constant increasing release of phosphate was measured in the presence but not in the absence of 5mM $MgCl_2$.

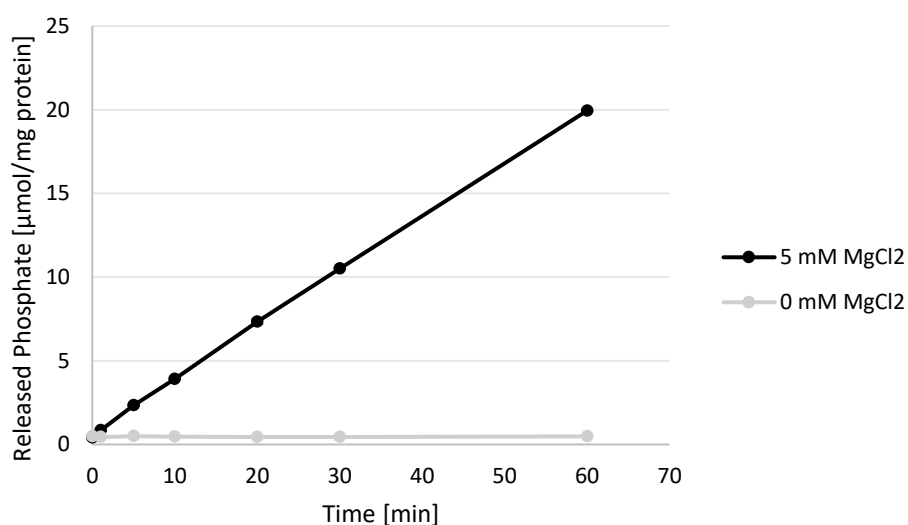


Figure 3-39: Mg^{2+} -dependency of HAD phosphatase activity. Phosphatase enzyme assay was performed with 2 mM PLP as substrate and 25 μ g purified HAD protein per ml in the presence and absence of 5 mM $MgCl_2$. Shown are mean values of five replicates, \pm SE (5mM $MgCl_2$) and two replicates (0mM $MgCl_2$).

The results demonstrate that the HAD is highly specific because among 14 different tested phosphorylated compounds (Table 3-16) (Caparrós-Martín *et al.*, 2013) only PLP was accepted as a substrate. Moreover, its activity relies on Mg^{2+} as a cofactor (Figure 3-39).

4 Discussion

Photorespiration was often described as a wasteful but necessary process in plants. However, this view begins to change: Recent studies demonstrate that photorespiration is not only essential for recycling toxic 2-phosphoglycolate but also plays additional roles in plants. However, it is unclear how impaired ATP/ADP translocation at the ER can cause a defect in photorespiration. A possible connection between these two processes is not directly evident. Therefore, the full picture of photorespiration is apparently much more complex than expected earlier. This study aims to gain deeper insights into the phenotype of *er-ant1* mutants and to approach a possible connection to photorespiration. Therefore, the new findings are discussed in the context of energy metabolism and/or photorespiration.

4.1.1 From PLP to photorespiration

The group of B₆ vitamins is composed of six vitamers: Pyridoxal (PL), pyridoxine (PN) and pyridoxamine (PM), and their phosphorylated forms PLP, PNP and PMP (Mooney and Hellmann, 2010). The *de novo* synthesis of the major active form PLP as well as its salvage into the other vitamers takes place in the cytosol. The non-phosphorylated forms can pass membranes via diffusion and by this also enter the chloroplast (Rueschhoff *et al.*, 2013). Here, they become phosphorylated by the chloroplastidic pyridoxal kinase SOS4.1, which is a splice variant of the cytosolic SOS4, and by this trapped in the stroma (Rueschhoff *et al.*, 2013). In this context it is important to mention that mutant plants lacking stromal SOS4.1 or with defects in cytosolic PLP synthesis show stunted growth, are chlorotic and show higher sensitivity to many stressors and thus in many essential aspects resemble *er-ant1* mutants.

Up to now, there is no information about the content of the different B₆ vitamers in *er-ant1*. However, several facts suggest that *er-ant1* suffers from PLP deficiency in chloroplasts. First, EMS mutagenesis and analyses of T-DNA insertion mutants revealed that missing HAD-type phosphatase activity alleviates the *er-ant1* phenotype. This enzyme resides in the chloroplast stroma (3.8.3.2) and is capable of dephosphorylating PLP (3.8.8). Consequently, missing activity of this phosphatase counteracts PLP dephosphorylation, which supports its trapping in the stroma. This result also suggests that SOS4.1 is functional in *er-ant1* chloroplasts.

Second, exogenous supply of pyridoxine (PN) was shown to increase biomass production of *er-ant1* but not of the wild type (Figure 11). After diffusion into the cell, PN can be converted into all other vitamers via the cytosolic salvage pathway (Colinas *et al.*, 2016). Consequently, PN feeding can enhance PLP supply to various enzymes in the cytosol. Moreover, the cytosolic conversion of PN into PL, its diffusion into the chloroplast and its phosphorylation by SOS4.1 may support PLP-dependent processes in the stroma.

Third, impaired chlorophyll biosynthesis of *er-ant1* (3.5.2) is also in line with a reduced PLP availability in the stroma. Mutant plants impaired in PLP synthesis (lacking PDX2) also show substantially reduced chlorophyll levels (Tambasco-Studart *et al.*, 2007). This is because first step in chlorophyll biosynthesis, the generation of 5-aminolevulinic acid (ALA), is catalysed by the PLP-dependent enzyme glutamate 1-semialdehyde aminotransferase (GSA1) (Tanaka *et al.*, 2011; Ilag *et al.*, 1994). Interestingly, the *GSA1* transcript level is lower in *er-ant1* but not in other strong photorespiration mutants (data not shown; Eisenhut *et al.*, 2017). Glutamate is an early precursor of ALA, and its reduced availability in *er-ant1* mutants might additionally impair chlorophyll synthesis. Therefore, the decrease in chlorophyll of *er-ant1* might be due to a limited PLP and glutamate availability in the chloroplast.

Fourth, missing HAD-activity in *er-ant1* led to partial restoration of the chlorophyll content and plant growth (*er-ant1* suppressor line 6.3, Figure 3-12 & Figure 3-13). Therefore, lesser PLP dephosphorylation in the *er-ant1* chloroplast seems to be beneficial for chlorophyll synthesis and the overall development of the mutant.

Notably, in *had-2 x er-ant1*, glycine levels remained more or less at *er-ant1* level, whereas the arginine levels resembled those of the wild type (Table 3-14). The decrease in arginine content in this mutant is probably not due to a stimulation of arginine catabolism in mitochondria (Ochocki *et al.*, 2018). This is because it is hard to imagine how missing PLP dephosphorylation in chloroplasts may stimulate PLP provision to other organelles. Alternatively, arginine accumulation might be prevented due to the restoration of the chlorophyll level, which would lead to higher photosynthetic activities and carbon fixation rates. The elevated carbohydrate availability thus shifts amino acid metabolism from the nitrogen store arginine to the biosynthesis of other amino acids. This could explain how missing HAD-activity can decrease the arginine accumulation in *er-ant1* to wild-type level.

Moreover, in *Arabidopsis*, PLP-dependent enzymes catalyse more than 140 reactions and are involved in essential cellular pathways (Colinas *et al.*, 2016; Parra *et al.*, 2018). Not only the PLP-dependent chlorophyll biosynthesis but also PLP-dependent amino acid metabolism is apparently disturbed in *er-ant1* (Figure 3-1; Figure 3-13) which might be a further hint towards an impaired PLP metabolism in this mutant.

For example, the arginine accumulation in *er-ant1* (Figure 3-1 F) might be due to a decreased PLP-dependent arginine catabolism in mitochondria (Ochocki *et al.*, 2018). In fact, *Arabidopsis* mutant plants with decreased Vitamin B₆ levels also accumulate arginine (Leuendorf *et al.*, 2010). Given that PLP provision to mitochondria also takes place via diffusion, PLP deprivation in the matrix may result from a limited availability of non-phosphorylated vitamers in the cytosol.

PLP is also of importance during photorespiration; it serves, for example, as a cofactor of the P subunit of the GDC (Heldt and Piechulla, 2012; Kandoth *et al.*, 2017). Using a mathematical model of mitochondrial GDC and SHMT, Nijhout *et al.*, 2009 have shown that PLP deficiency correlates with linearly increasing glycine levels while serine levels are only marginally affected (Nijhout *et al.*, 2009). Moreover, *Arabidopsis* mutant plants impaired in vitamin B₆ synthesis also accumulate glycine (Leuendorf *et al.*, 2010). Therefore, the increased glycine level and unchanged serine amounts in illuminated *er-ant1* leaves (Figure 3-1 A & B) may, in fact, result from insufficient PLP supply to the GDC. This may also be causative for the blocked photorespiration in *er-ant1* mutants.

The proposed defects in PLP-dependent processes of mitochondria (glycine decarboxylation and arginine catabolism) and chloroplasts (chlorophyll biosynthesis) are suggestive for an impaired production of non-phosphorylated vitamers in the cytosol. This is also in line with the observation that missing HAD-type phosphorylase activity has a positive impact on PLP-dependent processes in the chloroplast, whereas glycine accumulation remains high.

Also, the significantly decreased glutamate levels in illuminated leaves of *er-ant1* (Figure 3-1 D) may at least partially be due to generally reduced PLP levels in *er-ant1* mutants. In *Arabidopsis*, the *de novo* synthesis of PLP involves two PLP-synthases (PDXs). PDX2 hydrolyses glutamine to glutamate and ammonia (Tambasco-Studart *et al.*, 2007). Therefore, reduced glutamine hydrolysis via PDX2 may contribute to the reduced glutamate level of *er-ant1*. The

ammonia of the PDX2 reaction is used by PDX1 to form PLP from ribose-5-phosphate (RBP) and glyceraldehyde-3-phosphate (GAP). Since *er-ant1* mutants are downregulated in the expression of Calvin cycle enzymes (Figure 3-4) and contain lesser sugar than the wild type (Hoffmann *et al.*, 2013), it is possible that the limited availability of phosphorylated sugar precursors generally limits cytosolic B₆ vitamer production in this mutant.

4.1.2 From photorespiration to redox homeostasis

Conditions that increase the rate of photorespiration, such as heat and highlight, can induce adverse redox imbalances and fast alterations in the energy state of the cell: When stomata close, the CO₂ concentration decreases which rapidly leads to over-reduction of the chloroplast (Keech *et al.*, 2017). This is accompanied by an increase in the NADH/NAD and ATP/ADP ratio in the chloroplast, the cytosol and mitochondria (Igamberdiev *et al.*, 2001; Keech *et al.*, 2017).

In mitochondria, glycine is oxidised by the GDC, which leads to the release of NADH. The low-CO₂-induced increase of the mitochondrial NADH/NAD⁺ ratio is apparently directly coupled to mitochondrial glycine oxidation because the ratio was markedly lower after application of a GDC inhibitor (Wigge *et al.*, 1993).

er-ant1 mutants were reported to exhibit reduced GDC activity when compared to the wild type (Hoffmann *et al.*, 2013). Since photorespiratory glycine oxidation represents the major flux through mitochondria in the light (Bykova *et al.*, 2014), one might expect that *er-ant1* also shows a reduced NADH/NAD⁺ ratio when the CO₂ availability decreases. However, gene expression of both matrix-facing NAD(P)H dehydrogenases NAD1 and NAD2 was upregulated in *er-ant1* mutants (Table 3-7), which generally points to an elevated need for dissipating reducing equivalents and thus for higher NADH/NAD ratios.

In *er-ant1* mutants, the activity of GDC is decreased due to posttranslational modifications (Hoffmann *et al.*, 2013) and possibly due to limited PLP availability. GDC is feedback inhibited by its product (Bykova *et al.*, 2014) and given that *er-ant1* exhibits too high NADH/NAD ratios in mitochondria, the high NADH level might additionally reduce its activity. Notably, the mitochondrial malate dehydrogenase (mMDH) is supposed to play a crucial role in preventing

GDC inhibition by maintaining low levels of NADH (Bykova *et al.*, 2014). Interestingly, both genes encoding mMDHs in *Arabidopsis* are downregulated in *er-ant1* (Table 3-8).

Besides NAD(P)H dehydrogenases and mMDH, an additional important way to prevent over-reduction of the electron transport chain and corresponding ROS formation in mitochondria is the action of the alternative oxidase (AOX) (Vishwakarma *et al.*, 2015). To enable flexible adaptation of the cellular energy state towards changing conditions, AOX activity is strictly regulated at transcriptional, translational and post-translational level (Selinski *et al.*, 2018). It has been shown, that *er-ant1* mutant plants possess elevated ROS levels, and it was proposed that GDC of *er-ant1* is subject of oxidative modifications (Hoffmann *et al.*, 2013). The upregulation of several AOX isoforms is indicative for an over-energisation of the electron transport chain in *er-ant1*, which implies that the elevated ROS levels in *er-ant1* are generated in mitochondria.

Apart from its well-known function as a safety valve (Day *et al.*, 1996; Lambers, 1982) AOX were recently shown to play a more general role as they seem to be of high importance in balancing the mitochondrial ATP/ADP ratio (Selinski *et al.*, 2018). Therefore, the upregulation of AOX expression could also hint towards an elevated ATP/ADP ratio in *er-ant1* mitochondria. However, how the absence of an ER-located ATP/ADP transporter can cause such an increase in mitochondria becomes not immediately evident.

Inhibition of the mitochondrial TCA cycle enzyme aconitase results in citrate accumulation, rearrangement of metabolic fluxes and strong retrograde responses, including the induction of *AOX1A* expression (Wagner *et al.*, 2018). Therefore, the substantial accumulation of citrate (Hoffmann *et al.*, 2013) and the stimulation of the expression of *AOX1A* might be indicative for reduced fluxes via the TCA cycle in *er-ant1*. In fact, several TCA enzymes are inhibited by high ATP/ADP or NADH/NAD ratios (Berg *et al.*, 2002). Therefore, the citrate accumulation is a further hint towards an elevated energy and redox state in *er-ant1* mitochondria.

4.1.3 Hypoxia

Absence of ER-ANT1 is apparently associated with a high mitochondrial ATP/ADP ratio, whereas energy depletion in mitochondria seems to increase ER-ANT1 activity (Table 3-2). Since oxidative phosphorylation relies on O₂, hypoxia ultimately leads to blockage of

mitochondrial ATP production (Diab and Limami, 2016). Hypoxia induces multiple significant transcriptional changes, such as increased expression of genes associated with fermentation pathways (Diab and Limami, 2016) but also of *ER-ANT1* (Table 3-2). The increased expression of *ER-ANT1* suggests that ER-ANT1 is of particular importance during hypoxia or even more generally when mitochondrial ATP production is limited.

Interestingly, many transcripts encoding proteins required for fermentation are upregulated in *er-ant1* but not in all other strong photorespiration mutants (Table 3-10). Therefore, some specific alterations in *er-ant1* might provide the signal for the induction of the hypoxia-dependent gene expression already under normoxic conditions. It seems thus possible that *er-ant1* is not able to adapt its metabolism, even more, when real oxygen limitation occurs. The fact that *er-ant1* shoot and root growth on culture plates becomes highly impaired by elevated agar concentrations, known to decrease the diffusion of oxygen, strengthens this hypothesis (Leroch *et al.*, 2008; Hulst *et al.*, 1989).

Gene regulation and the overall survival of plants exposed to hypoxia was shown to rely on the availability of starch (Loreti *et al.*, 2018). The *er-ant1* mutant contains significantly lower levels of glucose, sucrose and starch than the wild type (Hoffmann *et al.*, 2013). Therefore, its growth impairment on increasing agar concentrations may also be due to the generally decreased carbohydrate availability, which might be insufficient for adequate fermentation when truly necessary. Indeed, the growth of the rice *er-ant1* mutant was significantly enhanced by exogenous sucrose supply (Zhang *et al.*, 2016).

The genevestigator perturbation study revealed that *er-ant1* expression is upregulated by heat and downregulated by cold (Table 3-2). This regulation is in line with the importance of ER-ANT1 under hypoxic conditions because the oxygen level in plant tissues is known to decrease with increasing temperatures (Borisjuk and Rolletschek, 2009). In this context, it is also interesting that induction of the expression of the heat shock factor A2 (HsfA2) by anoxia (Banti *et al.*, 2010) is also visible in *er-ant1* under normoxia (data not shown). Moreover, induction of *ER-ANT1* by heat apparently depends on specific heat shock proteins since it does not occur in *hsfa1a/1b* knockout mutants (Busch *et al.*, 2005). When *Arabidopsis* wild-type plants are treated with heat, they tolerate subsequent anoxia better than without heat

treatment (Banti *et al.*, 2010). This ability of heat-dependent acclimation to anoxia is lost in both, *hsfA2* and *hsfA1a/1b*, knockout mutants (Banti *et al.*, 2010).

Another hint for a misbalanced gene expression regulation of *er-ant1* in response to low oxygen is the upregulation of the zinc-finger transcription factor *STOP1* in *er-ant1* but not in the strong photorespiration mutants (data not shown; Eisenhut *et al.*, 2017). *STOP1* regulates the expression of genes encoding metabolic enzymes important for low oxygen tolerance such as enzymes belonging to the GABA-shunt, the glutamate dehydrogenases GDH1 and GDH2 and *HsfA2* (Enomoto *et al.*, 2019). Therefore, the significantly decreased glutamate content in illuminated *er-ant1* leaves could result from an increased flux of glutamate via GDH into the TCA or to the GABA shunt (Figure 3-1). In this context, it is important to note that *STOP1* is coexpressed with *ER-ANT1* during the whole plant development (Genevestigator coexpression study, data not shown).

Interestingly, also a key transcription factor of the ethylene signalling pathway, ETHYLENE INSENSITIVE 3 (*EIN3*), is coexpressed with *ER-ANT1* during development (Genevestigator coexpression study; data not shown). This transcription factor has been shown to promote GDH synthesis during anoxia (Tsai *et al.*, 2016).

In general, the efficiency for ATP production using fermentative pathways to maintain glycolysis is very low and highly carbohydrate-consuming (Diab and Limami, 2016). Consequently, the carbon storage depletes very quickly during hypoxia and ultimately results in carbon starvation (Diab and Limami, 2016). Since hypoxia-associated pathways are apparently upregulated already under normoxia, a prolonged glycolytic activity might explain the reduced sugar and starch levels of *er-ant1*.

Ethanol is a dead-end product in plants and thus results in carbon loss. However, carbon flux may be redirected from ethanolic fermentation to the alanine fermentative pathway via alanine aminotransferase (*AlaAT*) to safe carbohydrates (Diab and Limami, 2016). The corresponding synthesis of alanine from glutamate and pyruvate generates 2-oxoglutarate, which can enter the TCA cycle and provides one additional ATP per metabolised sucrose molecule (Diab and Limami, 2016) Therefore, alanine usually accumulates upon hypoxia (Diab and Limami, 2016). Different to the other hypoxia-associated responses, *er-ant1* does not accumulate alanine but rather shows decreased levels of this amino acid in roots and

illuminated leaves (Figure 3-1 G). In this context, it is important to note that *er-ant1* apparently suffers from general vitamin B₆ deficiency (4.1.1) and that AlaAT uses PLP as cofactor. PLP deprivation thus might be a limiting factor for alanine production in *er-ant1*. However, since starch and sugar levels are already depleted in *er-ant1* mutants, there is probably no carbon left to be saved in the form of alanine. Furthermore, also the precursor glutamate for alanine synthesis is decreased in *er-ant1*. This is in line with the observation, that alanine was increased when *er-ant1* was cultivated at high CO₂ conditions (Figure 3-2) and thereby has higher levels of sugar and starch and glutamate (Data not shown; (Leroch, 2006)).

4.1.4 Amino acid metabolism

Although *er-ant1* shows reduced alanine levels and depletion of sugars and starch, it accumulates arginine (Figure 3-1 F). Because of its highest N/C-ratio amongst the proteinogenic amino acids, arginine could serve to store for excessive nitrogen. Which is in line with the decreased carbohydrate pool and reduced expression of Calvin cycle enzymes (Hoffmann *et al.*, 2013; Figure 3-4).

The transcriptomic analysis revealed that the elevated arginine levels in *er-ant1* most likely not results from a stimulated *de novo* synthesis but rather from decreased arginine catabolism (Figure 3-5). Expression of *ARGAH2*, encoding arginase 2, which catalyses the hydrolysis of arginine to urea and ornithine, is downregulated in *er-ant1* but not in other strong photorespiration mutants (Figure 3-5). Interestingly ornithine, the product of arginine degradation, is further metabolised to glutamate-5-semialdehyde via the ornithine delta-aminotransferase (δ OAT), which is a PLP-dependent enzyme. Therefore, the reduced degradation of ornithine and thus also of arginine might result from a vitamin B₆ deficiency in *er-ant1* mutants. Interestingly, a very recent study revealed that repression of arginase 2 *de facto* allows saving substantial amounts of PLP, at least in human kidney cancer tumours (Ochocki *et al.*, 2018).

The glutamate-5-semialdehyde produced by (δ OAT) is further converted to glutamate (Funck *et al.*, 2008). It seems possible that the decreased glutamate levels in illuminated *er-ant1* leaves are a further consequence of the decreased arginine catabolism. As proline biosynthesis was shown to be independent of glutamate produced by arginine and ornithine

degradation, the unchanged level of proline in *er-ant1* mutants does not oppose this assumption (Funck *et al.*, 2008; Hoffmann *et al.*, 2013).

One might envision that the downregulation of several genes involved in JA-synthesis (Figure 3-6) is linked to the observation that *ARGAH2* is downregulated in *er-ant1*, as *ARGAH2* has been shown to be induced by jasmonate (Brownfield *et al.*, 2008; Jung *et al.*, 2007). Therefore, downregulation of JA-synthesis could support saving PLP due to less arginine catabolism.

Furthermore, JA has been shown to induce expression of *PGDH1* and *PSAT1* (Jung *et al.*, 2007) which are involved in the biosynthesis of serine via the phosphorylated pathway (PPSB) (Figure 3-7). Although serine metabolism is tightly connected with photorespiration, *er-ant1* differs in this context from other photorespiration mutants as the expression of *PGDH1* and *PSAT1* is not changed in *er-ant1* but induced in the strong photorespiration mutants (Table 3-3; Eisenhut *et al.*, 2017).

In *er-ant1*, missing induction of the PPSB would make sense because of several reasons. The PPSB starts with the conversion from 3-phosphoglycerate (3-PGA) to 3-phosphohydroxypyruvate, which is catalysed by *PGDH1*. 3-PGA is apparently decreased in *er-ant1*, possibly due to the depleted carbohydrate pool (Hoffmann *et al.*, 2013) and reduced expression of Calvin cycle enzymes (Figure 3-4). Therefore, missing substrate availability would make the upregulation of *PGDH1* useless. Moreover, induction of *PGDH1* might be even unfavourable, because the catalytic activity of *PGDH* leads to the formation of NADH (Figure 3-7) and would indirectly prevent ATP and NADPH consumption by 3-PGA conversion in the Calvin cycle. This would further increase the ATP/ADP and NADPH/NADP ratios in the chloroplast.

In the second step of the PPSB (Figure 3-7) the PLP-dependent *PSAT1* catalyses the amino group transfer from glutamate to 3-phosphohydroxypyruvate (Wulfert and Krueger, 2018; Ros *et al.*, 2014). However, glutamate and probably also PLP are limited in *er-ant1* (Figure 3-1 D) and the induction of *PSAT1* would further enhance the depletion of these molecules. Because PLP is *de novo* synthesised from carbohydrates, the induction of the PPSB would also indirectly lead to lesser PLP production. Thus, downregulation of JA-synthesis in illuminated leaves of

er-ant1 might prevent induction of the PPSB and by this the further increase of ATP/ADP and NAD(P)H/NAD(P)⁺ ratios, as well as additional glutamate and PLP consumption.

In the strong photorespiration mutants, the stimulation of the PPSB pathway apparently leads to increased serine levels. It is surprising, that although PPSB does not seem to be induced, serine levels in illuminated leaves of *er-ant1* resemble the wild type (Figure 3-1 A), since the photorespiration is supposed to be impaired in *er-ant* (Hoffmann *et al.*, 2013). In general, it might be that the glycolate pathway is still active in *er-ant1* even though photorespiration is somehow defective. Moreover, it is not clear why *er-ant1* plants exhibit elevated serine levels in roots and during the dark phase in leaves. Because of the relevance of the PPSB particularly under non-photosynthetic conditions, the corresponding increase might result from nocturnal and root-specific stimulation of this pathway. However, it is also imaginable that in non-photosynthetic tissues of *er-ant1*, the consumption of serine is lower than in the wild type. This might also apply to the photosynthetic tissues. Under the assumption that the glycolate pathway is impaired in *er-ant1*, lower serine consumption in the illuminated leaves might lead to serine levels similar to that of the wild type.

Serine synthesised by the PPSB can act, for example, as a precursor for the synthesis of homocysteine in the plastid (Okamura and Hirai, 2017). After transport to the cytosol, homocysteine is converted into methionine catalysed by methionine synthases (MS) (Wulfert and Krueger, 2018). Indeed, expression of *MS1* and *MS2*, encoding the two cytosolic isoforms of methionine synthase, is downregulated in *er-ant1* but not in all strong photorespiration mutants (Table 3-3). Therefore, it is imaginable that serine consumption in *er-ant1* is, among others, reduced by decreased synthesis of methionine.

Interestingly, only about 20 % of the plant methionine is incorporated into proteins, whereas 80 % is activated to S-adenosylmethionine (SAM) (Hesse *et al.*, 2004). The fact that the expression of three out of four SAM synthases was downregulated exclusively in *er-ant1* might be due to less methionine availability.

4.1.5 ER-ANT1 and cancer

Interestingly, the new findings concerning the *er-ant1* mutant somehow remind to the metabolic situation in cancer cells. First, under normoxic conditions, *er-ant1* shows increased

transcription of genes encoding proteins involved in fermentation. Notably, this does not apply to all strong photorespiration mutants (Table 3-10). Already in 1924, Otto Warburg observed that also cancer cells tend to “ferment” glucose even under normoxic conditions to support oxidative phosphorylation in mitochondria. The combined use of glycolysis and oxidative phosphorylation was recently shown to be due to a specific reprogramming of the cancer cell (Cesari et al., 2014). The reason for this mechanism is still elusive. At first glance, one might assume that the exclusive use of oxidative phosphorylation might be better suited to fulfil the enormous energy demands of proliferating cells.

Second, expression of *ER-ANT1* is reduced by MeJA treatment (Table 3-2) and transcripts for JA biosynthesis were downregulated in the *er-ant1* mutant but not in other strong photorespiration mutants (Figure 3-6). Generally, JA and MeJA fulfil an important role in plant development and growth. In mammalian cancer cells, MeJA has been shown to suppress growth and induce cell death, whereas other cells remain unaffected (Cesari et al., 2014). In the tumour cells, MeJA treatment results in ROS accumulation and dissociation of hexokinases from voltage-dependent anion channels (VDACs), which leads to the reduction of intracellular ATP levels and induction of fermentation (Cesari et al., 2014). This finally causes a mitochondrial burst and cell death (Cesari et al., 2014).

Interestingly, the hypoxia-induced transcriptional responses regarding energy production and consumption are conserved between animals and plants (Diab and Limami, 2016). Therefore, one might speculate that the MeJA-dependent effects on hexokinases and VDACs might also apply to plants. Indeed, plants contain even more VDAC isoforms which have been shown to play important roles in plant growth and are suggested to control ATP levels (Li et al., 2013). Moreover, also in *Arabidopsis* hexokinase 1 (Hxk1) interacts with VDAC and overexpression of Hxk1 prevents H₂O₂-induced programmed cell death (Li et al., 2013; Homblé et al., 2012). In this context, *er-ant1* mutants might reduce JA synthesis to maintain the proposed interaction between the hexokinases and the VDACs and by this prevent programmed cell death.

4.1.6 How can absence of ER-ANT1 affect PLP metabolism

The following scenario tries to bring ER-ANT1 into the context of high and low CO₂ and provides a possible solution to the question, why *er-ant1* plants suffer only under ambient conditions, but not under saturating CO₂.

Generally, in all eukaryotes, SLC-type transporters mediate energy provision to the ER (Klein *et al.*, 2018 unpublished data, Plant Physiology, TUK). These transporters exhibit a comparatively high affinity for ATP and ADP. Moreover, they are apparently well suited and sufficient to mediate ATP import into the plant ER under saturating CO₂. It has been shown that increasing CO₂ concentrations result in decreased ATP/ADP ratios in the cytosol, in mitochondria and in chloroplasts (Gardeström and Wigge, 1988) (Figure 4-1). In this context, it is important to mention that even under saturating CO₂, the cytosolic ATP concentration is almost 2-fold higher than that of ADP (Gardeström and Wigge, 1988). Therefore, the high-affinity SLC transporters might still favour ATP over ADP provision to the ER (Figure 4-1).

Moreover, saturating CO₂ increases the carbohydrate availability in the cell (Figure 4-1) and supports multiple anabolic processes, including transcription and amino acid production (given that nitrate and sulfate assimilation are well operating). The increased availability of substrates stimulates protein biosynthesis in the ER (Figure 4-1), which leads to efficient removal of ATP and thus ADP generation in the lumen. This minimises the chance of disadvantageous ATP export via the high-affine SLC transporters. Therefore, SLC transporters may guarantee the ATP supply to the ER when the cytosolic ATP/ADP ratio is low. However, this presupposes that protein biosynthesis in the lumen is efficiently operating. This is clearly given under saturating CO₂, nitrate and sulfate availability. Under these conditions, ER-ANT1 is apparently not required, and thus its absence has no substantial effect on plant vitality.

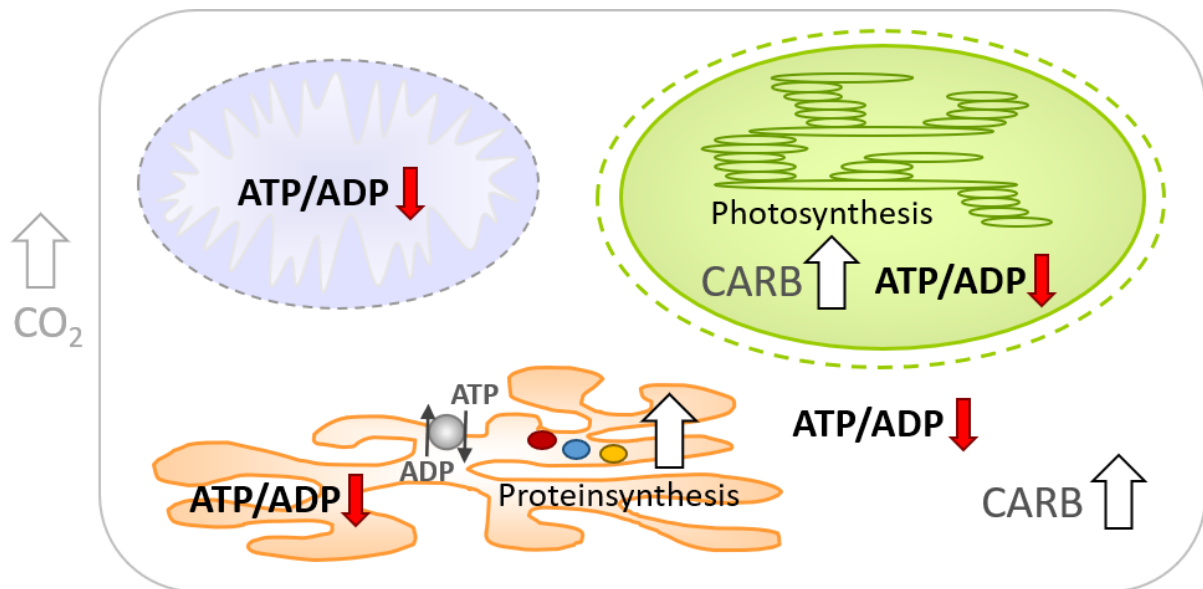


Figure 4-1 Schematic scenario displaying the energy status and carbohydrates under the conditions of elevated CO_2 . Decreased ratios of ATP/ADP under high CO_2 in mitochondria (purple), chloroplasts (green), ER (orange) and cytosol (white). SLC transporters (grey circle) provide ATP to the ER (orange) for protein synthesis. Carbohydrate levels are high. Figure provided by Ilka Haferkamp (TUK).

When protein synthesis slows down due to a decreased amino acid supply, the ATP/ADP ratio in the ER lumen increases (Figure 4-2). This also enhances the likelihood of unwanted ATP loss via the SLC-type ATP/ADP transporters and is quite likely under conditions of decreased CO_2 availability (Figure 4-2). It is important to note that ER-ANT1, in contrast to the SLC-type transporters, exhibits a comparatively low affinity for both, ATP and ADP. Therefore, it needs higher substrate levels to reach half-maximal velocity. Because low CO_2 increases the cytosolic ATP/ADP ratio, the higher ATP concentration would exclusively support ATP uptake into the ER via ER-ANT1 (Figure 4-2). Therefore, ER-ANT1 might help to maintain ATP provision to the ER under conditions when the ATP/ADP ratio in the lumen increases.

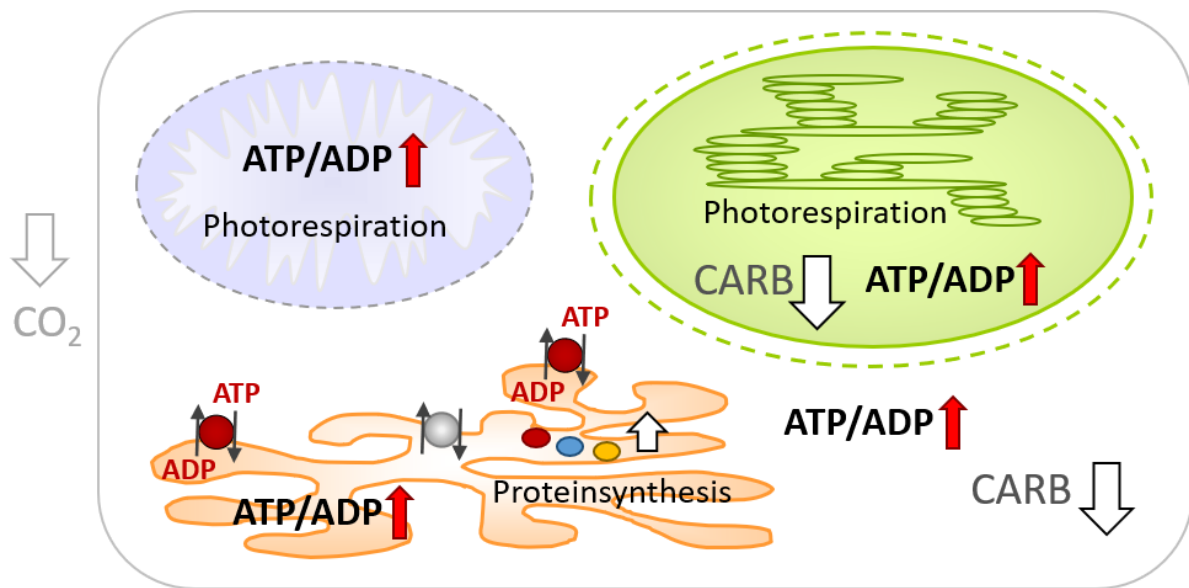


Figure 4-2 Schematic scenario displaying the energy status and carbohydrates under the conditions of low CO_2 . Elevated ratios of ATP/ADP under low CO_2 in mitochondria (purple), chloroplasts (green), ER (orange) and cytosol (white). ER-ANT1 (red circles) provides ATP to the ER (orange) for protein synthesis. Carbohydrate levels are decreased. Figure provided by Ilka Haferkamp (TUK).

Given that this hypothesis is correct, the absence of ER-ANT1 will cause a misbalance between the high cytosolic energy state and the reduced energy consumption in the ER (Figure 4-3). However, this misbalance requires a high cytosolic ATP/ADP ratio and thus can be prevented by high CO_2 . With decreasing CO_2 availability, the *er-ant1* mutant becomes confronted with two new situations (Figure 4-3). First, reduced protein synthesis in the ER and second, an increase in the cytosolic ATP/ADP ratio, which is even higher than in the wild type (Figure 4-3). In fact, the stimulation of several pathways for removal of excess energy and reduction equivalents is indicative of the increased cellular energy state. Induction of fermentation might be a further mechanism to counteract high cytosolic ATP/ADP ratios. However, the constant removal of excess energy consumes plenty of carbohydrates. Therefore, it is not surprising that *er-ant1* mutant plants are much smaller than the wild type under ambient conditions.

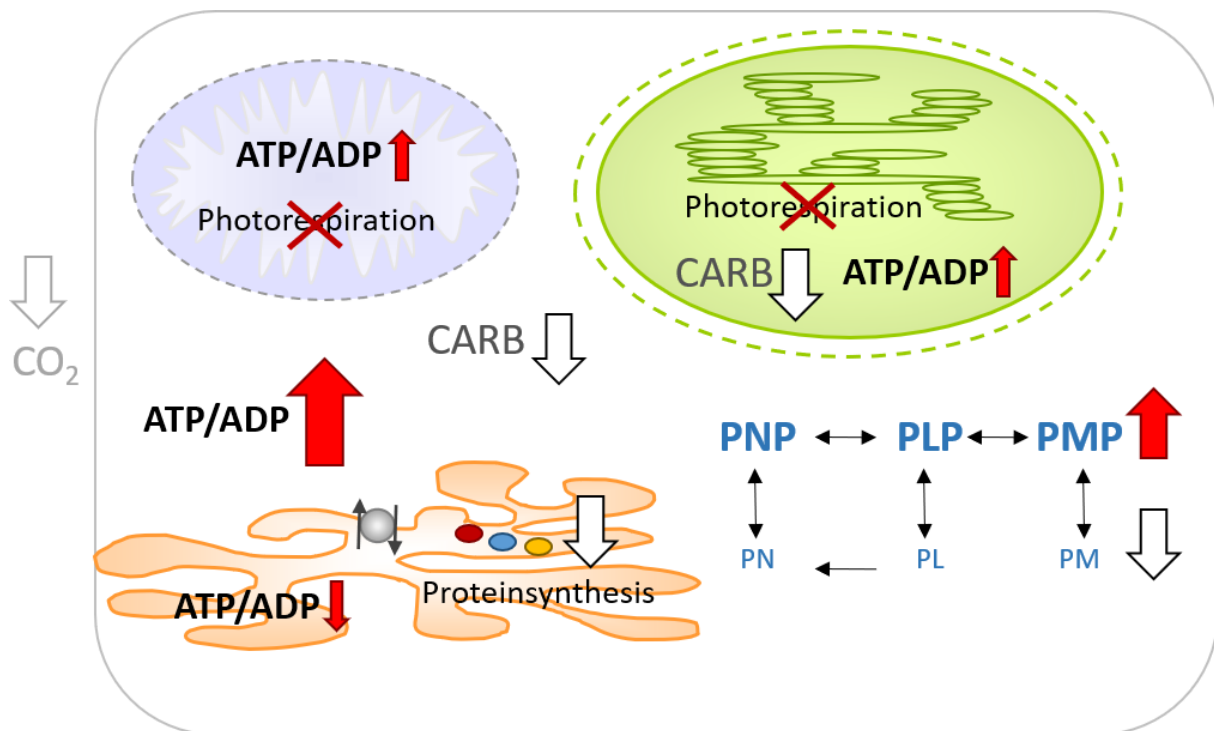


Figure 4-3 Schematic scenario displaying the energy status and carbohydrates under the conditions of low CO₂ in *A. thaliana* lacking ER-ANT1. High ratios of ATP/ADP under low CO₂ in mitochondria (purple), chloroplasts (green) and cytosol (white). Decreased ATP/ADP ratio in the ER (orange) and therefore decreased protein synthesis. Photorespiration is disturbed. Carbohydrates are low. Stimulated phosphorylation of PN, PL and PM due to high ATP/ADP ratio in the cytosol. Figure provided by Ilka Haferkamp (TUK).

The postulated over-energisation of the cytosol could also explain the perturbation of PLP metabolism. It is easy to envision that elevated ATP availability stimulates phosphorylation of the B₆ vitamers (Figure 4-3). Simultaneously, the availability of the membrane permeable, non-phosphorylated forms decreases. The reduced delivery of vitamers to the organelles might thus explain why the internal PLP-dependent processes are affected in *er-ant1* even though PLP *de novo* synthesis, salvage and SOS4.1 kinase are apparently operating in this mutant.

4.2 Outlook

This study revealed that a malfunction in B₆ vitamers metabolism and particularly limited PLP availability in the chloroplast might be causative for the photorespiratory phenotype. In this context, missing ATP import into the ER was supposed to result in a higher ATP/ADP ratio in the cytosol which favours the phosphorylation of the vitamers and by this hinders their entry into the chloroplast. The final prove, however, is missing and thus it is of utmost importance to determine the energy state of the cell as well as the content of phosphorylated versus non-phosphorylated B₆ vitamers. Moreover, it would be interesting to determine their ratios in the individual organelles. Limited PLP availability in mitochondria could further explain the observed glycine accumulation since GDC and SHMT activity relies on this cofactor.

High salt concentrations were shown to shift the cytosolic availability of non-phosphorylated to the phosphorylated vitamers and by this hinder their entry into the chloroplast. The lower plastidial PLP availability results in substantial growth defects and chlorosis. If the absence of the HAD-type phosphatase in fact enhances PLP trapping the chloroplast, the corresponding T-DNA insertion line should exhibit higher resistance to salt stress. Corresponding studies were already started and the results will be obtained soon.

Furthermore, the proposed function of ER-ANT1 in energy provision to the ER might be supported by complementation studies. Absence of ER-ANT1 might be restored by overexpression of other ER-targeted ATP/ADP transporters. Therefore, it might be interesting to test whether the AXER-homologs from *Arabidopsis* can rescue *er-ant1* mutants. Biochemical characterisation of the recombinant proteins revealed that ER-ANT1 has a quite low affinity for ATP, but might be very fast. The AXER homologs are highly affine for ATP but might be too slow to balance ATP homoeostasis. Therefore, the overexpression of one of the AXER homologs might restore missing ATP/ADP translocation across the ER membrane in *er-ant1*. Alternatively, an ER-resident nucleotide transporter (NTT5) from diatoms could be used for complementation. Interestingly, the affinities of NTT5 are approximately five times lower than those of the AXER homologs and thus rather resemble the characteristics of ER-ANT1. Therefore, the biochemical parameters classify the diatom carrier as a further promising candidate for a complementation study.

Loss of HAD function in the chloroplast was proven to alleviate the *er-ant1* phenotype. Initial characterisation of this protein suggests that it is highly specific for dephosphorylating PLP. Therefore, missing PLP phosphatase activity might increase the retention time of PLP in the stroma and thus its availability for enzymatic reactions. For the complete biochemical characterisation, some experiments remain open, for example, the determination of the Michaelis-Menten constant (K_M). Very recently, the first PLP-phosphatase of plants was discovered in tobacco. This protein exhibits a quite high K_M . It will be interesting to know whether the HAD-type phosphatase from *Arabidopsis* shows similarly low or even higher affinity for PLP. Although several phosphorylated metabolites were excluded as substrates, the capacity of HAD to dephosphorylate PMP and PNP remains to be tested.

The suppressor screen identified different suppressor candidates. Six M_3 lines contained mutations in the HAD-type phosphatase, and missing activity of this protein was verified to suppress the phenotype of *er-ant1*. However, at least seven lines have suppressor mutations in other regions. Moreover, the morphology and glycine content, as well as transcriptomic data, differ among the individual EMS mutants of the M_3 generation. In fact, there were other candidates worth analysing. Bioinformatic analyses revealed that certain candidates show high reliability of been the correct hits. Moreover, most of them are not characterised yet. The detailed investigation of these candidates will clearly support our knowledge on ER-ANT1 and will also provide new insights into plant metabolism in general.

5 Literature cited

- Abbas G., Murtaza B., Bibi I., Shahid M., Niazi N. K., Khan M. I., Amjad M., Hussain M.** (2018): Arsenic Uptake, Toxicity, Detoxification, and Speciation in Plants: Physiological, Biochemical, and Molecular Aspects. *International journal of environmental research and public health* **15**.
- Adrover M., Vilanova B., Frau J., Muñoz F., Donoso J.** (2008): The pyridoxamine action on Amadori compounds: A reexamination of its scavenging capacity and chelating effect. *Bioorganic & medicinal chemistry* **16**: pp. 5557–5569.
- Albrecht V., Simková K., Carrie C., Delannoy E., Giraud E., Whelan J., Small I. D., Apel K., Badger M. R., Pogson B. J.** (2010): The cytoskeleton and the peroxisomal-targeted snowy cotyledon3 protein are required for chloroplast development in Arabidopsis. *The Plant Cell* **22**: pp. 3423–3438.
- Alonso-Blanco C., Peeters A. J., Koornneef M., Lister C., Dean C., van den Bosch N., Pot J., Kuiper M. T.** (1998): Development of an AFLP based linkage map of Ler, Col and Cvi Arabidopsis thaliana ecotypes and construction of a Ler/Cvi recombinant inbred line population. *The Plant journal : for cell and molecular biology* **14**: pp. 259–271.
- Ames B. N.** (1966): [10] Assay of inorganic phosphate, total phosphate and phosphatases, Complex carbohydrates. In EF Neufeld, V Ginsburg, eds. Academic Press, New York [etc.], pp. 115–118.
- Armbruster U., Labs M., Pribil M., Viola S., Xu W., Scharfenberg M., Hertle A. P., Rojahn U., Jensen P. E., Rappaport F., Joliot P., Dörmann P., Wanner G., Leister D.** (2013): Arabidopsis CURVATURE THYLAKOID1 Proteins Modify Thylakoid Architecture by Inducing Membrane Curvature. *The Plant Cell* **25**: pp. 2661–2678.
- Armbruster U., Zühlke J., Rengstl B., Kreller R., Makarenko E., Rühle T., Schünemann D., Jahns P., Weisshaar B., Nickelsen J., Leister D.** (2010): The Arabidopsis thylakoid protein PAM68 is required for efficient D1 biogenesis and photosystem II assembly. *The Plant Cell* **22**: pp. 3439–3460.
- Aro E.-M., Suorsa M., Rokka A., Allahverdiyeva Y., Paakkarinen V., Saleem A., Battchikova N., Rintamäki E.** (2005): Dynamics of photosystem II: a proteomic approach to thylakoid protein complexes. *Journal of Experimental Botany* **56**: pp. 347–356.

- Bailey-Serres J., Voeselek L. A. C. J.** (2010): Life in the balance: a signaling network controlling survival of flooding. *Current opinion in plant biology* **13**: pp. 489–494.
- Baker N. R., Bradbury M., Farage P. K., Ireland C. R., Long S. P., Farquhar G. D., Lake J. V., Osmond C. B., Woolhouse H. W.** (1989): Measurements of the Quantum Yield of Carbon Assimilation and Chlorophyll Fluorescence for Assessment of Photosynthetic Performance of Crops in the Field [and Discussion]. *Philosophical Transactions of the Royal Society B: Biological Sciences* **323**: pp. 295–308.
- Banti V., Mafessoni F., Loreti E., Alpi A., Perata P.** (2010): The heat-inducible transcription factor HsfA2 enhances anoxia tolerance in Arabidopsis. *Plant Physiology* **152**: pp. 1471–1483.
- Bassi R., dal Belin Peruffo A., Barbato R., Ghisi R.** (1985): Differences in chlorophyll-protein complexes and composition of polypeptides between thylakoids from bundle sheaths and mesophyll cells in maize. *European journal of biochemistry* **146**: pp. 589–595.
- Benstein R. M., Ludewig K., Wulfert S., Wittek S., Gigolashvili T., Frerigmann H., Gierth M., Flügge U.-I., Krueger S.** (2013): Arabidopsis phosphoglycerate dehydrogenase1 of the phosphoserine pathway is essential for development and required for ammonium assimilation and tryptophan biosynthesis. *The Plant Cell* **25**: pp. 5011–5029.
- Berg J. M., Tymoczko J. L., Stryer L., Clarke N. d.** (2002): Biochemistry, Ed. 5. W. H. Freeman, New York, NY.
- Beynon E. R., Symons Z. C., Jackson R. G., Lorenz A., Rylott E. L., Bruce N. C.** (2009): The Role of Oxophytodienoate Reductases in the Detoxification of the Explosive 2,4,6-Trinitrotoluene by Arabidopsis. *Plant Physiology* **151**: pp. 253–261.
- Bilger W., Björkman O.** (1990): Role of the xanthophyll cycle in photoprotection elucidated by measurements of light-induced absorbance changes, fluorescence and photosynthesis in leaves of *Hedera canariensis*. *Photosynthesis research* **25**: pp. 173–185.
- Bilski P., Li M. Y., Ehrenshaft M., Daub M. E., Chignell C. F.** (2000): Vitamin B6 (pyridoxine) and its derivatives are efficient singlet oxygen quenchers and potential fungal antioxidants. *Photochemistry and photobiology* **71**: pp. 129–134.
- Björkman O., Demmig B.** (1987): Photon yield of O₂ evolution and chlorophyll fluorescence characteristics at 77 K among vascular plants of diverse origins. *Planta* **170**: pp. 489–504.

- Bloom A. J.** (2015): Photorespiration and nitrate assimilation: a major intersection between plant carbon and nitrogen. *Photosynthesis research* **123**: pp. 117–128.
- Blum H., Beier H., Gross H. J.** (1987): Improved silver staining of plant proteins, RNA and DNA in polyacrylamide gels. *Electrophoresis* **8**: pp. 93–99.
- Blume C., Ost J., Mühlenbruch M., Peterhänsel C., Laxa M.** (2019): Low CO₂ induces urea cycle intermediate accumulation in *Arabidopsis thaliana*. *PLoS ONE* **14**: pp. e0210342.
- Booher R., Beach D.** (1987): Interaction between *cdc13+* and *cdc2+* in the control of mitosis in fission yeast; dissociation of the G1 and G2 roles of the *cdc2+* protein kinase. *The EMBO Journal* **6**: pp. 3441–3447.
- Booher R. N., Alfa C. E., Hyams J. S., Beach D. H.** (1989): The fission yeast *cdc2/cdc13/suc1* protein kinase: regulation of catalytic activity and nuclear localization. *Cell* **58**: pp. 485–497.
- Borisjuk L., Rolletschek H.** (2009): The oxygen status of the developing seed. *The New phytologist* **182**: pp. 17–30.
- Bracher A., Sharma A., Starling-Windhof A., Hartl F. U., Hayer-Hartl M.** (2015): Degradation of potent Rubisco inhibitor by selective sugar phosphatase. *Nature plants* **1**: pp. 14002.
- Branco-Price C., Kaiser K. A., Jang C. J. H., Larive C. K., Bailey-Serres J.** (2008): Selective mRNA translation coordinates energetic and metabolic adjustments to cellular oxygen deprivation and reoxygenation in *Arabidopsis thaliana*. *The Plant journal : for cell and molecular biology* **56**: pp. 743–755.
- S. Brenner, J. H. Miller, W. J. Broughton**, eds, Encyclopedia of genetics. Academic Press, San Diego.
- Brooks M. D., Sylak-Glassman E. J., Fleming G. R., Niyogi K. K.** (2013): A thioredoxin-like/ β -propeller protein maintains the efficiency of light harvesting in *Arabidopsis*. *Proceedings of the National Academy of Sciences of the United States of America* **110**: pp. E2733-40.
- Brown H. M.** (1990): Mode of action, crop selectivity, and soil relations of the sulfonylurea herbicides. *Pesticide Science* **29**: pp. 263–281.
- Brownfield D. L., Todd C. D., Deyholos M. K.** (2008): Analysis of *Arabidopsis* arginase gene transcription patterns indicates specific biological functions for recently diverged paralogs. *Plant molecular biology* **67**: pp. 429–440.

- Bullock W. O.** (1987): XL1-Blue: a high efficiency plasmid transforming recA Escherichia coli strain with beta-galactosidase selection. *BioTechniques* **5**: pp. 376–378.
- Burroughs A. M., Allen K. N., Dunaway-Mariano D., Aravind L.** (2006): Evolutionary genomics of the HAD superfamily: understanding the structural adaptations and catalytic diversity in a superfamily of phosphoesterases and allied enzymes. *Journal of molecular biology* **361**: pp. 1003–1034.
- Busch W., Wunderlich M., Schöffl F.** (2005): Identification of novel heat shock factor-dependent genes and biochemical pathways in Arabidopsis thaliana. *The Plant journal : for cell and molecular biology* **41**: pp. 1–14.
- Bykova N. v., Møller I. M., Gardeström P., Igamberdiev A. U.** (2014): The function of glycine decarboxylase complex is optimized to maintain high photorespiratory flux via buffering of its reaction products. *Mitochondrion* **19 Pt B**: pp. 357–364.
- Caarls L., Elberse J., Awwanah M., Ludwig N. R., Vries M. de, Zeilmaker T., van Wees S. C. M., Schuurink R. C., van den Ackerveken G.** (2017): Arabidopsis JASMONATE-INDUCED OXYGENASES down-regulate plant immunity by hydroxylation and inactivation of the hormone jasmonic acid. *Proceedings of the National Academy of Sciences of the United States of America* **114**: pp. 6388–6393.
- Caldelari D., Wang G., Farmer E. E., Dong X.** (2011): Arabidopsis lox3 lox4 double mutants are male sterile and defective in global proliferative arrest. *Plant molecular biology* **75**: pp. 25–33.
- Caparrós-Martín J. A., McCarthy-Suárez I., Culiáñez-Macià F. A.** (2013): HAD hydrolase function unveiled by substrate screening: enzymatic characterization of Arabidopsis thaliana subclass I phosphosugar phosphatase AtSgpp. *Planta* **237**: pp. 943–954.
- Caparrós-Martín J. A., Reiland S., Köchert K., Cutanda M. C., Culiáñez-Macià F. A.** (2007): Arabidopsis thaliana AtGppl and AtGpp2: two novel low molecular weight phosphatases involved in plant glycerol metabolism. *Plant molecular biology* **63**: pp. 505–517.
- Caverzan A., Passaia G., Rosa S. B., Ribeiro C. W., Lazzarotto F., Margis-Pinheiro M.** (2012): Plant responses to stresses: Role of ascorbate peroxidase in the antioxidant protection. *Genetics and Molecular Biology* **35**: pp. 1011–1019.
- Cesari I. M., Carvalho E., Figueiredo Rodrigues M., Mendonça B. D. S., Amôedo N. D., Rumjanek F. D.** (2014): Methyl jasmonate: putative mechanisms of action on cancer cells cycle, metabolism, and apoptosis. *International journal of cell biology* **2014**: pp. 572097.

- Chauvin A., Lenglet A., Wolfender J.-L., Farmer E. E.** (2016): Paired Hierarchical Organization of 13-Lipoxygenases in Arabidopsis. *Plants* **5**.
- Chen Y., Zou T., McCormick S.** (2016): S-Adenosylmethionine Synthetase 3 Is Important for Pollen Tube Growth. *Plant Physiology* **172**: pp. 244–253.
- Cheng S.-B., Lin P.-T., Liu H.-T., Peng Y.-S., Huang S.-C., Huang Y.-C.** (2016): Vitamin B-6 Supplementation Could Mediate Antioxidant Capacity by Reducing Plasma Homocysteine Concentration in Patients with Hepatocellular Carcinoma after Tumor Resection. *BioMed research international* **2016**: pp. 7658981.
- Chetyrkin S. V., Zhang W., Hudson B. G., Serianni A. S., Voziyan P. A.** (2008): Pyridoxamine protects proteins from functional damage by 3-deoxyglucosone: mechanism of action of pyridoxamine. *Biochemistry* **47**: pp. 997–1006.
- Clairmont C. A., Maio A. de, Hirschberg C. B.** (1992): Translocation of ATP into the lumen of rough endoplasmic reticulum-derived vesicles and its binding to luminal proteins including BiP (GRP 78) and GRP 94. *The Journal of biological chemistry* **267**: pp. 3983–3990.
- Clifton R., Millar A. H., Whelan J.** (2006): Alternative oxidases in Arabidopsis: a comparative analysis of differential expression in the gene family provides new insights into function of non-phosphorylating bypasses. *Biochimica et biophysica acta* **1757**: pp. 730–741.
- Clough S. J., Bent A. F.** (1998): Floral dip: a simplified method for Agrobacterium-mediated transformation of Arabidopsis thaliana. *The Plant journal : for cell and molecular biology* **16**: pp. 735–743.
- Colinas M., Eisenhut M., Tohge T., Pesquera M., Fernie A. R., Weber A. P. M., Fitzpatrick T. B.** (2016): Balancing of B6 Vitamers Is Essential for Plant Development and Metabolism in Arabidopsis. *The Plant Cell* **28**: pp. 439–453.
- Collakova E., Goyer A., Naponelli V., Krassovskaya I., Gregory J. F., Hanson A. D., Shachar-Hill Y.** (2008): Arabidopsis 10-formyl tetrahydrofolate deformylases are essential for photorespiration. *The Plant Cell* **20**: pp. 1818–1832.
- Conn S. J., Hocking B., Dayod M., Xu B., Athman A., Henderson S., Aukett L., Conn V., Shearer M. K., Fuentes S., Tyerman S. D., Gilliham M.** (2013): Protocol: optimising hydroponic growth systems for nutritional and physiological analysis of Arabidopsis thaliana and other plants. *Plant methods* **9**: pp. 4.

- Dahal K., Vanlerberghe G. C.** (2018): Growth at Elevated CO₂ Requires Acclimation of the Respiratory Chain to Support Photosynthesis. *Plant Physiology* **178**: pp. 82–100.
- Das M., Reichman J. R., Haberer G., Welzl G., Aceituno F. F., Mader M. T., Watrud L. S., Pflieger T. G., Gutiérrez R. A., Schäffner A. R., Olszyk D. M.** (2010): A composite transcriptional signature differentiates responses towards closely related herbicides in *Arabidopsis thaliana* and *Brassica napus*. *Plant molecular biology* **72**: pp. 545–556.
- Day D. A., Krab K., Lambers H., Moore A. L., Siedow J. N., Wagner A. M., Wiskich J. T.** (1996): The Cyanide-Resistant Oxidase: To Inhibit or Not to Inhibit, That Is the Question. *Plant Physiology* **110**: pp. 1–2.
- Déjardin A., Sokolov L. N., Kleczkowski L. A.** (1999): Sugar/osmoticum levels modulate differential abscisic acid-independent expression of two stress-responsive sucrose synthase genes in *Arabidopsis*. *The Biochemical journal* **344 Pt 2**: pp. 503–509.
- Depaoli M. R., Hay J. C., Graier W. F., Malli R.** (2019): The enigmatic ATP supply of the endoplasmic reticulum. *Biological reviews of the Cambridge Philosophical Society* **94**: pp. 610–628.
- Diab H., Limami A. M.** (2016): Reconfiguration of N Metabolism upon Hypoxia Stress and Recovery: Roles of Alanine Aminotransferase (AlaAT) and Glutamate Dehydrogenase (GDH). *Plants* **5**.
- Dong Z., Chen Y.** (2013): Transcriptomics: advances and approaches. *Science China. Life sciences* **56**: pp. 960–967.
- Douce R., Bourguignon J., Neuburger M., Rébeillé F.** (2001): The glycine decarboxylase system: a fascinating complex. *Trends in plant science* **6**: pp. 167–176.
- Du M., Zhao J., Tzeng D. T. W., Liu Y., Deng L., Yang T., Zhai Q., Wu F., Huang Z., Zhou M., Wang Q., Chen Q., Zhong S., Li C.-B., Li C.** (2017): MYC2 Orchestrates a Hierarchical Transcriptional Cascade That Regulates Jasmonate-Mediated Plant Immunity in Tomato. *The Plant Cell* **29**: pp. 1883–1906.
- Eisenhut M., Bräutigam A., Timm S., Florian A., Tohge T., Fernie A. R., Bauwe H., Weber A. P. M.** (2017): Photorespiration Is Crucial for Dynamic Response of Photosynthetic Metabolism and Stomatal Movement to Altered CO₂ Availability. *Molecular plant* **10**: pp. 47–61.

- Eisenhut M., Planchais S., Cabassa C., Guivarc'h A., Justin A.-M., Taconnat L., Renou J.-P., Linka M., Gagneul D., Timm S., Bauwe H., Carol P., Weber A. P. M.** (2013): Arabidopsis A BOUT DE SOUFFLE is a putative mitochondrial transporter involved in photorespiratory metabolism and is required for meristem growth at ambient CO₂ levels. *The Plant journal : for cell and molecular biology* **73**: pp. 836–849.
- Enomoto T., Tokizawa M., Ito H., Iuchi S., Kobayashi M., Yamamoto Y. Y., Kobayashi Y., Koyama H.** (2019): STOP1 regulates the expression of HsfA2 and GDH genes critical for low-oxygen tolerance in Arabidopsis. *Journal of experimental botany*.
- Etherington G. J., Monaghan J., Zipfel C., MacLean D.** (2014): Mapping mutations in plant genomes with the user-friendly web application CandiSNP. *Plant methods* **10**: pp. 41.
- Flügel F., Timm S., Arrivault S., Florian A., Stitt M., Fernie A. R., Bauwe H.** (2017): The Photorespiratory Metabolite 2-Phosphoglycolate Regulates Photosynthesis and Starch Accumulation in Arabidopsis. *The Plant Cell* **29**: pp. 2537–2551.
- Forde B. G., Lea P. J.** (2007): Glutamate in plants: metabolism, regulation, and signalling. *Journal of Experimental Botany* **58**: pp. 2339–2358.
- Fox E. J., Reid-Bayliss K. S., Emond M. J., Loeb L. A.** (2014): Accuracy of Next Generation Sequencing Platforms. *Next generation, sequencing & applications* **1**.
- Froger A., Hall J. E.** (2007): Transformation of Plasmid DNA into E. coli Using the Heat Shock Method. *Journal of Visualized Experiments : JoVE*.
- Fu S.-F., Chen P.-Y., Nguyen Q. T. T., Huang L.-Y., Zeng G.-R., Huang T.-L., Lin C.-Y., Huang H.-J.** (2014): Transcriptome profiling of genes and pathways associated with arsenic toxicity and tolerance in Arabidopsis. *BMC plant biology* **14**: pp. 94.
- Fukao Y., Hayashi Y., Mano S., Hayashi M., Nishimura M.** (2001): Developmental analysis of a putative ATP/ADP carrier protein localized on glyoxysomal membranes during the peroxisome transition in pumpkin cotyledons. *Plant & cell physiology* **42**: pp. 835–841.
- Funck D., Stadelhofer B., Koch W.** (2008): Ornithine-delta-aminotransferase is essential for arginine catabolism but not for proline biosynthesis. *BMC plant biology* **8**: pp. 40.
- Gardeström P., Wigge B.** (1988): Influence of Photorespiration on ATP/ADP Ratios in the Chloroplasts, Mitochondria, and Cytosol, Studied by Rapid Fractionation of Barley (*Hordeum vulgare*) Protoplasts. *Plant Physiology* **88**: pp. 69–76.

- Genty B., Briantais J.-M., Baker N. R.** (1989): The relationship between the quantum yield of photosynthetic electron transport and quenching of chlorophyll fluorescence. *Biochimica et Biophysica Acta (BBA) - General Subjects* **990**: pp. 87–92.
- Giuntoli B., Licausi F., van Veen H., Perata P.** (2017): Functional Balancing of the Hypoxia Regulators RAP2.12 and HRA1 Takes Place in vivo in Arabidopsis thaliana Plants. *Frontiers in plant science* **8**.
- Grebner W., Stingl N. E., Oenel A., Mueller M. J., Berger S.** (2013): Lipoxygenase6-dependent oxylipin synthesis in roots is required for abiotic and biotic stress resistance of Arabidopsis. *Plant Physiology* **161**: pp. 2159–2170.
- Guo X., Stotz H. U.** (2007): Defense against Sclerotinia sclerotiorum in Arabidopsis is dependent on jasmonic acid, salicylic acid, and ethylene signaling. *Molecular plant-microbe interactions : MPMI* **20**: pp. 1384–1395.
- Gupta D. K., Srivastava S., Huang H. G., Romero-Puertas M. C., Sandalio L. M.** (2011): Arsenic Tolerance and Detoxification Mechanisms in Plants, Detoxification of Heavy Metals. In I Sherameti, A Varma, eds, Vol 30. Springer-Verlag Berlin Heidelberg, Berlin, Heidelberg, pp. 169–179.
- Haferkamp I., Schmitz-Esser S.** (2012): The plant mitochondrial carrier family: functional and evolutionary aspects. *Frontiers in plant science* **3**: pp. 2.
- Heard W., Sklenář J., Tomé D. F. A., Robatzek S., Jones A. M. E.** (2015): Identification of Regulatory and Cargo Proteins of Endosomal and Secretory Pathways in Arabidopsis thaliana by Proteomic Dissection. *Molecular & cellular proteomics : MCP* **14**: pp. 1796–1813.
- Heldt H.-W., Piechulla B.** (2012): Pflanzenbiochemie, Ed. 4. Spektrum, Akad. Verl., Heidelberg.
- Hesse H., Kreft O., Maimann S., Zeh M., Hoefgen R.** (2004): Current understanding of the regulation of methionine biosynthesis in plants. *Journal of Experimental Botany* **55**: pp. 1799–1808.
- Hirschberg C. B., Robbins P. W., Abeijon C.** (1998): Transporters of nucleotide sugars, ATP, and nucleotide sulfate in the endoplasmic reticulum and Golgi apparatus. *Annual review of biochemistry* **67**: pp. 49–69.

- Hoffmann C., Plochanski B., Haferkamp I., Leroch M., Ewald R., Bauwe H., Riemer J., Herrmann J. M., Neuhaus H. E.** (2013): From endoplasmic reticulum to mitochondria: absence of the Arabidopsis ATP antiporter endoplasmic Reticulum Adenylate Transporter1 perturbs photorespiration. *The Plant Cell* **25**: pp. 2647–2660.
- Höfgen R., Willmitzer L.** (1988): Storage of competent cells for Agrobacterium transformation. *Nucleic acids research* **16**: pp. 9877.
- Homblé F., Krammer E.-M., Prévost M.** (2012): Plant VDAC: facts and speculations. *Biochimica et biophysica acta* **1818**: pp. 1486–1501.
- Hooper C. M., Castleden I. R., Tanz S. K., Aryamanesh N., Millar A. H.** (2017): SUBA4: the interactive data analysis centre for Arabidopsis subcellular protein locations. *Nucleic acids research* **45**: pp. D1064-D1074.
- Hruz T., Laule O., Szabo G., Wessendorf F., Bleuler S., Oertle L., Widmayer P., Gruissem W., Zimmermann P.** (2008): Genevestigator v3: a reference expression database for the meta-analysis of transcriptomes. *Advances in bioinformatics* **2008**: pp. 420747.
- Hulst A. C., Hens H. J. H., Buitelaar R. M., Tramper J.** (1989): Determination of the effective diffusion coefficient of oxygen in gel materials in relation to gel concentration. *Biotechnology Techniques* **3**: pp. 199–204.
- Igamberdiev A. U., Bykova N. v., Lea P. J., Gardestrom P.** (2001): The role of photorespiration in redox and energy balance of photosynthetic plant cells: A study with a barley mutant deficient in glycine decarboxylase. *Physiologia Plantarum* **111**: pp. 427–438.
- Ihnatowicz A., Pesaresi P., Varotto C., Richly E., Schneider A., Jahns P., Salamini F., Leister D.** (2004): Mutants for photosystem I subunit D of Arabidopsis thaliana : effects on photosynthesis, photosystem I stability and expression of nuclear genes for chloroplast functions. *The Plant Journal* **37**: pp. 839–852.
- Jang Y. M., Kim D. W., Kang T.-C., Won M. H., Baek N.-I., Moon B. J., Choi S. Y., Kwon O.-S.** (2003): Human pyridoxal phosphatase. Molecular cloning, functional expression, and tissue distribution. *The Journal of biological chemistry* **278**: pp. 50040–50046.
- Järvi S., Suorsa M., Paakkarinen V., Aro E.-M.** (2011): Optimized native gel systems for separation of thylakoid protein complexes: novel super- and mega-complexes. *The Biochemical journal* **439**: pp. 207–214.

- Jung C., Lyou S. H., Yeu S., Kim M. A., Rhee S., Kim M., Lee J. S., Choi Y. D., Cheong J.-J.** (2007): Microarray-based screening of jasmonate-responsive genes in *Arabidopsis thaliana*. *Plant cell reports* **26**: pp. 1053–1063.
- Kandoth P. K., Liu S., Prenger E., Ludwig A., Lakhssassi N., Heinz R., Zhou Z., Howland A., Gunther J., Eidson S., Dhroso A., LaFayette P., Tucker D., Johnson S., Anderson J., Alaswad A., Cianzio S. R., Parrott W. A., Korkin D., Meksem K., Mitchum M. G.** (2017): Systematic Mutagenesis of Serine Hydroxymethyltransferase Reveals an Essential Role in Nematode Resistance1OPEN. *Plant Physiology* **175**: pp. 1370–1380.
- Karimi M., Inzé D., Depicker A.** (2002): GATEWAY vectors for *Agrobacterium*-mediated plant transformation. *Trends in plant science* **7**: pp. 193–195.
- Keech O., Gardeström P., Kleczkowski L. A., Rouhier N.** (2017): The redox control of photorespiration: from biochemical and physiological aspects to biotechnological considerations. *Plant, cell & environment* **40**: pp. 553–569.
- Kim Y., Schumaker K. S., Zhu J.-K.** (2006): EMS mutagenesis of *Arabidopsis*. *Methods in molecular biology (Clifton, N.J.)* **323**: pp. 101–103.
- Kirby E. G., Gallardo F., Man H., El-Khatib R.** (2006): The Overexpression of Glutamine Synthetase in Transgenic Poplar: A Review. *Silvae Genetica* **55**: pp. 278–284.
- Klein M.-C., Zimmermann K., Schorr S., Landini M., Klemens P. A. W., Altensell J., Jung M., Krause E., Nguyen D., Helms V., Rettig J., Fecher-Trost C., Cavalié A., Hoth M., Bogeski I., Neuhaus H. E., Zimmermann R., Lang S., Haferkamp I.** (2018): AXER is an ATP/ADP exchanger in the membrane of the endoplasmic reticulum. *Nature communications* **9**: pp. 3489.
- Koncz C., Schell J.** (1986): The promoter of TL-DNA gene 5 controls the tissue-specific expression of chimaeric genes carried by a novel type of *Agrobacterium* binary vector. *Molecular and General Genetics MGG* **204**: pp. 383–396.
- Koonin E. V., Tatusov R. L.** (1994): Computer analysis of bacterial haloacid dehalogenases defines a large superfamily of hydrolases with diverse specificity. Application of an iterative approach to database search. *Journal of molecular biology* **244**: pp. 125–132.
- Koornneef M., Meinke D.** (2010): The development of *Arabidopsis* as a model plant. *The Plant journal : for cell and molecular biology* **61**: pp. 909–921.

- Kouzai Y., Noutoshi Y., Inoue K., Shimizu M., Onda Y., Mochida K.** (2018): Benzothiadiazole, a plant defense inducer, negatively regulates sheath blight resistance in *Brachypodium distachyon*. *Scientific Reports* **8**: pp. 17358.
- Krishnakumar V., Hanlon M. R., Contrino S., Ferlanti E. S., Karamycheva S., Kim M., Rosen B. D., Cheng C.-Y., Moreira W., Mock S. A., Stubbs J., Sullivan J. M., Krampis K., Miller J. R., Micklem G., Vaughn M., Town C. D.** (2015): Araport: the Arabidopsis information portal. *Nucleic acids research* **43**: pp. D1003-9.
- Kumar V., Vogelsang L., Seidel T., Schmidt R., Weber M., Reichelt M., Meyer A., Clemens S., Sharma S. S., Dietz K.-J.** (2019): Interference between arsenic-induced toxicity and hypoxia. *Plant, cell & environment* **42**: pp. 574–590.
- Kunji E. R.S., Aleksandrova A., King M. S., Majd H., Ashton V. L., Cerson E., Springett R., Kibalchenko M., Tavoulari S., Crichton P. G., Ruprecht J. J.** (2016): The transport mechanism of the mitochondrial ADP/ATP carrier. *Biochimica et Biophysica Acta (BBA) - Molecular Cell Research* **1863**: pp. 2379–2393.
- Kuznetsova E.** (2009): Activity-based functional annotation of unknown proteins: HAD-like hydrolases from *E. coli* and *S. cerevisiae*. PhD thesis. University of Toronto, Toronto.
- Kuznetsova E., Nocek B., Brown G., Makarova K. S., Flick R., Wolf Y. I., Khusnutdinova A., Evdokimova E., Jin K., Tan K., Hanson A. D., Hasnain G., Zallot R., Crécy-Lagard V. de, Babu M., Savchenko A., Joachimiak A., Edwards A. M., Koonin E. V., Yakunin A. F.** (2015): Functional Diversity of Haloacid Dehalogenase Superfamily Phosphatases from *Saccharomyces cerevisiae*: BIOCHEMICAL, STRUCTURAL, AND EVOLUTIONARY INSIGHTS. *The Journal of biological chemistry* **290**: pp. 18678–18698.
- Lambers H.** (1982): Cyanide-resistant respiration: A non-phosphorylating electron transport pathway acting as an energy overflow. *Physiologia Plantarum* **55**: pp. 478–485.
- Laudert D., Pfannschmidt U., Lottspeich F., Hollnder-Czytko H., Weiler E. W.** (1996): Cloning, molecular and functional characterization of *Arabidopsis thaliana* allene oxide synthase (CYP 74), the first enzyme of the octadecanoid pathway to jasmonates. *Plant molecular biology* **31**: pp. 323–335.
- Leroch, M.** (2006): Molekulare, biochemische und physiologische Eigenschaften von Transportproteinen der MCF (mitochondrial carrier family) aus Pflanzen und Protisten. Molecular, biochemical and physiological analysis of transport proteins belonging to the MCF (Mitochondrial Carrier Family) of plants and protists, <https://kluedo.ub.uni-kl.de/files/1759/dissertation.pdf>.

- Leroch M., Neuhaus H. E., Kirchberger S., Zimmermann S., Melzer M., Gerhold J., Tjaden J.** (2008): Identification of a Novel Adenine Nucleotide Transporter in the Endoplasmic Reticulum of Arabidopsis. *The Plant Cell* **20**: pp. 438–451.
- Leuendorf J. E., Osorio S., Szewczyk A., Fernie A. R., Hellmann H.** (2010): Complex assembly and metabolic profiling of Arabidopsis thaliana plants overexpressing vitamin B₆ biosynthesis proteins. *Molecular plant* **3**: pp. 890–903.
- Li H., Durbin R.** (2009): Fast and accurate short read alignment with Burrows-Wheeler transform. *Bioinformatics (Oxford, England)* **25**: pp. 1754–1760.
- Li H., Handsaker B., Wysoker A., Fennell T., Ruan J., Homer N., Marth G., Abecasis G., Durbin R.** (2009): The Sequence Alignment/Map format and SAMtools. *Bioinformatics (Oxford, England)* **25**: pp. 2078–2079.
- Li X., Zhang Y.** (2016): Suppressor Screens in Arabidopsis. *Methods in molecular biology (Clifton, N.J.)* **1363**: pp. 1–8.
- Li Y., Lee K. K., Walsh S., Smith C., Hadingham S., Sorefan K., Cawley G., Bevan M. W.** (2006): Establishing glucose- and ABA-regulated transcription networks in Arabidopsis by microarray analysis and promoter classification using a Relevance Vector Machine. *Genome research* **16**: pp. 414–427.
- Li Z.-Y., Xu Z.-S., He G.-Y., Yang G.-X., Chen M., Li L.-C., Ma Y.** (2013): The voltage-dependent anion channel 1 (AtVDAC1) negatively regulates plant cold responses during germination and seedling development in Arabidopsis and interacts with calcium sensor CBL1. *International journal of molecular sciences* **14**: pp. 701–713.
- Linka N., Theodoulou F. L., Haslam R. P., Linka M., Napier J. A., Neuhaus H. E., Weber A. P.M.** (2008): Peroxisomal ATP Import Is Essential for Seedling Development in Arabidopsis thaliana. *The Plant Cell* **20**: pp. 3241–3257.
- Livak K. J., Schmittgen T. D.** (2001): Analysis of relative gene expression data using real-time quantitative PCR and the 2^{(-Delta Delta C(T))} Method. *Methods (San Diego, Calif.)* **25**: pp. 402–408.
- Loreti E., Valeri M. C., Novi G., Perata P.** (2018): Gene Regulation and Survival under Hypoxia Requires Starch Availability and Metabolism. *Plant Physiology* **176**: pp. 1286–1298.
- Loreti E., van Veen H., Perata P.** (2016): Plant responses to flooding stress. *Current opinion in plant biology* **33**: pp. 64–71.

- Maeda H., Song W., Sage T., Dellapenna D.** (2014): Role of callose synthases in transfer cell wall development in tocopherol deficient Arabidopsis mutants. *Frontiers in plant science* **5**: pp. 46.
- Mandaokar A., Thines B., Shin B., Lange B. M., Choi G., Koo Y. J., Yoo Y. J., Choi Y. D., Choi G., Browse J.** (2006): Transcriptional regulators of stamen development in Arabidopsis identified by transcriptional profiling. *The Plant journal : for cell and molecular biology* **46**: pp. 984–1008.
- Mao D., Yu F., Li J., van de Poel B., Tan D., Li J., Liu Y., Li X., Dong M., Chen L., Li D., Luan S.** (2015): FERONIA receptor kinase interacts with S-adenosylmethionine synthetase and suppresses S-adenosylmethionine production and ethylene biosynthesis in Arabidopsis. *Plant, cell & environment* **38**: pp. 2566–2574.
- Maple J., Møller S. G.** (2007): Mutagenesis in Arabidopsis. *Methods in molecular biology (Clifton, N.J.)* **362**: pp. 197–206.
- Marchler-Bauer A., Bo Y., Han L., He J., Lanczycki C. J., Lu S., Chitsaz F., Derbyshire M. K., Geer R. C., Gonzales N. R., Gwadz M., Hurwitz D. I., Lu F., Marchler G. H., Song J. S., Thanki N., Wang Z., Yamashita R. A., Zhang D., Zheng C., Geer L. Y., Bryant S. H.** (2017): CDD/SPARCLE: functional classification of proteins via subfamily domain architectures. *Nucleic acids research* **45**: pp. 200-203.
- Marchler-Bauer A., Bryant S. H.** (2004): CD-Search: protein domain annotations on the fly. *Nucleic acids research* **32**: pp. 327-331.
- Meinke D. W.** (2013): A survey of dominant mutations in Arabidopsis thaliana. *Trends in plant science* **18**: pp. 84–91.
- Meng J., Wang L., Wang J., Zhao X., Cheng J., Yu W., Jin D., Li Q., Gong Z.** (2018): METHIONINE ADENOSYLTRANSFERASE4 Mediates DNA and Histone Methylation. *Plant Physiology* **177**: pp. 652–670.
- Michalecka A. M., Svensson A. S., Johansson F. I., Agius S. C., Johanson U., Brennicke A., Binder S., Rasmusson A. G.** (2003): Arabidopsis genes encoding mitochondrial type II NAD(P)H dehydrogenases have different evolutionary origin and show distinct responses to light. *Plant Physiology* **133**: pp. 642–652.
- Millar A. H., Heazlewood J. L.** (2003): Genomic and proteomic analysis of mitochondrial carrier proteins in Arabidopsis. *Plant Physiology* **131**: pp. 443–453.

- Mitchell A. L., Attwood T. K., Babbitt P. C., Blum M., Bork P., Bridge A., Brown S. D., Chang H.-Y., El-Gebali S., Fraser M. I., Gough J., Haft D. R., Huang H., Letunic I., Lopez R., Luciani A., Madeira F., Marchler-Bauer A., Mi H., Natale D. A., Necci M., Nuka G., Orengo C., Pandurangan A. P., Paysan-Lafosse T., Pesseat S., Potter S. C., Qureshi M. A., Rawlings N. D., Redaschi N., Richardson L. J., Rivoire C., Salazar G. A., Sangrador-Vegas A., Sigrist C. J. A., Sillitoe I., Sutton G. G., Thanki N., Thomas P. D., Tosatto S. C. E., Yong S.-Y., Finn R. D.** (2019): InterPro in 2019: improving coverage, classification and access to protein sequence annotations. *Nucleic acids research* **47**: pp. D351-D360.
- Mithran M., Paparelli E., Novi G., Perata P., Loreti E.** (2014): Analysis of the role of the pyruvate decarboxylase gene family in *Arabidopsis thaliana* under low-oxygen conditions. *Plant biology (Stuttgart, Germany)* **16**: pp. 28–34.
- Miyashita Y., Dolferus R., Ismond K. P., Good A. G.** (2007): Alanine aminotransferase catalyses the breakdown of alanine after hypoxia in *Arabidopsis thaliana*. *The Plant journal : for cell and molecular biology* **49**: pp. 1108–1121.
- Mooney S., Hellmann H.** (2010): Vitamin B6: Killing two birds with one stone? *Phytochemistry* **71**: pp. 495–501.
- Mueller S., Hilbert B., Dueckershoff K., Roitsch T., Krischke M., Mueller M. J., Berger S.** (2008): General detoxification and stress responses are mediated by oxidized lipids through TGA transcription factors in *Arabidopsis*. *The Plant Cell* **20**: pp. 768–785.
- Muhitch M. J., Shaner D. L., Stidham M. A.** (1987): Imidazolinones and Acetohydroxyacid Synthase from Higher Plants: Properties of the Enzyme from Maize Suspension Culture Cells and Evidence for the Binding of Imazapyr to Acetohydroxyacid Synthase in Vivo. *Plant Physiology* **83**: pp. 451–456.
- Murchie E. H., Lawson T.** (2013): Chlorophyll fluorescence analysis: a guide to good practice and understanding some new applications. *Journal of experimental botany* **64**: pp. 3983–3998.
- Mustroph A., Zanetti M. E., Jang C. J. H., Holtan H. E., Repetti P. P., Galbraith D. W., Girke T., Bailey-Serres J.** (2009): Profiling translomes of discrete cell populations resolves altered cellular priorities during hypoxia in *Arabidopsis*. *Proceedings of the National Academy of Sciences of the United States of America* **106**: pp. 18843–18848.

- Narsai R., Law S. R., Carrie C., Xu L., Whelan J.** (2011): In-depth temporal transcriptome profiling reveals a crucial developmental switch with roles for RNA processing and organelle metabolism that are essential for germination in Arabidopsis. *Plant Physiology* **157**: pp. 1342–1362.
- Nguyen C. T., Martinoia E., Farmer E. E.** (2017): Emerging Jasmonate Transporters. *Molecular plant* **10**: pp. 659–661.
- Nijhout H. F., Gregory J. F., Fitzpatrick C., Cho E., Lamers K. Y., Ulrich C. M., Reed M. C.** (2009): A mathematical model gives insights into the effects of vitamin B-6 deficiency on 1-carbon and glutathione metabolism. *The Journal of nutrition* **139**: pp. 784–791.
- Ochocki J. D., Khare S., Hess M., Ackerman D., Qiu B., Daisak J. I., Worth A. J., Lin N., Lee P., Xie H., Li B., Wubbenhorst B., Maguire T. G., Nathanson K. L., Alwine J. C., Blair I. A., Nissim I., Keith B., Simon M. C.** (2018): Arginase 2 Suppresses Renal Carcinoma Progression via Biosynthetic Cofactor Pyridoxal Phosphate Depletion and Increased Polyamine Toxicity. *Cell metabolism* **27**: pp. 1263-1280.e6.
- Okamura E., Hirai M. Y.** (2017): Novel regulatory mechanism of serine biosynthesis associated with 3-phosphoglycerate dehydrogenase in Arabidopsis thaliana. *Scientific Reports* **7**: pp. 3533.
- Page D. R., Grossniklaus U.** (2002): The art and design of genetic screens: Arabidopsis thaliana. *Nature reviews. Genetics* **3**: pp. 124–136.
- Pallotta M. A., Graham R. d., Langridge P., Sparrow D. H. B., Barker S. J.** (2000): RFLP mapping of manganese efficiency in barley. *Theoretical and Applied Genetics* **101**: pp. 1100–1108.
- Palmieri F., Pierri C. L., Grassi A. de, Nunes-Nesi A., Fernie A. R.** (2011): Evolution, structure and function of mitochondrial carriers: a review with new insights. *The Plant journal : for cell and molecular biology* **66**: pp. 161–181.
- Pandey N., Ranjan A., Pant P., Tripathi R. K., Ateek F., Pandey H. P., Patre U. V., Sawant S. V.** (2013): CAMTA 1 regulates drought responses in Arabidopsis thaliana. *BMC genomics* **14**: pp. 216.
- Parra M., Stahl S., Hellmann H.** (2018): Vitamin B6 and Its Role in Cell Metabolism and Physiology. *Cells* **7**.

- Peeraer Y., Rabijns A., Collet J.-F., van Schaftingen E., Ranter C. de** (2004): How calcium inhibits the magnesium-dependent enzyme human phosphoserine phosphatase. *European journal of biochemistry* **271**: pp. 3421–3427.
- Perl M.** (1986): ATP synthesis and utilization in the early stage of seed germination in relation to seed dormancy and quality. *Physiologia Plantarum* **66**: pp. 177–182.
- Pesaresi P., Hertle A., Pribil M., Kleine T., Wagner R., Strissel H., Ihnatowicz A., Bonardi V., Scharfenberg M., Schneider A., Pfannschmidt T., Leister D.** (2009): Arabidopsis STN7 kinase provides a link between short- and long-term photosynthetic acclimation. *The Plant Cell* **21**: pp. 2402–2423.
- Peterhansel C., Horst I., Niessen M., Blume C., Kebeish R., Kürkcüoglu S., Kreuzaler F.** (2010): Photorespiration. *The arabidopsis book* **8**: pp. e0130.
- Peters J. L., Cnudde F., Gerats T.** (2003): Forward genetics and map-based cloning approaches. *Trends in plant science* **8**: pp. 484–491.
- Pfeiffer F., Gröber C., Blank M., Händler K., Beyer M., Schultze J. L., Mayer G.** (2018): Systematic evaluation of error rates and causes in short samples in next-generation sequencing. *Scientific Reports* **8**: pp. 10950.
- Pline W. A., WILCUT J. W., Edmisten K. L.** (2002): Postemergence Weed Control in Soybean (Glycine max) with Cloransulam-Methyl and Diphenyl Ether Tank-Mixtures 1. *Weed Technology* **16**: pp. 737–742.
- Porra R. J.** (2002): The chequered history of the development and use of simultaneous equations for the accurate determination of chlorophylls a and b. *Photosynthesis research* **73**: pp. 149–156.
- Potel F., Valadier M.-H., Ferrario-Méry S., Grandjean O., Morin H., Gaufichon L., Boutet-Mercey S., Lothier J., Rothstein S. J., Hirose N., Suzuki A.** (2009): Assimilation of excess ammonium into amino acids and nitrogen translocation in Arabidopsis thaliana--roles of glutamate synthases and carbamoylphosphate synthetase in leaves. *The FEBS journal* **276**: pp. 4061–4076.
- Qin Y., Leydon A. R., Manziello A., Pandey R., Mount D., Denic S., Vasic B., Johnson M. A., Palanivelu R.** (2009): Penetration of the stigma and style elicits a novel transcriptome in pollen tubes, pointing to genes critical for growth in a pistil. *PLoS genetics* **5**: pp. e1000621.

- Qiu J.-L., Zhou L., Yun B.-W., Nielsen H. B., Fiil B. K., Petersen K., Mackinlay J., Loake G. J., Mundy J., Morris P. C.** (2008): Arabidopsis mitogen-activated protein kinase kinases MKK1 and MKK2 have overlapping functions in defense signaling mediated by MEKK1, MPK4, and MKS1. *Plant Physiology* **148**: pp. 212–222.
- Qu L.-J., Qin G.** (2014): Generation and identification of Arabidopsis EMS mutants. *Methods in molecular biology (Clifton, N.J.)* **1062**: pp. 225–239.
- Ravanel S., Block M. A., Rippert P., Jabrin S., Curien G., Rébeillé F., Douce R.** (2004): Methionine metabolism in plants: chloroplasts are autonomous for de novo methionine synthesis and can import S-adenosylmethionine from the cytosol. *The Journal of biological chemistry* **279**: pp. 22548–22557.
- Rawat R., Sandoval F. J., Wei Z., Winkler R., Roje S.** (2011): An FMN hydrolase of the haloacid dehalogenase superfamily is active in plant chloroplasts. *The Journal of biological chemistry* **286**: pp. 42091–42098.
- Reinhold T., Alawady A., Grimm B., Beran K. C., Jahns P., Conrath U., Bauer J., Reiser J., Melzer M., Jeblick W., Neuhaus H. E.** (2007): Limitation of nocturnal import of ATP into Arabidopsis chloroplasts leads to photooxidative damage. *The Plant journal : for cell and molecular biology* **50**: pp. 293–304.
- Rensink W. A., Buell C. R.** (2005): Microarray expression profiling resources for plant genomics. *Trends in plant science* **10**: pp. 603–609.
- Reyes F., León G., Donoso M., Brandizzi F., Weber A. P. M., Orellana A.** (2010): The nucleotide sugar transporters AtUTr1 and AtUTr3 are required for the incorporation of UDP-glucose into the endoplasmic reticulum, are essential for pollen development and are needed for embryo sac progress in Arabidopsis thaliana. *The Plant journal : for cell and molecular biology* **61**: pp. 423–435.
- Ros R., Muñoz-Bertomeu J., Krueger S.** (2014): Serine in plants: biosynthesis, metabolism, and functions. *Trends in plant science* **19**: pp. 564–569.
- Rueschhoff E. E., Gillikin J. W., Sederoff H. W., Daub M. E.** (2013): The SOS4 pyridoxal kinase is required for maintenance of vitamin B6-mediated processes in chloroplasts. *Plant physiology and biochemistry : PPB* **63**: pp. 281–291.
- Sa N., Rawat R., Thornburg C., Walker K. D., Roje S.** (2016): Identification and characterization of the missing phosphatase on the riboflavin biosynthesis pathway in Arabidopsis thaliana. *The Plant journal : for cell and molecular biology* **88**: pp. 705–716.

- Sambrook J., Russell D. W.** (2001): Molecular cloning. A laboratory manual, Ed. 3. Cold Spring Harbor Laboratory Press, Cold Spring Harbor, N.Y.
- Sandoval F. J., Roje S.** (2005): An FMN hydrolase is fused to a riboflavin kinase homolog in plants. *The Journal of biological chemistry* **280**: pp. 38337–38345.
- Sauter M., Moffatt B., Saechao M. C., Hell R., Wirtz M.** (2013): Methionine salvage and S-adenosylmethionine: essential links between sulfur, ethylene and polyamine biosynthesis. *The Biochemical journal* **451**: pp. 145–154.
- Schägger H., Jagow G.** von (1991): Blue native electrophoresis for isolation of membrane protein complexes in enzymatically active form. *Analytical biochemistry* **199**: pp. 223–231.
- Selinski J., Scheibe R.** (2014): Pollen tube growth: where does the energy come from? *Plant signaling & behavior* **9**: pp. e977200.
- Selinski J., Scheibe R., Day D. A., Whelan J.** (2018): Alternative Oxidase Is Positive for Plant Performance. *Trends in plant science* **23**: pp. 588–597.
- Senkler J., Senkler M., Eubel H., Hildebrandt T., Lengwenus C., Schertl P., Schwarzländer M., Wagner S., Wittig I., Braun H.-P.** (2017): The mitochondrial complexome of Arabidopsis thaliana. *The Plant journal : for cell and molecular biology* **89**: pp. 1079–1092.
- Sessions A., Weigel D., Yanofsky M. F.** (1999): The Arabidopsis thaliana MERISTEM LAYER 1 promoter specifies epidermal expression in meristems and young primordia. *The Plant journal : for cell and molecular biology* **20**: pp. 259–263.
- Shimoni E., Rav-Hon O., Ohad I., Brumfeld V., Reich Z.** (2005): Three-Dimensional Organization of Higher-Plant Chloroplast Thylakoid Membranes Revealed by Electron Tomography. *The Plant Cell* **17**: pp. 2580–2586.
- ShuoHao H., Jing L., Jie Z., JianYun Z., LongQuan H.** (2019): Identification and characterization of a pyridoxal 5'-phosphate phosphatase in tobacco plants. *Plant science : an international journal of experimental plant biology* **278**: pp. 88–95.
- Singh P., Kuo Y.-C., Mishra S., Tsai C.-H., Chien C.-C., Chen C.-W., Desclos-Theveniau M., Chu P.-W., Schulze B., Chinchilla D., Boller T., Zimmerli L.** (2012): The lectin receptor kinase-VI.2 is required for priming and positively regulates Arabidopsis pattern-triggered immunity. *The Plant Cell* **24**: pp. 1256–1270.

- Slocum R. D.** (2005): Genes, enzymes and regulation of arginine biosynthesis in plants. *Plant physiology and biochemistry : PPB* **43**: pp. 729–745.
- Song J., Li Z., Liu Z., Guo Y., Qiu L.-J.** (2017): Next-Generation Sequencing from Bulk-Segregant Analysis Accelerates the Simultaneous Identification of Two Qualitative Genes in Soybean. *Frontiers in plant science* **8**.
- Sousa C.A.F. de, Sodek L.** (2003): Alanine metabolism and alanine aminotransferase activity in soybean (*Glycine max*) during hypoxia of the root system and subsequent return to normoxia. *Environmental and Experimental Botany* **50**: pp. 1–8.
- Stepansky A., Leustek T.** (2006): Histidine biosynthesis in plants. *Amino acids* **30**: pp. 127–142.
- Stintzi A., Browse J.** (2000): The *Arabidopsis* male-sterile mutant, *opr3*, lacks the 12-oxophytodienoic acid reductase required for jasmonate synthesis. *Proceedings of the National Academy of Sciences of the United States of America* **97**: pp. 10625–10630.
- Stotz H. U., Sawada Y., Shimada Y., Hirai M. Y., Sasaki E., Krischke M., Brown P. D., Saito K., Kamiya Y.** (2011): Role of camalexin, indole glucosinolates, and side chain modification of glucosinolate-derived isothiocyanates in defense of *Arabidopsis* against *Sclerotinia sclerotiorum*. *The Plant journal : for cell and molecular biology* **67**: pp. 81–93.
- Suorsa M., Rantala M., Mamedov F., Lespinasse M., Trotta A., Grieco M., Vuorio E., Tikkanen M., Järvi S., Aro E.-M.** (2015): Light acclimation involves dynamic re-organization of the pigment-protein megacomplexes in non-appressed thylakoid domains. *The Plant journal : for cell and molecular biology* **84**: pp. 360–373.
- Sussman I., Avron M.** (1981): Characterization and partial purification of dl-glycerol-1-phosphatase from *Dunaliella salina*. *Biochimica et Biophysica Acta (BBA) - Enzymology* **661**: pp. 199–204.
- Tadege M.** (1999): Ethanol fermentation: new functions for an old pathway. *Trends in plant science* **4**: pp. 320–325.
- Tambasco-Studart M., Tews I., Amrhein N., Fitzpatrick T. B.** (2007): Functional Analysis of PDX2 from *Arabidopsis*, a Glutaminase Involved in Vitamin B6 Biosynthesis. *Plant Physiology* **144**: pp. 915–925.
- Taylor R. G., Walker D. C., McInnes R. R.** (1993): *E. coli* host strains significantly affect the quality of small scale plasmid DNA preparations used for sequencing. *Nucleic acids research* **21**: pp. 1677–1678.

- The UniProt Consortium** (2019): UniProt: a worldwide hub of protein knowledge. *Nucleic acids research* **47**: pp. D506-D515.
- Thimm O., Bläsing O., Gibon Y., Nagel A., Meyer S., Krüger P., Selbig J., Müller L. A., Rhee S. Y., Stitt M.** (2004): MAPMAN: a user-driven tool to display genomics data sets onto diagrams of metabolic pathways and other biological processes. *The Plant journal : for cell and molecular biology* **37**: pp. 914–939.
- Thines B., Mandaokar A., Browse J.** (2013): Characterizing jasmonate regulation of male fertility in Arabidopsis. *Methods in molecular biology (Clifton, N.J.)* **1011**: pp. 13–23.
- Thole J. M., Vermeer J. E. M., Zhang Y., Gadella T. W. J., Nielsen E.** (2008): Root hair defective4 encodes a phosphatidylinositol-4-phosphate phosphatase required for proper root hair development in Arabidopsis thaliana. *The Plant Cell* **20**: pp. 381–395.
- Thomas P. D., Campbell M. J., Kejariwal A., Mi H., Karlak B., Daverman R., Diemer K., Muruganujan A., Narechania A.** (2003): PANTHER: a library of protein families and subfamilies indexed by function. *Genome research* **13**: pp. 2129–2141.
- Titiz O., Tambasco-Studart M., Warzych E., Apel K., Amrhein N., Laloi C., Fitzpatrick T. B.** (2006): PDX1 is essential for vitamin B6 biosynthesis, development and stress tolerance in Arabidopsis. *The Plant journal : for cell and molecular biology* **48**: pp. 933–946.
- Tjaden J., Mohlmann T., Kampfenkel K., Neuhaus G. H. a. E.** (1998): Altered plastidic ATP/ADP-transporter activity influences potato (*Solanum tuberosum*L.) tuber morphology, yield and composition of tuber starch. *The Plant Journal* **16**: pp. 531–540.
- Trentmann O., Horn M., van Scheltinga A. C. T., Neuhaus H. E., Haferkamp I.** (2007): Enlightening energy parasitism by analysis of an ATP/ADP transporter from chlamydiae. *PLoS biology* **5**: pp. e231.
- Trentmann O., Jung B., Neuhaus H. E., Haferkamp I.** (2008): Nonmitochondrial ATP/ADP Transporters Accept Phosphate as Third Substrate. *The Journal of biological chemistry* **283**: pp. 36486–36493.
- Tsai K.-J., Lin C.-Y., Ting C.-Y., Shih M.-C.** (2016): Ethylene-Regulated Glutamate Dehydrogenase Fine-Tunes Metabolism during Anoxia-Reoxygenation. *Plant Physiology* **172**: pp. 1548–1562.

- Uchida N., Sakamoto T., Tasaka M., Kurata T.** (2014): Identification of EMS-induced causal mutations in *Arabidopsis thaliana* by next-generation sequencing. *Methods in molecular biology (Clifton, N.J.)* **1062**: pp. 259–270.
- van Aken O., Zhang B., Law S., Narsai R., Whelan J.** (2013): AtWRKY40 and AtWRKY63 modulate the expression of stress-responsive nuclear genes encoding mitochondrial and chloroplast proteins. *Plant Physiology* **162**: pp. 254–271.
- van Dijk E. L., Auger H., Jaszczyszyn Y., Thermes C.** (2014): Ten years of next-generation sequencing technology. *Trends in genetics : TIG* **30**: pp. 418–426.
- van Leeuwen J., Pons C., Boone C., Andrews B. J.** (2017): Mechanisms of suppression: The wiring of genetic resilience. *BioEssays : news and reviews in molecular, cellular and developmental biology* **39**.
- Varotto C., Pesaresi P., Meurer J., Oelmüller R., Steiner-Lange S., Salamini F., Leister D.** (2000): Disruption of the *Arabidopsis* photosystem I gene *psaE1* affects photosynthesis and impairs growth. *The Plant Journal* **22**: pp. 115–124.
- Vishwakarma A., Bashyam L., Senthilkumaran B., Scheibe R., Padmasree K.** (2014): Physiological role of AOX1a in photosynthesis and maintenance of cellular redox homeostasis under high light in *Arabidopsis thaliana*. *Plant physiology and biochemistry : PPB* **81**: pp. 44–53.
- Vishwakarma A., Tetali S. D., Selinski J., Scheibe R., Padmasree K.** (2015): Importance of the alternative oxidase (AOX) pathway in regulating cellular redox and ROS homeostasis to optimize photosynthesis during restriction of the cytochrome oxidase pathway in *Arabidopsis thaliana*. *Annals of botany* **116**: pp. 555–569.
- Voon C. P., Guan X., Sun Y., Sahu A., Chan M. N., Gardeström P., Wagner S., Fuchs P., Nietzel T., Versaw W. K., Schwarzländer M., Lim B. L.** (2018): ATP compartmentation in plastids and cytosol of *Arabidopsis thaliana* revealed by fluorescent protein sensing. *Proceedings of the National Academy of Sciences of the United States of America* **115**: pp. E10778-E10787.
- Wagner S., van Aken O., Elsässer M., Schwarzländer M.** (2018): Mitochondrial Energy Signaling and Its Role in the Low-Oxygen Stress Response of Plants. *Plant Physiology* **176**: pp. 1156–1170.
- Wang K., Li M., Hakonarson H.** (2010): ANNOVAR: functional annotation of genetic variants from high-throughput sequencing data. *Nucleic acids research* **38**: pp. e164.

- Wang X., Xu C., Cai X., Wang Q., Dai S.** (2017): Heat-Responsive Photosynthetic and Signaling Pathways in Plants: Insight from Proteomics. *International journal of molecular sciences* **18**.
- Wasternack C., Hause B.** (2013): Jasmonates: biosynthesis, perception, signal transduction and action in plant stress response, growth and development. An update to the 2007 review in *Annals of Botany*. *Annals of botany* **111**: pp. 1021–1058.
- Weigel D., Glazebrook J.** (2002): *Arabidopsis*. A laboratory manual. Cold Spring Harbor Laboratory Press, Cold Spring Harbor, N.Y.
- Winkler H. H., Neuhaus H. E.** (1999): Non-mitochondrial ATP transport. *Trends in biochemical sciences* **24**: pp. 64–68.
- Winter G., Todd C. D., Trovato M., Forlani G., Funck D.** (2015): Physiological implications of arginine metabolism in plants. *Frontiers in plant science* **6**: pp. 534.
- Wittig I., Braun H.-P., Schagger H.** (2006): Blue native PAGE. *Nature protocols* **1**: pp. 418–428.
- Wu Y., Shi L., Li L., Fu L., Liu Y., Xiong Y., Sheen J.** (2019): Integration of nutrient, energy, light, and hormone signalling via TOR in plants. *Journal of experimental botany* **70**: pp. 2227–2238.
- Wulfert S., Krueger S.** (2018): Phosphoserine Aminotransferase1 Is Part of the Phosphorylated Pathways for Serine Biosynthesis and Essential for Light and Sugar-Dependent Growth Promotion. *Frontiers in plant science* **9**.
- Xiong Y., McCormack M., Li L., Hall Q., Xiang C., Sheen J.** (2013): Glucose-TOR signalling reprograms the transcriptome and activates meristems. *Nature* **496**: pp. 181–186.
- Xu F., Xu S., Wiermer M., Zhang Y., Li X.** (2012): The cyclin L homolog MOS12 and the MOS4-associated complex are required for the proper splicing of plant resistance genes. *The Plant journal : for cell and molecular biology* **70**: pp. 916–928.
- Yang Y., Zhang Y., Ding P., Johnson K., Li X., Zhang Y.** (2012): The ankyrin-repeat transmembrane protein BDA1 functions downstream of the receptor-like protein SNC2 to regulate plant immunity. *Plant Physiology* **159**: pp. 1857–1865.
- Yekondi S., Liang F.-C., Okuma E., Radziejwoski A., Mai H.-W., Swain S., Singh P., Gauthier M., Chien H.-C., Murata Y., Zimmerli L.** (2018): Nonredundant functions of Arabidopsis LecRK-V.2 and LecRK-VII.1 in controlling stomatal immunity and jasmonate-mediated stomatal closure. *The New phytologist* **218**: pp. 253–268.

- Yoo S.-D., Cho Y.-H., Sheen J.** (2007): Arabidopsis mesophyll protoplasts: a versatile cell system for transient gene expression analysis. *Nature protocols* **2**: pp. 1565–1572.
- Zhang S., Wei J., Le Kang** (2012): Transcriptional analysis of Arabidopsis thaliana response to lima bean volatiles. *PLoS ONE* **7**: pp. e35867.
- Zhang X., Zheng X., Ke S., Zhu H., Liu F., Zhang Z., Peng X., Guo L., Zeng R., Hou P., Liu Z., Wu S., Song M., Yang J., Zhang G.** (2016): ER-localized adenine nucleotide transporter ER-ANT1: an integrator of energy and stress signaling in rice. *Plant molecular biology* **92**: pp. 701–715.
- Zhou Q., Liu W., Zhang Y., Liu K. K.** (2007): Action mechanisms of acetolactate synthase-inhibiting herbicides. *Pesticide Biochemistry and Physiology* **89**: pp. 89–96.
- Zimmermann P., Hirsch-Hoffmann M., Hennig L., Gruissem W.** (2004): GENEVESTIGATOR. Arabidopsis microarray database and analysis toolbox. *Plant Physiology* **136**: pp. 2621–2632.
- Zulet A., Gil-Monreal M., Zabalza A., van Dongen J. T., Royuela M.** (2015): Fermentation and alternative oxidase contribute to the action of amino acid biosynthesis-inhibiting herbicides. *Journal of plant physiology* **175**: pp. 102–112.
- Zybilov B., Rutschow H., Friso G., Rudella A., Emanuelsson O., Sun Q., van Wijk K. J.** (2008): Sorting Signals, N-Terminal Modifications and Abundance of the Chloroplast Proteome. *PLoS ONE* **3**.

6 Appendix

6.1 Gene ontology *er-ant1*

Table 6-1: Gene ontology (GO) biological process analysis of all genes upregulated in *er-ant1* after 4 d shift from high to ambient CO₂ but not in other photorespiration mutants analysed by Eisenhut *et al.*, 2017. Shown are significantly enriched GO terms (Threshold: log₂ fold change ≥ 1; Test type: Fisher's test; Correction: false discovery rate-corrected for P < 0.05).

GO upregulated genes (biological process)	<i>A. thaliana</i> (27581)	<i>er-ant1</i> (510)	<i>er-ant1</i> (expected)	<i>er-ant1</i> (fold Enrichment)
box C/D snoRNP assembly	5	3	0.9	32.45
peptidyl-arginine methylation, to asymmetrical-dimethyl arginine	7	4	0.13	30.90
polyadenylation-dependent snoRNA 3'-end processing	7	4	0.13	30.90
nuclear polyadenylation-dependent tRNA catabolic process	7	4	0.13	30.90
U4 snRNA 3'-end processing	11	6	0.20	29.50
exonucleolytic trimming to generate mature 3'-end of 5.8S rRNA from tricistronic rRNA transcript (SSU-rRNA, 5.8S rRNA, LSU-rRNA)	8	4	0.15	27.04
Response to X-ray	6	3	0.11	27.04
nuclear-transcribed mRNA catabolic process, exonucleolytic, 3'-5'	13	6	0.24	24.96
histone arginine methylation	11	5	0.20	24.58
nuclear polyadenylation-dependent rRNA catabolic process	9	4	0.17	24.04
nuclear mRNA surveillance	14	6	0.26	23.18
positive regulation of mitochondrial translation	10	4	0.18	23.18
rRNA modification	37	6	0.68	8.77
maturation of LSU-rRNA	32	5	0.59	8.45
ribosomal large subunit assembly	42	6	0.78	7.73
maturation of SSU-rRNA	51	6	0.94	6.36
protein targeting to mitochondrion	62	7	1.15	6.11
amide biosynthetic process	617	25	11.41	2.19

Table 6-2: Gene ontology (GO) molecular function analysis of all genes upregulated in *er-ant1* after 4 d shift from high to ambient CO₂ but not in other photorespiration mutants analysed by Eisenhut *et al.*, 2017. Shown are significantly enriched GO terms (Threshold: log₂ fold change ≥ 1; Test type: Fisher's test; Correction: false discovery rate-corrected for P < 0.05).

GO upregulated genes (molecular function)	<i>A. thaliana</i> (27581)	<i>er-ant1</i> (510)	<i>er-ant1</i> (expected)	<i>er-ant1</i> (fold Enrichment)
protein-arginine omega-N asymmetric methyltransferase activity	8	4	0.15	27.04
mitochondrial ribosome binding	11	5	0.20	24.58
histone-arginine N-methyltransferase activity	9	4	0.17	24.04
translation activator activity	10	4	0.18	21.63
snoRNA binding	20	5	0.37	13.52
catalytic activity, acting on RNA	425	24	7.86	3.05

Table 6-3: Gene ontology (GO) cellular component analysis of all genes upregulated in *er-ant1* after 4 d shift from high to ambient CO₂ but not in other photorespiration mutants analysed by Eisenhut *et al.*, 2017. Shown are significantly enriched GO terms (Threshold: log₂ fold change ≥ 1; Test type: Fisher's test; Correction: false discovery rate-corrected for P < 0.05).

GO upregulated genes (cellular component)	<i>A. thaliana</i> (27581)	<i>er-ant1</i> (510)	<i>er-ant1</i> (expected)	<i>er-ant1</i> (fold Enrichment)
cytoplasmic exosome (RNase complex)	14	7	0.26	27.04
Pwp2p-containing subcomplex of 90S preribosome	6	3	0.11	27.04
nuclear exosome (RNase complex)	15	6	0.28	21.63
box C/D snoRNP complex	11	3	0.20	14.75
small-subunit processome	49	13	0.91	14.35
RNA polymerase I complex	19	4	0.35	11.39
preribosome, large subunit precursor	20	4	0.37	10.82
RNA polymerase III complex	29	5	0.54	9.32
integral component of mitochondrial inner membrane	28	4	0.52	7.73
cytosolic large ribosomal subunit	137	11	2.53	4.34

Table 6-4: Gene ontology (GO) biological process analysis of all genes downregulated in *er-ant1* after 4 d shift from high to ambient CO₂ but not in other photorespiration mutants analysed by Eisenhut *et al.*, 2017. Shown are significantly enriched GO terms (Threshold: log₂ fold change ≤ -1; Test type: Fisher's test; Correction: false discovery rate-corrected for P < 0.05).

GO downregulated genes (biological process)	<i>A. thaliana</i> (27581)	<i>er-ant1</i> (606)	<i>er-ant1</i> (expected)	<i>er-ant1</i> (fold Enrichment)
S-adenosylmethionine biosynthetic process	4	3	0.09	34.13
jasmonic acid biosynthetic process	25	9	0.55	16.38
anthocyanin-containing compound biosynthetic process	16	5	0.35	14.22
regulation of flavonoid biosynthetic process	25	5	0.55	9.10
protein N-linked glycosylation	43	8	0.94	8.47
flavonoid biosynthetic process	59	9	1.30	6.94
response to jasmonic acid	216	24	4.75	4.85
response to wounding	216	21	4.75	4.42
response to heat	220	17	4.83	3.52
response to water deprivation	346	23	7.60	3.03
Defense response to fungus	232	15	5.10	2.94
response to salt stress	590	34	12.96	2.62
response to oxygen-containing compound	575	28	12.63	2.22
Transmembrane transport	708	33	15.56	2.12

Table 6-5: Gene ontology (GO) molecular function analysis of all genes downregulated in *er-ant1* after 4 d shift from high to ambient CO₂ but not in other photorespiration mutants analysed by Eisenhut *et al.*, 2017. Shown are significantly enriched GO terms (Threshold: log₂ fold change ≤ -1; Test type: Fisher's test; Correction: false discovery rate-corrected for P < 0.05).

GO downregulated genes (molecular function)	<i>A. thaliana</i> (27581)	<i>er-ant1</i> (606)	<i>er-ant1</i> (expected)	<i>er-ant1</i> (fold Enrichment)
glucomannan 4-β-mannosyltransferase	8	4	0.18	22.76
carbohydrate derivative transmembrane transporter activity	77	9	1.69	5.32
active transmembrane transporter activity	683	34	15.01	2.27

Table 6-6: Gene ontology (GO) cellular component analysis of all genes downregulated in *er-ant1* after 4 d shift from high to ambient CO₂ but not in other photorespiration mutants analysed by Eisenhut *et al.*, 2017. Shown are significantly enriched GO terms (Threshold: log₂ fold change \leq -1; Test type: Fisher's test; Correction: false discovery rate-corrected for P < 0.05).

GO downregulated genes (cellular component)	<i>A. thaliana</i> (27581)	<i>er-ant1</i> (606)	<i>er-ant1</i> (expected)	<i>er-ant1</i> (fold Enrichment)
endoplasmic reticulum chaperone complex	4	3	0.09	34.13
proton-transporting V-type ATPase, V1 domain	6	3	0.13	22.76
endoplasmic reticulum lumen	39	8	0.86	9.34
plant-type vacuole membrane	119	12	2.61	4.59
Golgi membrane	376	24	8.26	2.91
cytoskeleton	381	20	8.37	2.39

6.2 Chromosomal mapping approach (example for line 4.4)

For the identification of the EMS-mutagenized loci, which led to enhanced growth of *er-ant1* suppressor mutants, chromosomal gene mapping was performed (Alonso-Blanco *et al.*, 1998). For that purpose, the M₃ generation plants of *er-ant1* suppressor line 4.4 (see 3.5.1), which had Columbia-0 (Col-0) ecotype background, was crossed with *A. thaliana* wild-type plants of the ecotype Landsberg erecta (Ler) (Figure 6-1). This crossing resulted in an F₁ generation with heterozygous hybrids. After the self-pollination of the F₁ generation, the resulting F₂ generation was used for chromosomal mapping (mapping population).

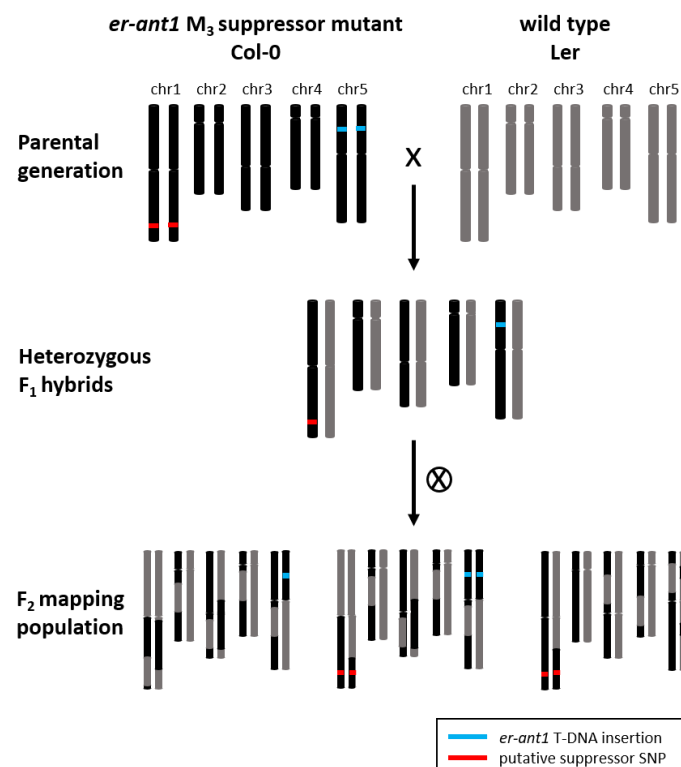


Figure 6-1: Crossing strategy for the production of the mapping population used for chromosomal gene mapping.

From this mapping population, approximately 50 plants were chosen per line, which showed enhanced growth at ambient air conditions compared to original *er-ant1* mutant plants. Subsequently, gDNA from these plants was isolated, and a T-DNA screen was performed to identify homozygous *er-ant1* knockout plants. Then, only homozygous *er-ant1* T-DNA insertion plants were used for a PCR-based genetic screen using markers for simple sequence length polymorphisms (SSLP; <http://www.amp.genomic.org.cn>). PCR products obtained with the specific SSLP primer combinations differ in size, depending on if the tested DNA region has Col-0 or Ler background. Doing this with several plants and primer combinations results in information about which chromosomal parts are interchangeable and do not play a role in the growth enhancement of the respective plant. Simultaneously, loci which contain the suppressor mutation always show Col-0 specific PCR products, because the EMS mutagenesis was conducted on *er-ant1* seeds with Col-0 background.

After a rough mapping with SSLP primer combinations covering all five *A. thaliana* chromosomes, a single region (apart from the already known *er-ant1* region on chromosome 5) was obtained in which Col-0 specific PCR products were found exclusively (Figure 6-2). A new set of SSLP primer was used, covering only this particular region but in much closer proximity than within the rough mapping. By that, the area could be narrowed down to a smaller region of 3.4 million base pairs. Within this region, 1041 putative loci were identified. To further narrow this down, further crossing steps would have been needed or even an outcross in a Near Isogenic Line. Doing this would have consumed a lot more time and effort. Therefore, and because of the availability of alternative possibilities which seemed to be more efficient concerning time and workload, the strategy was changed.

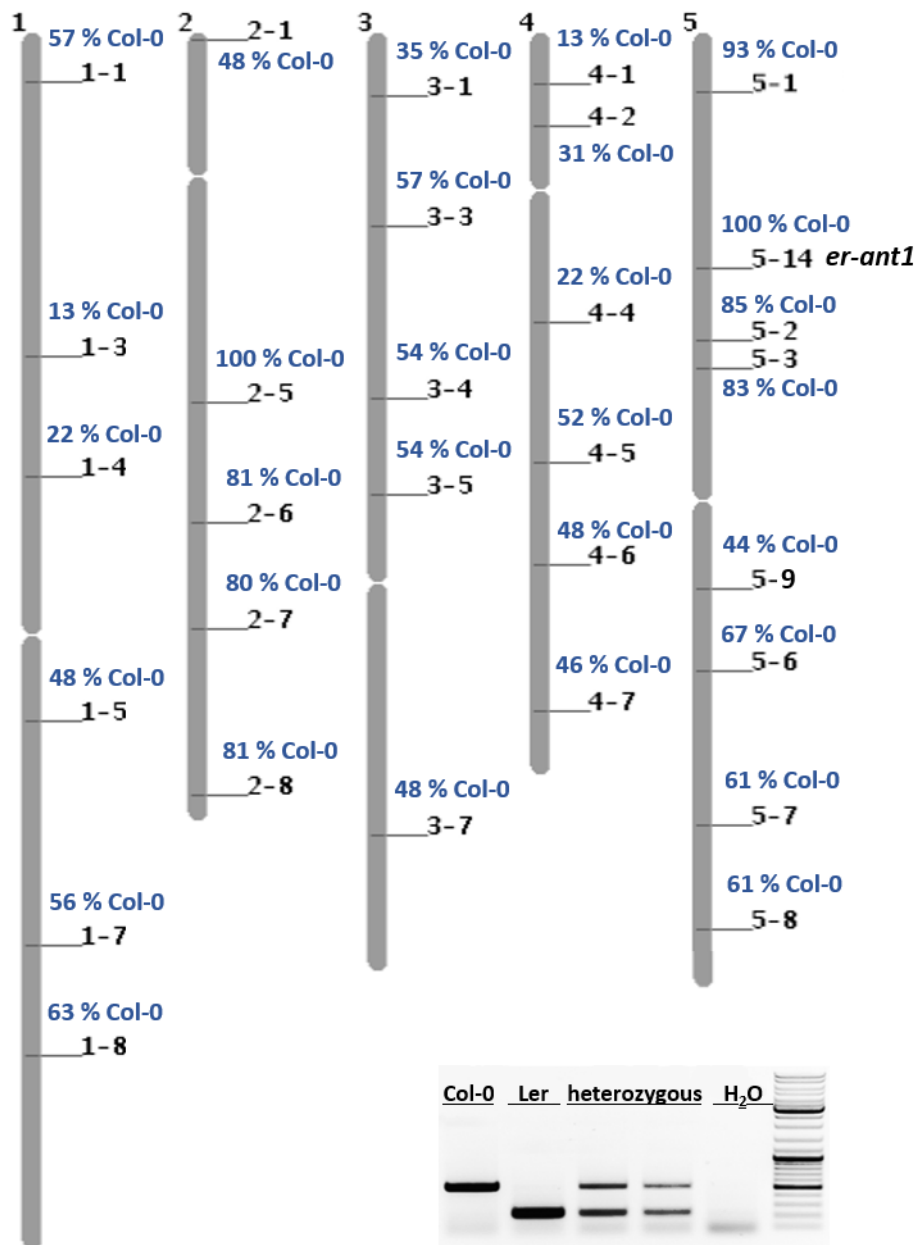


Figure 6-2: Rough chromosomal mapping results of *er-ant1* suppressor mutant line 4.4. Black chromosome labels indicate the SSLP position. Blue labels show percentage of Col-0 specific PCR-products of 27 tested plants of the mapping population. Gel picture for visualisation for possible PCR results of one SSLP primer combination.

6.3 Mapping Statistics

The mapping rates of samples reflect the similarity between each sample and the reference genome. The depth and coverage are indicators of the evenness and homology with the reference genome.

Table 6-7: Mapping statistics.

Sample	Mapped reads	Total reads	Mapping rate (%)	Average depth (x)	Coverage at least 1x (%)	Coverage at least 4x (%)
<i>er-ant1</i>	45369272	47946686	94.62	47.43	99.98	99.96
neg_1_2	47866704	49483480	96.73	48.12	99.98	99.96
neg_1_3	49005334	49970678	98.07	41.82	99.97	99.96
neg_4_1	58995978	63119214	93.47	48.17	99.98	99.96
neg_4_2	51946036	53981484	96.23	44.96	99.98	99.96
neg_4_3	54687985	57776730	94.65	43.35	99.98	99.96
neg_4_4	45414706	46892656	96.85	44.73	99.98	99.96
neg_5_4	46045326	47436708	97.07	45.03	99.98	99.96
neg_5_5	43675205	47359492	92.22	43.66	99.98	99.96
neg_5_6	62678722	64343774	97.41	52.50	99.98	99.96
neg_6_3	47183300	48514958	97.26	42.89	99.98	99.96
neg_8_3	44919361	48176140	93.24	44.86	99.98	99.96
neg_16_2	49697464	52465504	94.72	42.87	99.98	99.96
neg_17_1	59383702	61110918	97.17	50.33	99.98	99.96
pos_1_2	50722265	52861804	95.95	50.85	99.98	99.96
pos_1_3	59021928	60719054	97.20	51.15	99.98	99.96
pos_4_1	56307252	58000454	97.08	49.32	99.98	99.96
pos_4_2	41065934	42626008	96.34	41.63	99.98	99.96
pos_4_3	58502853	59309858	98.64	49.80	99.98	99.96
pos_4_4	45961042	46915736	97.97	46.35	99.98	99.96
pos_5_4	50672935	51801310	97.82	50.67	99.98	99.97
pos_5_5	44935099	47336870	94.93	45.33	99.98	99.96
pos_5_6	53220001	54081746	98.41	47.76	99.98	99.96
pos_6_3	56564399	57471136	98.42	49.92	99.98	99.96
pos_8_3	46873068	48859450	95.93	47.13	99.98	99.96
pos_16_2	59639496	61565880	96.87	51.68	99.98	99.96
pos_17_1	66361757	68235866	97.25	56.45	99.98	99.96

6.4 Alignments of AT2G33255

Table 6-8: Similarity scores from ClustalW multiple sequence alignments with AT2G33255 and the eight characterised HADSF subfamily IA members. The identity and similarity values in per cent describe the proteins' sequence similarity to the protein sequence of AT2G33255.

	SOQ1	PYRP2	FHY	FHY1	CBBY	GPP2	GPP1	SGPP
% Identity	3 %	7 %	8 %	8 %	11 %	12 %	13 %	13 %

The ClustalW multiple sequence alignment performed in this study did not reveal HAD homologs within the group of characterised HADSF subfamily IA members in *A. thaliana*. However, the HAD protein sequence had the highest sequence similarity within this group with GPP1 and SGPP. For this reason, single sequence alignments were performed with the protein sequences of both GPP proteins and HAD (Figure 6-3) and pairwise sequence alignment with the protein sequence of HAD and SGPP (Figure 6-4).

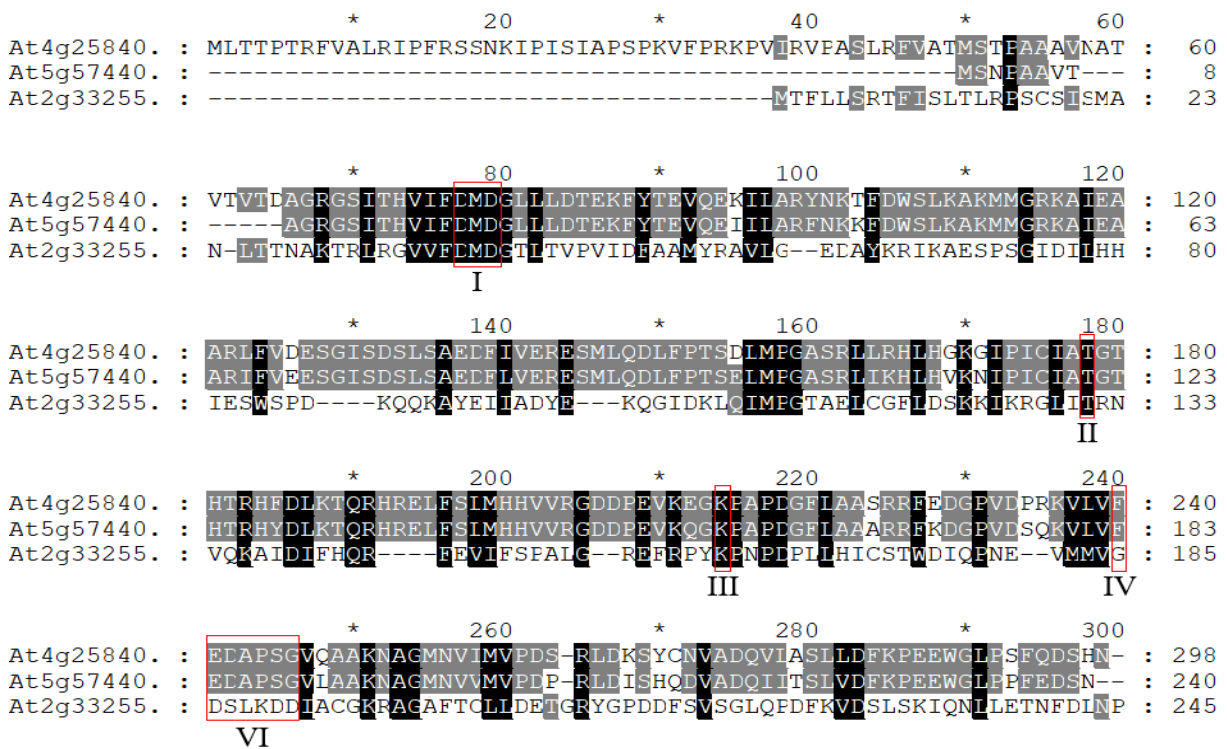


Figure 6-3: Alignment of the predicted amino acid sequences of GPP1 (At4g25840), GPP2 (At5g57440) and HAD (AT2G33255). Residues identical among sequences are indicated by black shading. Residues conserved by two proteins are indicated by grey shading. Red boxes mark conserved HADSF motifs I-IV (I: DxD; II, T/S; III: K/R; IV: E/DD, GDxxD, or GDxxxD). Dashes represent introduced sequenced gaps for alignment improvement. Numbers on the right indicate amino acid positions.



Figure 6-4 Alignment of the predicted amino acid sequences of SGPP2 and HAD (AT2G33255). Residues identical or with similar properties among sequences are indicated by black shading. Residues which are not identical are highlighted by different shading (grey/white). Red boxes mark conserved HADSF motifs I-IV (I: Dx D; II, T/S; III: K/R; IV: E/DD, GDxxD, or GDxxx D). Dashes represent introduced sequenced gaps for alignment improvement. Numbers on the right indicate amino acid positions.

Within the EMBOSS Needle pairwise sequence alignment, HAD protein sequence shares more percent identity with SGPP (19.7 %) than with the GPP protein sequences.

Danksagung

An erster Stelle möchte ich mich bei Herrn Prof. Dr. H Ekkehard Neuhaus für die Vergabe des interessanten Forschungsthemas, das Vertrauen und die sehr gute Betreuung während meiner Promotionszeit herzlich bedanken.

Außerdem möchte ich mich bei Herrn Dr. Mathias Pribil bedanken, der mich während meiner Aufenthalte in Kopenhagen ebenfalls sehr gut betreut und meine unzähligen Fragen per Mail beantwortet hat.

Furthermore, I'd like to thank Poul Erik Jensen, who kindly assesses my thesis.

Dr. Sebastian Hassler gebührt ebenfalls ein großer Dank, da er das EMS-Projekt gestartet und mich in der ersten Zeit betreut hat.

Ein großer Dank auch an Dr. Tatjana Kleine, dafür, dass sie die EMS-Mutagenese der Samen übernommen und mir viele Mails mit Fragen zum NGS beantwortet hat.

Ein Dank, der mir besonders am Herzen liegt, gilt Dr. Ilka Haferkamp, dafür, dass sie mich mit ihrem Enthusiasmus so sehr angesteckt hat, so dass ich mittlerweile der Meinung bin das tollste Promotionsthema aller Zeiten gehabt zu haben. Dafür, dass sie mir den Spaß am Forschen vermittelt hat und ich immer sein durfte, wie ich bin. Fürs Gedankenentwirren, fürs Geduldigsein, fürs Mutmachen, für's Mentorin-sein und für Merlin. Danke, du Superhirn und Freundin.

Natürlich danke ich Kathrin Patzke, die den Soundtrack zur gesamten Promotionszeit täglich neu komponiert hat. Zu zweit ist alles einfacher und ich bin froh, dass ich den Riesenweg mit dir als Freundin gemeinsam gehen konnte. Die vielen Insider werden uns auf ewig verbinden.

Dr. Oliver Trentmann möchte ich dafür danken, dass er immer da ist, wenn man ihn braucht. Gemeinsam mit Ilka bringst du ein bisschen Heimat ins Labor. Danke, dass du MacGyver-mäßig alles in Schuss hältst und immer eine Lösung findest. Dein Pragmatismus lässt mich immer wieder durchatmen und die Dinge in angemessener Relation betrachten.

Christa Jung danke ich für jegliche Hilfe bei bürokratischem Wirrwarr. Noch mehr danke ich dir für die Mini-Therapiesitzungen und die Erkenntnis, dass Eichhörnchen eigentlich ganz okay sind.

Generell danke ich allen Leuten der AG Pflanzenphysiologie für die gute und vor allem harmonische Zusammenarbeit. Besonders danke ich Regina Rode dafür, dass sie unheimlich spontan, schnell und genau Aufgaben erledigt, für die meine zwei linken Hände ungeeignet sind. Und danke für die unfassbar hübschen und leckeren Kuchen!

Vanessa Scherer gebührt besonderem Dank, da sie im Rahmen ihrer Masterarbeit maßgeblich an der Charakterisierung der HAD beteiligt war. Vielen Dank auch, dass du dich

so super um die Pflanzen gekümmert hast, während ich in Kopenhagen war. Auf dich ist echt Verlass!

Danke auch an den treuesten Hiwi der Welt, Timo Zeh. Ohne dich würde ich wahrscheinlich jetzt noch Samen ernten. Pommes!

Thanks to Omar, Anurag, James, Silas, Guillem and Wendy! Omar, for all the beer and showing me how to do thylakoid isolation and BN-PAGE, and how to repair a di-pump with bubble-gum and a needle. I want to thank Anurag, not only for teaching me everything about TEM, but also showing me mantras for my head (your "little fella" tries to unclutter her mind and is more often deeeeeply relaxed 😊.) Silas, tak for the translation, this is awesome! I'd further like to thank Lene Rasmussen for the help with the paperwork and Annemarie Matthes for all the chocolate 😊.

Danke Anne, dafür, dass du mir in all den Jahren eine wahre Freundin warst. Alles ist (noch immer) gut. Du wirst mich nie mehr los.

Danke, liebe Familie, sorry, dass ich in den letzten Jahren nicht oft da war... Ich verspreche, es wird besser. Ich danke meiner Mutter, Renate Altensell, dafür, dass sie mir das Abitur ermöglicht hat und mich nie zu etwas gedrängt hat. Meiner unfassbar klugen Cousine, Jasmin deBeyer, danke ich dafür, dass sie jedes Problem innerhalb von Sekunden analysiert und direkt hundert Lösungsvorschläge parat hat. An dir ist eine Naturwissenschaftlerin verloren gegangen. Danke auch meiner „neuen“ Familie, besonders Elke und Wolfgang Weigand, für die moralische Unterstützung und die Versorgungspakete.

Danke Ben, dafür dass du mein Partner und bester Freund bist. Gemeinsam schaffen wir alles.

Lebenslauf

Promotion:

06/2015- Heute Wissenschaftliche Mitarbeitern im Rahmen einer
Promotion
AG Pflanzenphysiologie,
Fachbereich Biologie
Technische Universität Kaiserslautern

06/2015- Heute PhD Student
Department of Plant and Environmental Sciences,
Faculty of Science,
University of Copenhagen

Studium:

10/2012-05/2015 Master of Science Microbial and Plant Biotechnology,
Technische Universität Kaiserslautern

10/2009-7/2012 Bachelor of Science Biowissenschaften,
Technische Universität Kaiserslautern

Eidesstattliche Erklärung

Hiermit erkläre ich, dass ich die vorliegende Dissertation selbständig und ohne unerlaubte Hilfe verfasst und keine anderen Quellen und Hilfsmittel als die angegebenen verwendet habe.

Ich versichere, dass ich weder an der Technischen Universität Kaiserslautern, noch anderweitig versucht habe, eine Dissertation einzureichen oder mich einer Doktorprüfung zu unterziehen.

Kaiserslautern, den 12.06.2019: